HHS Public Access

Author manuscript

Chem Rev. Author manuscript; available in PMC 2018 November 08.

Published in final edited form as:

Chem Rev. 2017 November 08; 117(21): 13320–13352. doi:10.1021/acs.chemrev.7b00180.

Biomimetic Reactivity of Oxygen-Derived Manganese and Iron Porphyrinoid Complexes

Regina A. Baglia, **Jan Paulo T. Zaragoza**, and **David P. Goldberg***

Department of Chemistry, The Johns Hopkins University, 3400 North Charles Street, Baltimore, Maryland 21218, United States

Abstract

Heme proteins utilize the heme cofactor, an iron porphyrin, to perform a diverse range of reactions including dioxygen binding and transport, electron transfer, and oxidation/oxygenations. These reactions share several, key metalloporphyrin intermediates, typically derived from dioxygen and its congeners such as hydrogen peroxide, and which are comprised of metal-dioxygen, metal-superoxo, metal-peroxo, and metal-oxo adducts. A wide variety of synthetic metalloporphyrinoid complexes have been synthesized to generate and stabilize these intermediates, and then employed to determine the spectroscopic features, structures, and reactivities of such species in controlled and well-defined environments. In this review, we summarize recent findings on the reactivity of these species with common porphyrinoid scaffolds employed for biomimetic studies. The proposed mechanisms of action are emphasized. The review is organized by structural type of metal-oxygen intermediate, and broken into subsections based on the metal (manganese, iron) and porphyrinoid ligand (porphyrin, corrole, corrolazine).

TABLE OF CONTENTS FIGURE

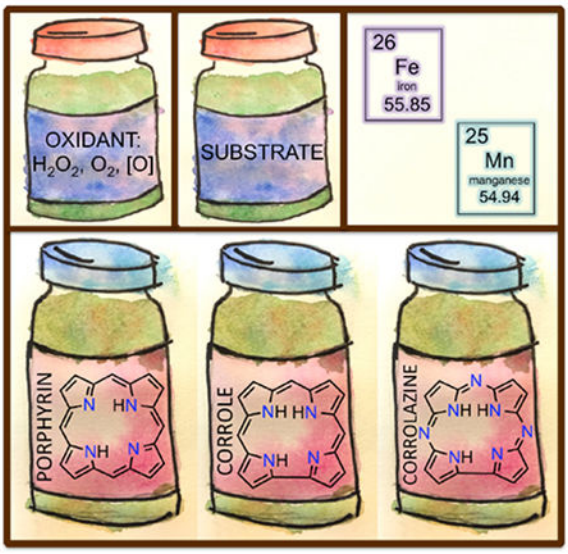

* *Corresponding Author*: dpg@jhu.edu.

The authors declare no competing financial interest.

1.1 Introduction

Porphyrins and related macrocycles have been well studied because of their role as biological ligands. The heme cofactor, which consists of an iron-bound porphyrin, is at the active site of many metalloproteins and performs a diverse range of chemistry such as oxygen transport and storage, electron transfer, and oxidation/oxygenation reactions (using O_2/H_2O_2 as the oxidant and in many cases the O-atom source).[1-3]

Examples of monooxygenation reactions catalyzed by heme enzymes include aromatic and alkane hydroxylations, olefin epoxidations, as well as N-, S- or O-dealkylations. One class of enzymes that performs many of these transformations, which use dioxygen (O_2) as the oxidant and O-atom source, is a large class of thiolate-ligated heme enzymes called Cytochrome P450s (CYPs), which are found in most mammalian tissues and organs as well as other organisms such as plants, bacteria, and yeast. Heme-dependent dioxygenases, which incorporate both oxygen atoms into the substrate, are a smaller class of enzymes that oxidize tryptophan or other indole derivatives to give N-formylkynurenine products. While there is a lot of information regarding the mechanism of CYP, less is known about the mechanism of dioxygenases.[1,4] Peroxidases, catalases, and choroperoxidases (CPOs) all utilize hydrogen peroxide as oxidant and substrate but differ in their functions and proximal ligand; peroxidase heme iron is bound by histidine, catalase heme iron is bound by tyrosinate, and CPO heme is bound by cysteinate. Peroxidases utilize hydrogen peroxide (H_2O_2) to oxidize such substrates as phenols and aromatic amines. Catalases perform the disproportionation of hydrogen peroxide to dioxygen and water. Heme chloroperoxidase is a halogenating enzyme that uses hydrogen peroxide to chlorinate aliphatic substrates; however, it is functionally tolerant of other substrates in that it is also capable of catalyzing peroxidase, catalase, and P450-type reactions. Finally, heme degradation is performed by heme oxygenase enzymes, in which the oxygenation of the porphyrin ligand itself occurs.

All of the enzymes discussed here utilize only a few common intermediates derived from dioxygen or hydrogen peroxide in their mechanistic cycles. These intermediates are metal-superoxo ($O_2^{\bullet-}$), - peroxo (O_2^{2-}), - hydroperoxo (OOH^-), and - oxo (O^{2-}) species (Scheme 1). Synthetic analogs target these intermediates and allow for the structural and spectroscopic features of these species to be analyzed. The development of synthetic analogs of these intermediates provides systems in which bond-making and bond-breaking events that occur at the metal can be studied in well-controlled environments. In this review, we focus on the biomimetic reactivity of synthetic oxygen-derived metalloporphyrinoid compounds.

The environment surrounding the heme in the active site varies depending on the system. The iron center is coordinated axially on the proximal side by an N, O, or S donor derived from the amino acids histidine, tryptophan, tyrosine, or cysteine. The identity of the amino acids surrounding the distal side of the metalloporphyrin also play important roles, such as providing hydrogen bond donors or acceptors that can interact with the reactive intermediates during the catalytic cycle. These structural features combine to provide selectivity and control reactivity of the metalloenzyme, allowing for a wide variety of reaction outcomes (Scheme 2). For example, within the broad class of heme proteins,

myoglobin and CYP utilize heme iron at their active sites, but have entirely different functions and O_2 reactivities due to differences in the chemical environment surrounding the heme sites. Myoglobin is a simple dioxygen- binding and transport protein. At the active site, the heme is ligated by an axial histidine nitrogen, and contains a nearby histidine on the distal side, which provides selectivity for O_2 over other toxic small molecules such as carbon monoxide (CO). In CYP, a monooxygenase, the heme iron is ligated by a cysteinate on the proximal side, and several residues and a hydrogen-bonded water network on the distal side control O_2 binding, cleavage, and subsequent substrate oxidation. Scheme 3 illustrates the "push/pull" effects of these interactions in CYP that influence this reactivity.[1]

Because the heme cofactor utilizes the porphyrin framework, synthetic metalloporphyrin complexes have proved useful as model systems to study the factors that control the reactivity of heme proteins. Porphyrins are heterocyclic macrocycles composed of four pyrrole units joined by methine bridges. They are aromatic, 18-π electron systems, and this high degree of conjugation allows for intense absorption bands in the visible region. Physicochemical properties of the porphyrin ring, such as electronic effects, steric effects, and solubility, can be varied by substituting at the *meso*- positions of the macrocycle or the β- positions of the pyrrole unit. The porphyrinoid family encompasses the common structural types shown in Chart 1. This family includes ring-contracted analogs in which one *meso* position is missing from the framework (as in corroles and corrolazines). Ring contracted analogs such as subporphyrins, subphthalocyanines, and subporphyrazines, which are missing a pyrrole unit, are also members of the porphyrinoid family, but are only known as the boron-bound derivatives.[5,6] Ring-expanded porphyrins are another large category within the porphyrinoid family, in which one or more *meso*- positions *or* pyrrole units are added to the framework. There are some excellent reviews on the synthesis of ring-expanded porphyrinoid compounds and their reactivities including articles by Dolphin,[7] Sessler,[8] and most recently Osuka.[9] In this review, we focus on porphyrins and the contracted corrole and corrolazine systems, which have been used in a range of biomimetic studies over the past several years.

In metalloporphyin models of heme proteins, the "active site" has been synthetically constructed in levels by building out from the porphyrin framework. The first level of synthetic design is to modify the porphyrin substituents on the periphery of the ring. The second level is to change the first coordination sphere of the central metal atom by adding axial ligands. The third level is to add steric encumbrance on functional groups orthogonal to the macrocycle plane, which may interact with oxygen-derived intermediates through non-covalent interactions such as hydrogen-bond donors or acceptors. An example of the latter comes from the synthesis of so-called "Pacman" porphyrins.[10] The fourth level of synthetic modification is through the encapsulation of the metalloporphyrin in a larger scaffold such as MOFs, dendrimers, or short peptides.[11,12] Finally, the ability to encapsulate the metalloporphyin in artificial or engineered proteins has seen a recent surge in effort.[13-16]

In many cases, the reactive intermediates of interest (e.g. metal-oxo, metal-O_2) in metalloporphyrin systems are transient species at room temperature and must be generated or trapped at low temperatures for characterization and study. Ring-contracted porphyrinoid complexes such as corrole and corrolazine (Chart 1) provide enhanced thermal stabilization

for some of these intermediates and allow for their direct characterization or even isolation in some cases. Corroles contain a direct pyrrole-pyrrole linkage and thus differ by the deletion of a *meso*-carbon atom relative to porphyrins. Fully deprotonated, they are trianionic (3−) ligands, and the higher charge and smaller cavity size provide a stabilizing environment for metal ions in higher oxidation states (≥ 3). Corrolazines are also ring-contracted like corroles, but contain *meso*-nitrogen atoms in place of *meso*-carbons. The biomimetic reactivity of these three ligand systems (porphyrins, corroles, and corrolazines) will be covered here. The synthesis of corroles, corrolazines, and their metalated forms has been recently reviewed in the Handbook of Porphyrin Science (2011).[17] Herein recent developments on the biomimetic reactivity of such systems are reviewed. The review is organized by structural type of metalloporphyrinoid species. Complexes are restricted to those able to participate in one or more of the biomimetic reaction types defined in the following section.

1.2 Biomimetic reaction types

Shown in Chart 2 are several biomimetic reactions performed by metalloporphyrin complexes. Oxygen atom transfer (OAT) is a two-electron process which results in the net transfer of an oxygen atom to a substrate and can occur by at least two different mechanisms, with two of the most common for metal-oxo species shown in Scheme 4. The first of these is a concerted mechanism, in which the oxygen atom is transferred in one step. Another common mechanism is a stepwise mechanism, in which the substrate is oxidized by one electron either by an outer-sphere or inner-sphere oxidation, followed by fast oxygen transfer. Typically this reaction is facile when a substrate is nucleophilic and the oxidant is an electrophilic oxo complex. The substrate for OAT is often an alkene, sulfide, or phosphine, resulting in an epoxide, sulfoxide, or phosphine oxide, respectively.

Hydrogen-atom abstraction is the net transfer of an H-atom, which can occur by several different mechanisms. H-atom abstraction is usually proposed as the first step in the oxidation of inert C–H bonds by high-valent metal-oxo species in biological systems, followed by rebound of the newly formed carbon radical with a metal-hydroxo intermediate. Mechanistically, understanding H-atom abstraction can be complex because H• transfer can occur in a step-wise fashion (proton transfer followed by electron transfer or vice versa) or in a concerted fashion. The kinetics and thermodynamics are intertwined, and the thermodynamic parameters (pK_a, $E°$) associated with H-atom transfer are illustrated in the square scheme in Scheme 5. The square scheme is similar to a thermodynamic Hess cycle, in which the sum of the ΔG°s of the horizontal (from the $E°$ of ET) and vertical (from the pK_a of PT) steps adds up to give the ΔG° of the diagonal step.

There are many examples of hydroxylation reactions by high-valent metal-oxo porphyrin species. These reactions typically are initiated by H-atom abstraction of a substrate by the metal-oxo species to give a high-valent metal hydroxide and a substrate radical, followed by oxygen rebound in which the substrate radical “combines” with the hydroxyl radical from the metal-hydroxide. Thus far, there are no examples in the biomimetic literature, in which this second step, involving oxygen rebound, has been examined directly via reaction of a high-valent metal-hydroxide complex with an organic radical to give an ROH product.

Oxygen (O_2) activation is another common biomimetic reaction. This umbrella term encompasses O_2 binding/transport (reversible O_2 activation), the two-electron/two-proton reduction of O_2 to hydrogen peroxide (H_2O_2), and the four-electron/four-proton reduction of O_2 to water. The binding and activation of H_2O_2 is related to this process, and shares common metal-oxygen intermediates. The extent of O_2 activation by a metal porphyrinoid complex is controlled by many different factors, including the metal identity, oxidation state, and ligand electronic properties, as well as any exogenous or ligand-appended hydrogen-bond donor groups in the secondary coordination sphere.

2. Metal-Oxo Porphyrinoid Complexes as Models for Biological Oxidations

2.1 Iron-Oxo Complexes

2.1.1 Iron-Oxo Porphyrins—Reactions carried out by iron-oxo porphyrins have received considerable attention because of their synthetic utility in the oxidation of organic substrates and their relevance to enzymatic heme-catalyzed processes such as those found in cytochrome P450, peroxidases, and catalases. The key reactive intermediates are postulated as high-valent iron-oxo porphyrin species defined in the biological context as Cpd I (Fe^{IV}(O)(porphyrin$^{\bullet+}$)), formally a Fe^{V}(O) complex, and Cpd II ((Fe^{IV}(O)(porphyrin)). The terms “compound I” and “compound II” were historically applied to the reactive ferryl species found in horseradish peroxidases (HRP), but are now used to describe isoelectronic iron-oxo porphyrin species in other heme enzymes.[18] Studies of synthetic high-valent iron-oxo porphyrin complexes have provided valuable insights into the reactivity of these species because of the relative ease of control of the ligand steric and electronic properties, and reaction environment, as compared to heme enzymes. In 1979, Groves *et al.* demonstrated alkene epoxidation and alkane hydroxylation using iodosylbenzene (PhIO) with an Fe^{III}(Cl)(TPP) (TPP = tetraphenylporphyrin) catalyst at room temperature.[19] One of the proposed intermediates for this catalytic oxidation was an iron-oxo complex. An early analog of the proposed catalytic intermediate came from the oxidation of Fe^{III}(Cl)(TMP) (TMP = tetramesitylporphyrin) with 1.5 equiv of mCPBA at −78 °C to form Fe^{IV}(O)(TMP$^{\bullet+}$), a porphyrin π-radical cation complex (Scheme 6).[20] The large downfield shifts in the ^{1}H NMR peaks of the mesityl groups and the UV-visible spectrum suggested a porphyrin π-radical cation. The small Mossbauer isomer shift of 0.05 mm/s (ΔE_Q = 1.49 mm/s) was in the range expected for an iron(IV) species. This complex is also reactive with olefins to form epoxides even at low temperatures. When the oxidation reaction was performed in the presence of $H_2{}^{18}O$, almost complete (99%) ^{18}O incorporation in the epoxide was observed.

After these initial reports, a number of studies on iron-oxo porphyrins were made in efforts to define possible mechanisms of substrate oxidation by heme enzymes. Excellent reviews on the reactivity of iron-oxo porphyrin complexes can be found in the literature, including those from Fujii (2000,[21] 2002[22], 2016[23]) Meunier et al. (2004),[24] Groves (2006),[25] Newcomb (2006),[26] Nam (2007),[27] Costas (2011),[28] Ray and Meyer (2012),[29] and Rutkowska-Zbik (2014)[30]. Dedicated chapters in *The Porphyrin Handbook (2000),*[18,31-34] *Handbook of Porphyrin Science,*[35] and other compilations[36-38] can also be found. This section will focus on recently published works in this area.

Although iron complexes with the tetrakis(meso-phenyl) porphyrin general structure led to some metastable iron-oxo complexes that mimic cytochrome P450 compound I reactivity, their catalytic activities were plagued with porphyrin decomposition and μ-oxo dimer formation. These problems were overcome by introducing alkyl, halogen, or other substituents to either the meso-aryl or the β-pyrrole positions of the porphyrin ring. The result was increased catalytic activity and stability of the porphyrin ligand towards decomposition.[38,39] For example, Groves has reported high rates for C-H hydroxylation in aqueous solution for $Fe^{IV}(O)(TMPyP^{\bullet+})$ (TMPyP = tetrakis(N-methyl-4-pyridinium)porphyrin) (Scheme 7).[40] Reaction of $Fe^{IV}(O)(TMPyP^{\bullet+})$ with xanthene gave the hydroxylation product, 9-xanthydrol (90%), and performing the reaction in the presence of 47.5 % $H_2{}^{18}O$ led to 21% ^{18}O incorporation. This incorporation is consistent with an oxygen-rebound scenario, where a high-valent $Fe^{IV}(O)(porphyrin^{\bullet+})$ species abstracts an H-atom from xanthene to give a carbon radical, and an $Fe^{IV}(OH)$ rebound intermediate. This species "rebounds" the •OH group to the carbon radical in the solvent cage to form the alcohol product and the resting ferric state. The rate constant for this reaction was found to be $3.6 \times 10^6\ M^{-1}\ s^{-1}$, with a modest kinetic isotope effect of 2.1. A variety of C-H hydroxylation substrates (fluorene-4-carboxylic acid, 4-isopropyl and 4-ethylbenzoic acid) were tested as well, and the hydroxylation rates correlate well with the substrate BDEs (C-H). The BDE(O-H) for Fe^{IV}(O-H)(TMPyP) was estimated from a Brønsted–Evans–Polanyi relationship to be ~100 kcal/mol, much larger than the values estimated for Fe^{IV}(O-H)(TMP) (92 kcal/mol),[41] and Fe^{III}(O-H)(TPFPP) (~86 kcal/mol)[42]. The high kinetic reactivity of this complex can be traced to the redox and basicity tuning of the iron-oxo porphyrin, expected from a porphyrin ligand with electronegative and positively charged substituents. It was further suggested that the increase in reactivity could be due to a spin-state crossing phenomena occurring in the course of the reaction.

An alternative method of producing high valent iron-oxo species was reported by the groups of Zhang, Fung, and Newcomb.[41] In this method, $Fe^{III}(ClO_4)$(TMP) was oxidized to the metastable $Fe^{IV}(ClO_4)_2$(TMP) which, when irradiated with 355 nm laser light, gave a new transient species which could be characterized only by UV-visible spectroscopy (Scheme 8). Preparative reaction of this transient iron-oxo species with cyclooctene gave cyclooctene epoxide in 28% yield. This species also reacts with alkanes and benzylic C-H substrates with rates up to 5 orders of magnitude larger than the cpd I analog $Fe^{IV}(O)(TMP^{\bullet+})$. For this reason, this species was speculated to be an $Fe^{V}(O)$(TMP) complex on the basis of its reactivity. Although this speculation is reasonable from kinetic data, this oxidation state assignment should remain tentative until appropriate spectroscopic evidence such as EPR, Mössbauer, or X-ray absorption spectroscopy is presented. These laser flash photolysis (FLP) studies were further extended to other porphyrin analogs, TPP (tetraphenylporphyrin) and OEP (octaethylporphyrin), and the order of reactivity was found to be OEP>TPP>TMP (Scheme 8). These putative transient iron-oxo species, characterized by their unique UV-visible spectra, exhibited similar rate constants to the similarly generated $Mn^{V}(O)$ porphyrins. Rate constants for benzylic C-H bond cleavage correlated with the C-H BDEs, and Hammett correlations with *para*-substituted styrenes gave slopes between −0.5 and −0.7, reflecting the electrophilic character of these reactions.[43]

Zhang and coworkers recently reported a method of generating $Fe^{IV}(O)(porphyrin^{\bullet+})$ or $Fe^{IV}(O)$(porphyrin) (porphyrin = TMP, TPP, TPFPP) complexes by simple visible light irradiation of $Fe^{III}(OBrO_2)$(porphyrin) complex.[44] The photolysis reaction is proposed to go through the heterolytic cleavage of the O-Br bond, forming a putative $Fe^{V}(O)$ complex which then relaxes to an $Fe^{IV}(O)(porphyrin^{\bullet+})$. This was observed in electron-rich porphyrins such as TMP and TPP. With Fe^{III}(TPFPP) (TPFPP = tetrakis(pentafluorophenyl)porphyrin), however, a final $Fe^{IV}(O)$(TPFPP) product was observed, which is proposed to result from the $Fe^{V}(O)$(TPFPP) comproportionating with residual Fe^{III}(TPFPP). The formation of cpd I and cpd II analogs was further confirmed by comparable rate constants obtained in the HAT and OAT reactions of iron-oxo porphyrins generated using visible light generation vs addition of mCPBA. DFT studies show that an $Fe^{V}(O)$ ground state is favored *in vacuo*. However, the $Fe^{IV}(O)(porphyrin^{\bullet+})$ configuration is favored in the solvent or protein environment.[45]

Newcomb and coworkers have shown that single-turnover hydroxylation reactions of ethyl benzene and benzyl alcohol with $Fe^{IV}(O)(TMP^{\bullet+})$, generated from the addition of m-CPBA to Fe^{III}(TMP) in CH_3CN, give large temperature-dependent KIEs, which are ascribed to H-atom tunneling.[46] The substrates were oxidized in the benzylic C-H position, to give 1-phenylethanol and benzaldehyde respectively, as determined by gas chromatography (GC).

It has been shown that axial ligands of heme enzymes also play an important role in their reactivity. In work from Fujii and coworkers, the factors that affect H-tunneling processes were explored by studying the C-H hydroxylations of xanthene and tetralin with $Fe^{IV}(O)(TMP^{\bullet+})(L)$ with different axial ligands (L = NO_3^-, Cl^-, imidazole) (Scheme 9).[47] The $Fe^{IV}(O)(TMP^{\bullet+})(L)$ complex was generated with excess O_3 (ozone) in CH_2Cl_2 at low temperatures (−20 to −95 °C). Non-linear Arrhenius plots were observed, providing strong evidence for the participation of H-tunneling in the rate-limiting H-transfer process. In addition, the authors showed that H-tunneling is controlled by temperature, the BDE of the C-H substrate, and the reactivity and Fe-O bond strength of the $Fe^{IV}(O)(TMP^{\bullet+})(L)$ complex.

The strong electron-donation from the cysteinyl thiolate ligand in cytochrome P450s is proposed to influence the driving force for C-H bond cleavage.[48] Efforts have been made to synthesize thiolate-ligated heme models with the goal of studying the role of thiolate ligation on reactivity, and these are summarized in a review.[49] The facile oxidation of thiolate ligands to disulfide remains an outstanding difficulty in the synthesis of thiolate-ligated heme models, and this is usually prevented by using a large excess of the thiolate ligand or by covalently attaching the thiolate group to the porphyrin scaffold.[38,49-51] A stable thiolate-ligated complex (called SR complex, Swan Resting) was prepared by Higuchi and co-workers by covalently attaching an alkane-thiolate group to the porphyrin, and bulky pivaloyl groups were added to protect the sulfur atom from oxidation, and amide NH groups for hydrogen-bonding with the sulfur atom (Scheme 10).[52] However, although the SR complex is known to react with oxygen atom donors and peroxyacids, it does not form a stable dioxygen adduct due to the absence of a binding pocket. In addition to the instability of thiolate-ligated heme-dioxygen adducts, the increasingly complicated synthesis of these model complexes has limited the number of examples of these systems in the literature.

Substitution of a thiolate ligand (RS^-) with a sulfonate (RSO_3^-) ligand reduces the charge density at the metal and tunes the $Fe^{III/II}$ redox couple to a more positive potential close to that found in $P450_{cam}$.[53] Woggon and van Eldik showed that the cpd I analog $Fe^{IV}(O)(porphyrin^{\bullet+})(RSO_3^-)$ can be generated with m-CPBA under saturation kinetics, which suggests the formation of an acyl-peroxo adduct intermediate, eventually converting to the cpd I analog (Scheme 11).[54] There has been speculation that an $Fe^{III}(OOH)$(porphyrin) complex (compound 0), the precursor to compound I, can act as a *second* oxidant for certain substrates in cytochrome P450. Thus, the generation of an Fe^{III}-acylperoxo complex with m-CPBA can be utilized as a model to study the possible involvement of an Fe^{III}-OOH species in heme enzyme oxidations.

Nam and coworkers have shown that $Fe^{IV}(O)(TMP^{\bullet+})$ is the active oxidant in olefin epoxidation with cyclohexene, aromatic ring oxidation with anthracene, C–H bond activation with dihydroanthracene, and alcohol oxidation with benzyl alcohol in CH_3CN/CH_2Cl_2 (1:1 v/v) at −40 °C. These results contrast with the poor oxidizing ability of the Fe^{III}(m-CPBA) adduct of this complex.[55] Similarly, van Eldik and coworkers reported kinetic evidence showing that oxygen atom transfer for Fe^{III}(m-CPBA)(TMP) was orders of magnitude slower than the $Fe^{IV}(O)(TMP^{\bullet+})$ complex in epoxidation and sulfoxidation reactions.[56]

Heme synthetic models with axial ligands covalently tethered to the porphyrin ligand can provide insights into effects of axial ligation on reactivity. However, the synthesis of these tethered systems are usually difficult and low-yielding. An alternative approach is by adding exogenous ligands to the cpd I and cpd II analogs. Large increases in cyclooctene epoxidation rates were observed upon addition of axial ligands to the $Fe^{IV}(O)(porph^{\bullet+})$ (porph = TMP, TMTMP) (TMTMP = 2,7,12,17-tetramethyl-3,8,13,18-tetramesitylporphyrin) complex, and the epoxidation rates increase in the order of $L = NO_3^- < Cl^- <$ 3-fluoro-4-nitrophenolate<imidazole.[57] Interestingly, the measured redox potentials for $Fe^{IV}(O)(porph)(L)/Fe^{IV}(O)(porph^{\bullet+})(L)$ follow the opposite trend, i.e., a positive shift was observed with anionic axial ligands (more oxidizing) and a negative shift was observed with neutral ligands (less oxidizing).[58] The reactivity of $Fe^{IV}(O)(L)(porphyrin^{\bullet+})$ correlates instead with the Fe^{III}/Fe^{II} redox potential of the reaction product, Fe^{III}(L)(porphyrin), suggesting that axial ligands affect the reactivity of $Fe^{IV}(O)(porphyrin^{\bullet+})$ complexes by stabilizing the reaction product.[59] In a separate study, the reactivity of $Fe^{IV}(O)(TMP^{\bullet+})$ in olefin epoxidation, aromatic hydroxylation, alcohol oxidation and alkane hydroxylation was measured in the presence of *para*-substituted pyridine N-oxide derivatives (*para*-Y-C_5H_5NO, Y = -OCH_3, -CH_3 -H, -Cl) as axial donors. It was found that the binding of these axial ligands lead to enhanced reactivities in all of the oxidation reactions.[60] The most electron-donating pyridine N-oxide (*p*-OCH_3-C_5H_5NO) gives the most reactive $Fe^{IV}(O)(TMP^{\bullet+})(L)$ complex in both O-atom transfer and H-atom transfer reactions. This increased reactivity was attributed to a stronger Fe(O-H) bond formed in HAT reactions, and a weaker reactant Fe=O bond broken in OAT reactions.

DFT calculations on the effects of various anionic axial ligands on aromatic hydroxylation with $Fe^{IV}(O)(porphyrin^{\bullet+})$ have shown that stronger axial ligands give rise to higher pKas of the corresponding Fe^{IV}(OH)(porphyrin) complex, while electronic effects are less affected.

Moreover, the barrier for aromatic hydroxylation appear to be proportional to the strength of the O-H bond formed in the $Fe^{IV}(OH)$ complex.[61] A similar trend was observed in alkane hydroxylation,[62] with the strength of the C-H bond of the substrate also correlating with the reaction barrier. For sulfoxidation[63] and alkene epoxidation[64,65] reactions however, the barrier height correlates with the ionization potential of the substrate, supporting an ET rate-determining step in the oxidation process. Calculations were also performed to determine the source of regioselectivity in the oxidation of ethylbenzene by $Fe^{IV}(O)(porphyrin^{\bullet+})$ to form 1-phenylethanol (alkane hydroxylation product) and p-ethylphenol (aromatic hydroxylation product). The calculations indicate that an axial acetonitrile ligand favors aromatic hydroxylation, whereas a Cl^- axial ligand favors alkane hydroxylation.[66] The anionic ligand, such as Cl^-, makes the oxidant less electrophilic due to orbital mixing which disfavors the aromatic hydroxylation mechanism and favors the alternative alkane hydroxylation mechanism.

A high-valent terminal iron-oxo species generated from a nitrido-bridged-diiron porphyrin complex was trapped and characterized, and was found to oxidize C-H bonds as strong as that of methane (BDE = 104 kcal/mol).[67] Addition of *m*-CPBA to $[(TPP)Fe^{III}(N)Fe^{IV}(TPP)]$ in CH_2Cl_2 at −80 °C results in formation of a peroxo complex which undergoes heterolytic cleavage to form the diiron, terminal oxo species $[(TPP)(m\text{-}CBA)Fe^{IV}(N)Fe^{IV}(O)(TPP^{\bullet+})]^-$, characterized by UV-vis, ESI-MS, EPR and Mössbauer spectroscopies (Scheme 12 and Figure 1). This species was found to have superior oxidizing properties towards alkanes when compared with the model complex $Fe^{IV}(O)(TPP^{\bullet+})$, and KIEs of about 3 support a rate-limiting C-H cleavage. To avoid uncertainties as a result of the possible oxidation of organic solvent by strongly oxidizing species, heterogeneous oxidation of CH_4 was performed starting with the $[(TPP)Fe^{III}(N)Fe^{IV}(TPP)]$ catalyst combined with silica and dried at 50 °C. The supported catalyst, *m*-CPBA and methane gas were added in an autoclave reactor heated to 60 °C. Methane was oxidized to HCOOH (formic acid) from GC and LC analyses. This report showed the enhancement of C-H bond oxidations induced by an N-bridging ligand on an iron-oxo complex.

Chloroperoxidase (CPO) and myeloperoxidase (MPO) are heme enzymes that catalyze the oxidation of Cl^- with H_2O_2, and are responsible for the biosynthesis of chlorinated compounds in microorganisms.[68,69] Studies have suggested that a cpd I intermediate oxidizes Cl^- to form a transient $Fe^{III}(OCl)$ species. Studies from the Fujii group have shown different ways of accessing $Fe^{III}(OCl)$ species from an $Fe^{III}(TPFP)$ complex (Scheme 13). Addition of Cl^- ions to a solution of $Fe^{IV}(O)(tpfp^{\bullet+})$ at −90 °C leads to reduction of the Fe complex, giving $Fe^{IV}(O)(tpfp)$. The Cl^- ion is proposed to be oxidized to chlorine radical ($Cl\bullet$).[70] A study from Fujii[58] showed that the redox couple for $Fe^{IV}(O)(tpfp)(ClO_4^-)^{+/0}$ is 1.39 V vs SCE in dichloromethane at −60 °C. This finding indicates that the iron-oxo porphyrin complex should be capable of oxidizing chloride ion (1.11 V vs SCE in H_2O).[71] Single turn-over chlorination reactions with organic substrates led to modest yields of chlorinated products. In an alternative route, protonation of $Fe^{IV}(O)(TPFP^{\bullet+})$ with TFA results in the tautomerization of this complex to $Fe^{III}(L')(TPFP^{++})$ (L' = anion other than Cl^-), and further addition of Cl^- ions lead to conversion to $Fe^{III}(L')(Cl)(TPFP\text{-}Cl)$, a *meso*-chloro-isoporphyrin.[72] This complex can chlorinate electron-rich benzene and alkene derivatives catalytically through an electrophilic aromatic substitution (for benzene) or

electrophilic addition mechanism (for alkenes). An $Fe^{III}(OCl)$ species was independently formed by addition of 4 equiv of OCl^- to $Fe^{III}(OH)(TPFP)$ in 1:1 CH_2Cl_2-CH_3CN at −60°C.[73] Based on spectroscopic data, the species was characterized as $Fe^{III}(OCl)_2(TPFP)^-$, which eventually decomposed to $Fe^{IV}(O)(TPFP)$ (Scheme 13). Imidazole derivatives of this complex were also synthesized. The O-atom transfer and chlorination reactivity of the $Fe^{III}(OCl)$ complexes were tested with thioanisole, cyclohexene and 1,3,5-trimethoxybenzene substrates. The imidazole derivatives were found to have attenuated reactivity compared to the bis-hypochlorite analog. These biomimetic studies find their importance in comparison with CPO/MPO heme enzymes, where $Fe^{III}(OCl)$ species are indicated, but spectroscopic evidence for such species is scarce.

The last step in perchlorate (ClO_4^-) degradation by microbes is the decomposition of chlorite (ClO_2^-) to dioxygen (O_2) and chloride (Cl^-) mediated by the heme enzyme chlorite dismutase. From stopped-flow and EPR experiments, the mechanism was proposed to go through a cpd I intermediate.[74,75] This process was mimicked outside of a protein with water-soluble porphyrins, where chlorite is decomposed to chloride and chlorate in a 1:2 stoichiometry (Scheme 14).[76,77] Based on experimental observations and kinetic studies, two competing cycles were proposed. The first $Fe^{IV}(O)P^{\bullet+}/Fe^{III}$ cycle produces Cl^- and O_2, as in the heme enzyme. However, the $Fe^{IV}(O)P^{\bullet+}$ can also comproportionate with Fe^{III} to form $Fe^{IV}(O)P$. The second competing cycle involves an O-atom transfer from $Fe^{IV}(O)P$ to ClO_2^- to form Fe^{II} (P) and ClO_3^-.

Aromatic hydroxylation is another reaction studied extensively with iron porphyrin models. Its mechanism differs from alkane hydroxylation in that small KIEs and 1,2-hydride shifts (NIH shift) are observed, precluding the usual oxygen rebound mechanism proposed for alkane hydroxylations. Mechanistic information on aromatic hydroxylation of a series of *para*-substituted benzene derivatives with $Fe^{IV}(O)(TPFPP^{\bullet+})$ was obtained by the groups of Jang and Nam.[78] A large negative Hammett slope (ρ) of −8.0 and a KIE value of ~0.8 were observed, consistent with the formation of a cationic σ adduct upon addition of an electrophilic iron-oxo species. Fujii and coworkers studied the ability of a series of $Fe^{IV}(O)(porphyrin^{\bullet+})$ with electron-withdrawing porphyrins to hydroxylate aromatic substrates (benzene, anisole, naphthalene), and were able to show the involvement of an electron transfer process in these reactions.[79] Plots of (RT/F) $\ln(k_2)$ vs $\Delta E_{1/2}$ (where k_2 is the second-order rate constant of aromatic hydroxylation and $E_{1/2}$ is the redox potential for the cpd I/II couple) were constructed, and revealed slopes that are in between 0.5 and 1.0, indicating that the electron transfer process is coupled to the subsequent O–C bond formation (instead of proton transfer, which is not found to be in the rate-limiting step). Direct electron transfer between the substrate and $Fe^{IV}(O)(porphyrin^{\bullet+})$ can be ruled out because the reaction is highly endergonic ($\Delta G_{ET} >> 0$). However, this uphill electron transfer step is followed by a downhill O-C bond formation, making the over-all process thermodynamically favorable. The proposed mechanism (Scheme 15) brings together and reasonably explains the previously observed results.

N-oxygenation and N-dealkylation reactions are some of the many oxidations performed by compound I. The mechanism for N-dealkylation is proposed to go through either an H-atom transfer mechanism or a rate-limiting electron transfer step coupled with a proton transfer

step (Scheme 16). DFT calculations showed that both N-oxygenation and N-dealkylation proceed from the low spin state of compound I, and the computed KIEs for the rate-determining HAT step fits well with experimental data.[80]

Aside from exogenous substrates, the high-valent iron porphyrin complex is also capable of performing heme degradation reactions as observed in the enzyme heme oxygenase. One of the proposed reaction pathways for the first step of this reaction is the formation of a transient cpd-I ($Fe^{IV}(O)(porphyrin^{\bullet+})$), through the heterolytic cleavage of an $Fe^{III}(OOH)$(porphyrin) species. Karlin and co-workers have described a heme oxygenase model system in which an iron(III) tetraarylporphyrin complex is selectively oxidized to the final verdoheme-like product using a sacrificial oxidant, cerium(IV) ammonium nitrate (CAN), in the presence of water (Scheme 17).[81] A combination of UV-vis, EPR, and ESI-MS observations provided evidence for the formation of 1) an isoporphyrin complex resulting from the attack of water/hydroxide on a cpd-I analog, 2) a porphyrin degradation product resembling benzoyl biliverdin, and 3) a verdoheme-like product as well as a benzoyl fragment. From ^{18}O labeling experiments, water was shown to be the O-atom source in the final oxidized products. In addition, the intermediacy of a cpd-II-like complex ($Fe^{IV}(O)$(porphyrin)) was ruled out, as no further oxidation with this complex was detected, while direct observation of the conversion of cpd-I (generated at −80 °C) to the isoporphyrin complex was observed.

Iron(IV)-oxo porphyrins, one-electron reduced analogs of iron(IV)-oxo porphyrin π-radical cation complexes, were first synthesized in 1980 by Balch and La Mar by the addition of nitrogen bases (*N*-methylimidazole, pyridine, piperidine) to Fe^{III} peroxo-bridged porphyrins at −80 °C (Scheme 18).[82,83] The $Fe^{IV}(O)$ complex is EPR silent and shows paramagnetic proton resonances, while its magnetic susceptibility and UV-visible absorption spectrum resembled that of compound II horseradish peroxidase.

Other than homolytic cleavage of the O-O bond of Fe^{III} peroxo-bridged porphyrins, iron(IV)-oxo porphyrins can be prepared from the starting Fe^{III} porphyrin by a) chemical oxidation with mCPBA or PhIO under certain conditions, b) electrochemical oxidation and c) addition of hydroperoxides (see ref. [38] and related references therein). Iron(IV)-oxo porphyrins were initially considered as poor oxidants.[83] However, it has been shown that iron(IV)-oxo porphyrins react with substituted styrenes to give epoxide, although with poor selectivity towards cis vs trans epoxide formation.[84] Nam and coworkers reported the reactivity of $Fe^{IV}(O)$(porphyrin) complexes with benzylic C-H substrates and NADH analogues to give the corresponding oxidized products (Scheme 19).[42] A linear correlation is observed between the rate constant log k_2' and the C-H substrate BDEs, in addition to large KIEs of up to 21 for DHA and xanthene, providing evidence for an H-atom abstraction mechanism. Among the three porphyrins tested, there is a modest increase in HAT and hydride transfer reaction rates with the more electron-deficient porphyrins.

A DFT study on the comparative reactivity of $Fe^{IV}(O)(porphyrin^{\bullet+})$ and $Fe^{IV}(O)$(porphyrin) with 10-methyl-9,10-dihydroacridine show that $Fe^{IV}(O)(porphyrin^{\bullet+})$ reacts with a much lower barrier.[85] The main difference, however, is that $Fe^{IV}(O)$(porphyrin) reacts via hydrogen atom transfer, while $Fe^{IV}(O)(porphyrin^{\bullet+})$ reacts via hydride transfer. This

difference in mechanism was rationalized to be a result of differences in electron abstraction abilities of these two oxidants.

The ability to selectively produce cpd 0, I, and II with Fe^{III}(TMP) under different conditions was exploited by van Eldik and coworkers to compare directly their reactivity towards O-atom transfer, H-atom transfer, and hydride transfer reactions at low temperatures.[86] As expected, the $Fe^{IV}(O)(TMP^{\bullet+})$ (cpd I) complex turned out to be the most reactive species. Interestingly, for hydride transfer reactions, the reactivity order was found to be cpd II > cpd 0 > cpd I. In the initial electron-transfer step, Cpd II is reduced to an iron (III)–oxo species, which would be the most basic intermediate and would therefore promote the subsequent proton abstraction step. A similar study from the same group on the comparison of reactivity of $Fe^{IV}(O)(TMP^{\bullet+})$(2-MeIm) and Fe^{IV}(O)(TMP)(2-MeIm) also confirmed the high reactivity of the cpd I analog towards epoxidation, H-atom abstraction, and heteroatom oxidation.[87] Compound I and II mimics were also stabilized in aqueous solution using the water soluble porphyrin Fe^{III}(TMPS), and their formation was found to be pH-dependent.[88] Combined temperature and pressure measurements have shown that, for selected substrates, oxidation with the Cpd II mimic is an enthalpy-controlled process whereas it is entropy-controlled for Cpd I.

Iron(IV)-oxo porphyrins were also shown to carry out oxidative N-dealkylation of *N,N*-dialkylanilines via a rate-limiting electron transfer coupled with proton transfer (ET-PT.[89] The large negative slopes obtained from the plots of log k_{obs} vs Hammett parameter σ (ρ = −3.3) and $E°_{ox}$ of para-substituted N,N-dimethylanilines (slope = −5.0) suggest a rate-limiting electron transfer. In addition, the use of several mechanistic probes and a modest inter- and intramolecular KIE of 2.8 and 4.2 all pointed to an ET-PT mechanism. An Fe^{IV}(O) porphyrin complexed with a per-o-methylated ß-cyclodextrin dimer was found to oxidize $ROCH_3$ to $ROCH_2OH$, which further decomposes to ROH and HCHO, and the corresponding Fe^{II}(porphyrin) complex (Scheme 20).[90] An initial H-atom abstraction followed by an oxygen rebound mechanism similar to compound I has been proposed for this system. Work from the same group showed that an Fe^{IV}(O) porphyrin complexed to a per-o-methylated ß-cyclodextrin dimer was capable of a direct oxygen transfer reaction to the sulfide bond found intramolecularly on the linker.[91]

As shown previously, there have been several instances of iron(IV)-oxo porphyrin complexes acting as competent oxidants for various substrates. A DFT electronic structure analysis of alkane hydroxylation with Fe^{IV}(O)(porph) and its hydrosulfide-ligated analog was performed, with methane as a model substrate for alkanes. DFT calculations on the ground triplet and excited quintet spin state surfaces revealed that H-atom abstraction is the rate-determining step, and a two-state reactivity (TSR) mechanism is plausible for C-H activation with Fe^{IV}(O)(porph), but not for the $[Fe^{IV}(O)(porph)(SH)]^-$ analog, where C-H activation can only occur on the triplet surface.[92]

It was shown by pH-jump stopped-flow UV-vis spectroscopy that iron(IV)-oxo porphyrins can be protonated twice to form the iron(III)-aquo porphyrin$^{\bullet+}$ valence tautomer (Scheme 21).[93] The two-proton pK_a values of sulfonated, water-soluble Fe^{IV}(O) porphyrins were identified and it was found that the most basic Fe^{IV}(O) complex had the largest C-H bond

cleavage rates. For $Fe^{IV}(O)(TMPS^{\bullet+})$, a KIE of 1.80 was observed with xanthene-d_2, and a solvent KIE of 1.65 was seen with D_2O, giving a combined substrate-solvent isotope effect of 2.2. A mechanism which involves both the substrate proton and the solvent proton was proposed which accounts for all of the observed data (Scheme 21).

2.1.2 Iron-Oxo Corroles and Corrolazines—The ring contracted porphyrinoid compounds corroles and corrolazines are designed to stabilize high-valent transition metals. Although a number of high-valent complexes have been prepared with these porphyrinoid ligands, the iron-oxo corroles and corrolazines are rare and less studied than the iron-oxo porphyrins.[94] The synthesis of well-characterized, high-valent, mononuclear iron-oxo corroles is challenging in part because of the propensity of iron corroles to form μ-oxo dimers upon oxidation of Fe(III) corrole.[95-97] In addition, the inherent non-innocence in iron(IV) corroles obscures their electronic structure assignment, with both Fe^{IV}(corrole) (S = 1) and $Fe^{III}(corrole^{\bullet+})$ (S = 1) states as limiting possibilities.[98,99]

The use of laser flash photolysis (LFP) – induced ligand cleavage of $Mn^{IV}(OX)$ (X = ClO_2, NO_2) corroles to generate $Mn^{V}(O)$ corroles was extended by Newcomb and Zhang to the analogous $Fe^{IV}(OX)$ (X = ClO_2, NO_2 or Fe^{IV}) corroles[100-102] to generate a proposed $Fe^{V}(O)$ corrole (Scheme 22). This species was formulated as $Fe^{V}(O)$, as opposed to $Fe^{IV}(O)(corrole^{\bullet+})$, because of its increased reactivity compared to the analogous $Fe^{IV}(O)(porphyrin^{\bullet+})$. However, the inability to characterize this highly reactive complex by methods other than UV-vis spectroscopy has precluded definitive oxidation state assignment. The proposed species shows an intense Soret band that decays after 20 ms at 22 °C, which is similarly observed from the reaction of Fe^{III} corrole with excess mCPBA, and displays high oxidative reactivity towards alkenes (cyclohexene, cyclooctene). A KIE of 3.6 for the oxidation reaction of ethylbenzene was also observed, suggesting that C-H bond cleavage is the rate-determining step.

The isoelectronic $Fe^{IV}(O)(corrole^{\bullet+})$ has been proposed to be energetically accessible based on calculations,[103] which also found the $Fe^{V}(O)$(corrole) complex to be equienergetic. Neither of these species have been experimentally observed. However, more recent DFT calculations from Valentine, Nam, and de Visser[104] find that the $Fe^{IV}(O)(corrole^{\bullet+})$ valence tautomer is lower in energy than the $Fe^{V}(O)$(corrole). The H-atom abstraction reactivity of this complex towards a broad range of C-H bond substrates was explored by DFT calculations, and it was shown to react via a single, dominant low spin surface. These results are in stark contrast with the $Fe^{IV}(O)(porphyrin^{\bullet+})$ analog, which is computationally predicted to react via a two-state reactivity surface.

Iron(IV)-oxo corroles, which are compound II analogs, are proposed as an intermediate in the catalytic decomposition of peroxynitrite ($ONOO^-$) with water-soluble sulfonated Fe^{III} corroles.[105] An Fe^{III}(corrole)-mediated O-O bond cleavage of peroxynitrite forms nitrogen dioxide (N_2O) and a hydroxo or oxo-iron(IV) corrole, which was found to decay via multiple pathways of similar rates of about 10^6 M^{-1} s^{-1} (Scheme 23). However, this highly reactive species has only been observed with stopped-flow UV-vis measurements. Fe^{III} corroles are also shown to catalyze the oxidation of hydrocarbons with t-butylhydroperoxide,[106] and xanthene-modified and hangman Fe^{IV}(Cl) corroles are shown to

catalyze the disproportionation of hydrogen peroxide via the catalase reaction.[107,108] In both cases, the formation of an $Fe^{IV}(O)$ corrole intermediate is invoked, but no direct evidence was provided.

In 2009, Goldberg and coworkers reported the synthesis and the first direct spectroscopic observation of a compound I analog in a corrole-like scaffold, an $Fe^{IV}(O)(TBP_8Cz^{\bullet+})$ (TBP_8Cz = octakis(tert-butylphenyl)corrolazine) complex.[109] The Fe^{III} precursor complex was synthesized by reaction of metal-free corrolazine with $Fe(acac)_3$ in refluxing pyridine,[110,111] to give $Fe^{III}(TBP_8Cz)$. Addition of an O-atom transfer reagent (mCPBA, PFIB, or PhIO) to the Fe^{III} precursor complex in 1:1 CH_2Cl_2/CH_3OH at −78 °C resulted in the formation of Fe^{IV} $(O)(TBP_8Cz^{\bullet+})$ (Scheme 24). The $Fe^{IV}(O)(TBP_8Cz^{\bullet+})$ complex (Figure 2) has been invoked as the key oxidizing species in the catalytic oxidation of olefinic and benzylic C-H substrates with PFIB as oxidant and $Fe^{III}(TBP_8Cz)$ as catalyst.[109]

EPR[110] and X-ray absorption spectroscopy (XAS) measurements[112] of this iron-oxo corrolazine led to an assignment of an S = 1 Fe^{IV} metal center antiferromagnetically coupled to an S = ½ corrolazine π-radical cation, giving a total spin ground state of S = 1/2. Best fits to the EXAFS data showed a short Fe–O bond distance of 1.64 Å, in excellent agreement with the $Fe^{IV}(O)$ assignment. The $Fe^{IV}(O)(TBP_8Cz^{\bullet+})$ complex is stable at −78 °C for hours, but reverts to $Fe^{III}(TBP_8Cz)$ at room temperature. This iron-oxo corrolazine complex is capable of O-atom transfer, H-atom abstraction, and electron transfer (Scheme 1).

Addition of PPh_3 to this complex at −78 °C converts the species back to the starting Fe^{III} complex. The ability of $Fe^{IV}(O)(TBP_8Cz^{\bullet+})$ to cleave activated C-H bonds was studied.[112] A KIE of 5.7 was obtained for xanthene, and a linear correlation between the rate constants (log *k*) and BDE(C-H) of the C-H substrates show that these reactions occur via a rate-determining H-atom transfer. However, the putative $Fe^{IV}(OH)$ intermediate was not observed. A temperature dependence on the product distribution was observed for the reaction between $Fe^{IV}(O)(TBP_8Cz^{\bullet+})$ and xanthene, where the oxygen-rebound product (xanthydrol) is favored at lower temperatures (−25 °C) over the radical dimerization (9,9'bixanthene) product. Thus, lowering the reaction temperature increases the efficiency of oxygen rebound.

2.2. Manganese-Oxo Complexes

2.2.1 Manganese-Oxo Porphyrins—Iron-oxo intermediates are found in the catalytic cycles of heme enzymes, and Mn has been used as an analog of Fe in models of these systems in part due to the enhanced stability of Mn-oxo species over the corresponding Fe-oxo species. While Mn(porphyrins) have yet to be identified as natural cofactors in metalloenzymes, synthetic manganese porphyrins have been used as catalysts in the biomimetic oxidation of organic substrates. These reactions usually proceed through a high-valent metal-oxo intermediate in mechanisms similar to those proposed for heme enzymes. Manganese-oxo porphyrins have been identified in the Mn^{IV}-oxo and Mn^{V}-oxo states. An early example of a well-characterized manganese(IV)-oxo porphyrin complex was reported in 1995, in which the $Mn^{IV}(O)$ complex was synthesized from oxidation of the Mn(III)porphyrin with potassium peroxycarbonate, and structurally characterized by XAS.[113] Typically, $Mn^{IV}(O)$ porphyrin species are less reactive than their $Mn^{V}(O)$ counterparts.[31]

Spectroscopic characterization of a $Mn^{V}(O)$ porphyrin species remained elusive until relatively recently.[114,115] The complex ($Mn^{V}(O)$(TMPyP) (TMPyP = *meso*-tetrakis(4-methylpyridinium)porphyrinato^{2-})) was generated in aqueous solution at 25 °C and characterized by UV-vis and ^{1}H NMR spectroscopy. High-valent Mn-oxo porphyrins, including the previous example, have been reviewed in The Porphyrin Handbook (2000-2003)[18,31] and Chemical Reviews[116,117] and won't be reiterated here.

In 2002, Nam and coworkers presented UV-vis and EPR evidence for the formation of a $Mn^{V}(O)$ porphyrin complex from the reaction of Mn^{III}(por) and H_2O_2 in aqueous solution (Scheme 26).[118] The reaction between $Mn^{III}(TF_4TMAP)$ (TF_4TMAP = *meso*-tetrakis(2,3,5,6-tetrafluoro-*N,N,N*-trimethyl-4-aniliniumyl)porphyrinato^{2-}) and H_2O_2 was highly pH dependent, with O–O bond homolysis proposed to occur at low pH to generate an $Mn^{IV}(O)(TF_4TMAP)$ and O–O bond heterolysis proposed at high pH to generate an $Mn^{V}(O)(TF_4TMAP)$. These two high-valent species could be differentiated by their UV-vis and NMR spectra. When alkyl or acyl hydroperoxide was used as oxidant, the electron-donating or -withdrawing properties of the oxidant controlled the mechanism of O–O cleavage, with the former cleaving homolytically to generate the $Mn^{IV}(O)$ species and the latter cleaving heterolytically to give the $Mn^{V}(O)$ species. The high-valent Mn-oxo species also had differing reactivity. The $Mn^{V}(O)(TF_4TMAP)$ was a very efficient epoxidizing agent, whereas the lower-valent $Mn^{IV}(O)(TF_4TMAP)$ was unable to oxidize alkenes. This result was consistent with earlier findings that a $Mn^{IV}(O)$(TM-2-PyP) (TM-2-PyP = *meso*-tetrakis(*N*-methyl-2-pyridyl)porphyrinato^{2-}) complex was unable to oxidize olefins.[115] Electrochemical evidence for $Mn^{V}(O)(TF_4TMAP)$ generated from H_2O_2 and Mn^{III} has been obtained.[119]

A dimanganese complex of a dimeric tetraaryl porphyrin was reported by Naruta and coworkers to generate a dinuclear $Mn^{V}(O)$ complex (Scheme 27).[120] When two equivalents of mCPBA were added to the Mn^{III}_2 porphyrin dimer [Mn_2(DTMP)(OH)] (TMP = *meso*-(tetramesityl) porphyrinato^{2-}) in CH_2Cl_2/CH_3CN (1:1 v/v), a new species assigned as an $(Mn^{V}(O))_2$ species was generated. This new species was stable in the presence of excess tetrabutylammonium hydroxide; however, when excess triflic acid was added to the complex in the presence of 10% water, fast reduction to a dinuclear manganese(III) species occurred with simultaneous evolution of O_2. A 92% yield of O_2 relative to the starting dimeric complex was obtained by mass spectrometry and when 18-O labeled water/hydroxide was used, $^{18}O_2$ was observed. Based on the available data, the authors proposed that the $(Mn^{V}(O))_2$ species underwent O–O bond formation to evolve dioxygen, either by nucleophilic attack of solvent water on an $Mn^{V}(O)(H_2O)$ species or by coupling the two $Mn^{V}(O)$ units.

Evidence for the formation of a $Mn^{V}(O)$ porphyrin species has come from laser flash photolysis (LFP) studies.[121] It is important to note that in the following photochemical studies, the high-valent Mn-oxo species were characterized mainly by transient UV-vis spectroscopy, and further characterization (e.g. Raman, XAS) is needed to confirm their identity. Irradiation of a Mn^{III}(TPFPP) (TPFPP = *meso*-tetrakis(pentafluorophenyl)porphyrinato^{2-}) in acetonitrile in the presence of the perchlorate anion resulted in the formation of a transient UV-vis spectrum for a new species assigned as

Mn^{V}(O)(TPFPP) based on its reactivity. In the presence of alkene substrates, this species decayed back to Mn^{III}(TPFPP) at a rate faster than the self-decay process. The new species was able to oxidize stilbene to stilbene oxide with high stereoselectivity in a >95:5, cis:trans ratio. Furthermore, when ethylbenzene and ethylbenzene-d_{10} were used as substrates, a kinetic isotope effect of 2.3 was obtained, implicating C–H cleavage in the rate determining step. The LFP generation method was subsequently applied to a wider series of manganese porphyrin complexes (Mn^{III}(TPFPP), Mn^{III}(TPP), and Mn^{III}(TMPyP)) in which the electron-donating properties were varied (Scheme 28).[122] When LFP was initiated in the presence of NO_3^- or ClO_3^-, a species assigned as an Mn^{IV}(O)(por) complex was obtained, which results from the homolytic cleavage of the N–O or Cl–O bonds. LFP in the presence of ClO_4^- resulted in the formation of a species assigned as an Mn^{V}(O)(por) complex, which results from heterolytic Cl–O cleavage. The presence of water further stabilized the higher-valent species. The reactivity of the postulated Mn^{V}(O)(por) species were studied with various substrates. Smooth two-electron chemistry was observed, with no intermediacy of an Mn^{IV}(O)(por) species. The reaction rates with a given substrate depended on the electronics of the porphyrin ligand. The most electron-withdrawing porphyrin was TPFPP, and the Mn^{V}(O)(TPFPP) species was the most reactive, followed by the Mn^{V}(O)(TMPyP) and Mn^{V}(O)(TPP) species. The Mn^{IV}(O)(por) species were found to be less reactive than the Mn^{V}(O)(por) species. Furthermore, the effect of the electronics of the ligand in reactions with substrates was found to be reversed relative to the Mn^{V}(O)(por). Thus, the rates of reaction were found to be as follows: Mn^{IV}(O)(TPP) > Mn^{IV}(O)(TMPyP) > Mn^{IV}(O)(TPFPP). This surprising trend was rationalized by the rapid disproportionation equilibrium of Mn^{IV}(O)(por) to form Mn^{V}(O)(por) and Mn^{III}(por)(X), with the Mn^{V}(O)(por) performing the actual oxidation of the substrate. The disproportionation equilibrium controls the amount of Mn^{V}(O)(por) in solution and therefore the “apparent” rate of the reaction. A related photochemical method of generating high-valent Mn-oxo porphyrins was reported for a dinuclear Mn^{III} complex. Upon visible light irradiation, bis-porphyrin dimanganese(III)-μ-oxo complexes could be photo-disproportionated to Mn^{IV}(O) porphyrin and Mn^{II} porphyrin.[123]

The effects of oxo-hydroxo tautomerism (Scheme 29) on the reactivity of Mn^{V}(O) porphyrins were studied in two isomeric porphyrin complexes.[124] It was found that Mn^{V}(O)(X)(4-TMPyP) was more reactive with Br^- ions to form hypobromite (BrO^-) than the less electron-rich Mn^{V}(O)(X)(2-TMPyP). This result is due to the higher basicity of the Mn^{V}(O)(4-TMPyP) complex, resulting in the presence of more Mn^{V}(O)(H_2O) (which is the active oxidizing species) rather than Mn^{V}(O)(OH) in this complex. This finding is consistent with the idea that an anionic axial donor would make the Mn^{V}(O) less electrophilic. Density functional theory (DFT) calculations of the possible spin states (singlet, triplet, and quintet) of the three possible Mn^{V}-oxo isomers (dioxo, oxo-hydroxo, and oxo-aquo complexes) reveal a singlet ground state for all three complexes. However, for the oxo-hydroxo and oxo-aquo complexes, the triplet and quintet states are relatively close in energy to the singlet ground state. This small energy difference could allow for a possible spin-crossing event during oxygen transfer, leading to enhanced rates of reaction with substrates.

The importance of spin states on Mn-oxo reactivity has been studied extensively by DFT. A DFT study on C–H hydroxylation by Mn^{V}(O)(X)(TPP) (X = O^{2-}, OH^-, and H_2O) suggested

that a rebound mechanism is possible in the triplet and quintet states, but not along the singlet pathway.[125] The higher selectivity for the rebound mechanism in the triplet and quintet states was attributed to an increased oxyl radical character found in these higher spin-states, which caused the reaction to occur in two distinct one-electron steps, with a spin cross-over from singlet to triplet in the initial step.[126] The extent of oxyl radical character influenced the bond order of the Mn–O interaction. The bond order was found to increase with protonation of the axial ligand X (X = O^{2-}, OH^-, and H_2O) according to the following series $Mn^V(O)_2$<$Mn^V(O)(OH)$<$Mn^V(O)(H_2O)$.[127] However, the multiplicity of the ground states and the extent of oxyl character were highly dependent on the functional used.[126] Furthermore, the effect of the axial ligand in the calculations was found to decrease the singlet-triplet and singlet-quintet gaps along this series, and this gap is the dominant factor in controlling the calculated reactivity, with the $Mn^V(O)(H_2O)$ species as the most reactive, as found experimentally.[124,128] The protonated bis-hydroxy complex $Mn^V(OH)(OH)$(por) was also found to be a viable, potent C–H hydroxylation oxidant by DFT.[129,130] Recently, an ab initio benchmarking study on the spin-state energetics and oxyl character of Mn-oxo porphyrins was reported, in which the authors suggest that the best electronic description of these species can be achieved with pure functionals.[131]

N-donor axial ligands are common additives to C–H bond activation reactions catalyzed by Mn-porphyrins, for which $Mn^V(O)$-porphyrin intermediates are often proposed. Addition of axial N-donors is in part motivated by the prominent role played by the axial ligands (e.g. histidine, tyrosine, cysteine) in heme enzymes. A DFT study on the effect of Mn–O bond length versus axial N–donor strength found that the Mn–O bond lengthens with decreasing $Mn–N_{axial}$ bond distance, indicating that the stronger the axial ligand, the weaker the Mn–O bond, which in turn leads to predicted enhanced reactivity.[132] Furthermore, the ability of the axial N-donor to interact with the *meso*-phenyl rings of an Mn(O)(por) through non-covalent interactions, such as hydrogen-bonding, was also an indicator of reactivity.[133] DFT calculations showed that the ortho-C–F bonds in the phenyl rings of $Mn^V(O)$(TPFPP) were able to hydrogen-bond with the C–H groups of axially ligated pyridine derivatives, providing a stronger $Mn–N_{axial}$ interaction, and a lower barrier for C–H activation.

An unusual substrate for $Mn^V(O)$ porphyrin is the Br^- anion. It was shown that $Mn^V(O)$(TDMImP) (TDMImP = *meso*-tetrakis(dimethylimidazolium)porphyrinato^{2-}) was capable of oxidizing the bromide ion to form hypobromite (OBr^-), and this reaction was reversible.[134] The equilibrium for the reaction $Mn^V(O)$(TDMImP) + $Br^- \rightleftharpoons Mn^{III}$(TDMImP) + OBr^- could be controlled by changing the pH. The formation of the $Mn^V(O)$(TDMImP) and Br^- was favored under basic conditions, whereas the formation of Mn^{III}(TDMImP) and the O–Br bond was favored under acidic conditions.

Nam, Solomon, and coworkers synthesized a high-valent Mn porphyrin complex by reaction of Mn(III) porphyrins with one of various oxidants including mCPBA, iodosylarenes, and hydrogen peroxide. This product was formulated as an $Mn^V(O)$ complex based on UV-vis, EPR, ^1H and ^{19}F NMR, resonance Raman, and XAS.[135] The XAS data led to identification of an Mn–O distance of 1.68 Å for the proposed $Mn^V(O)$(TDCPP) (TDCPP = *meso*-tetrakis(2,6-dichlorophenyl)porphyrinato^{2-}) and indicated that the central Mn was likely 6-coordinate with an axial ^-OH ligand. However, the Mn–O distance of 1.68 Å was

significantly longer than other Mn^{V}–O distances, including that reported for a related Mn^{V}(O) corrolazine.[136] Reactions of the high-valent Mn complex with various substrates were analyzed kinetically. A linear Hammett plot was obtained for reactions with *para*-substituted thioanisoles of varying electron-donating or electron-withdrawing substituents. The negative slope for this plot indicated that the Mn complex was electrophilic in nature. When the reaction with cyclooctene and cyclooctane was examined, no oxidized organic products were observed. The authors postulated that, in light of the EXAFS results showing that an axial ligand was present, an anionic $^{-}$OH ligand could decrease the electrophilicity of the proposed Mn^{V}(O)(TDCPP) complex and stabilize it. However, the structure of this complex was not assigned correctly and it was subsequently reformulated as a trans-dioxo Mn^{V} porphyrin complex, based on reinterpretation of the spectroscopic data and independent generation of another example of a trans-dioxo Mn^{V} porphyrin complex.[137]

The formal bonding picture of Mn^{V}(O) porphyrins, known since the 1960s, predicted that mono-oxo complexes should be stable species, but trans-dioxo Mn^{V} complexes would be inaccessible. However, an example of a trans-dioxo Mn^{V} was reported by Groves and Spiro in 2007. Trans-dioxo Mn^{V}-oxo porphyrins were generated by exploiting pH-dependent oxo-hydroxo tautomerism.[138] Under highly basic conditions, a series of trans-dioxo Mn^{V}(O) porphyrin complexes were generated in organic solvent. These species were half- or fully-labelled isotopically by using ^{18}O-sources, allowing for the key identification of the symmetric and asymmetric Mn–O stretches by resonance Raman and IR spectroscopy. A correlation could be obtained between the force constant for Mn–O stretches and Mn–O bond lengths for a series of comparable manganese-oxo complexes. This correlation, known as Badger's rule, allowed for a bond length prediction of ~1.7 Å for the Mn=O double bonds.

The isolated trans-dioxo complexes were unreactive towards olefins, but addition of one equivalent of trifluoroacetic acid caused instantaneous reaction with cyclooctene at −70 °C. The authors suggested that the acid protonated one of the oxo ligands and lowered the net negative charge on the $[Mn^{V}(O)_2]^{-}$ complex, thereby enhancing its electrophilicity. While unreactive with olefins, trans-dioxo Mn^{V}-oxo porphyrins were found to perform hydride abstraction from dihydronicotinamide adenine dinucleotide (NADH) analogues, such as 10-methyl-9,10-dihydroacridine ($AcrH_2$).[139] The hydride abstraction rates were sensitive to the electron-donating properties of the $AcrH_2$ derivative, as well as the electronics of the porphyrin ligand, with the most electron-deficient porphyrin having the fastest hydride transfer rates. Large deuterium kinetic isotope effects were also observed for the $AcrH_2$ substrates. The kinetic data indicated that the hydride transfer reaction was occurring through a mechanism involving initial rate-determining proton-coupled electron transfer followed by fast electron transfer.

Manganese-porphyrins were found to photocatalytically oxygenate $AcrH_2$, exploiting the facile reaction between Mn^{V}(O)(por) and this hydride donor.[140] A mechanism was invoked in which the resting state of the catalyst, the Mn^{III}(por), is irradiated and generates a photoexcited $[Mn^{III}]$* which reacts with O_2 to generate a Mn^{IV}-superoxo species (Scheme 30). The superoxo species cleaves the C–H bond of the $AcrH_2$ to generate a Mn^{IV}-hydroperoxo species and the acridinyl radical AcrH•. The O–O bond of the Mn^{IV}-OOH

species goes through oxygen rebound homolysis to generate the $Mn^{V}(O)$ species and a hydroxylated AcrH–OH molecule. The Mn^{III}(por) catalyst is regenerated by the further oxidation of the AcrH–OH molecule to the ketone, acridone, or by the oxidation of another $AcrH_2$ molecule.

Early work on high-valent Mn–oxo porphyrins showed that $Mn^{V}(O)$ and $Mn^{IV}(O)$ porphyrins had distinct reactivity, with the lower valent $Mn^{IV}(O)$ complexes being less reactive in oxidations such as epoxidation of alkenes.[31] A comparison of the differing reactivity in OAT and HAT reactions for trans-dioxo Mn^{V} and $Mn^{IV}(O)$ generated in aqueous solutions was described by Fukuzumi and Nam. The trans-dioxo complex $Mn^{V}(O)_2(tf_4tmap)$ (tf_4map = *meso*-tetrakis(2,3,5,6-tetrafluoro-*N*,*N*,*N*-trimethyl-4-aniliniumyl)porphyrinato^{2-}), and the oxo-hydroxo complex, $Mn^{IV}(O)(OH)(tf_4tmap)$, were generated in H_2O by oxidation with H_2O_2 and *tert*-butyl hydroperoxide, respectively, and characterized by UV-vis and EPR spectroscopies. The two high-valent Mn(O) complexes were reacted with various C–H substrates and O-atom acceptor reagents and the kinetics of these reactions were analyzed (Scheme 31).[141] It was found that only the $Mn^{V}(O)_2$ complex was capable of OAT to thioanisole substrates, and this reaction gave a Mn^{III} product and the corresponding methyl phenyl sulfoxide. A linear Hammett plot for *para*-substituted thioanisole derivatives showed a negative slope which indicated a mechanism where the nucleophilic sulfide substrate attacks the electrophilic $Mn^{V}(O)_2$. The $Mn^{IV}(O)(OH)$ species was able to perform OAT to triarylphosphines, a highly nucleophilic substrate, to give a Mn^{II} product and triphenylphosphine oxide. When C–H substrates were added to $Mn^{V}(O)_2(tf_4map)$, the product of the H-atom abstraction reaction was $Mn^{IV}(O)(OH)(tf_4tmap)$. When C–H substrates were added to the independently generated $Mn^{IV}(O)(OH)(tf_4tmap)$, slow formation of $Mn^{III}(tf_4tmap)$ was observed. No substrate hydroxylation was observed for either Mn-oxo species. A mechanism was suggested from DFT calculations by showing that the energy barrier for the oxygen rebound step is higher than that for the escape of the carbon radical from the cage. These DFT calculations along the reaction coordinate showed that oxygen rebound was disfavored, especially for a dioxo-manganese complex $Mn^{V}(O)_2$ relative to the oxo-hydroxo complex $Mn^{V}(O)(OH)$, which suggests that the strongly bound oxo (O^{2-}) ligand may play a role in controlling the reaction barrier associated with oxygen rebound.[142] The H-atom abstraction rate constants for both $Mn^{V}(O)_2$ and $Mn^{IV}(O)(OH)$ complexes were found to be linearly dependent on the strength of the C–H bond, with the stronger C–H bonds giving slower reaction rates, and large kinetic isotope effects (k_H/k_D = 8-24) for the deuterated substrates were also observed. These data support C–H cleavage as the rate-determining step and implicate a hydrogen atom transfer mechanism for both high-valent Mn-oxo species. The authors conclude that the reaction between H-atom donor and $Mn^{IV}(O)(OH)(tf_4tmap)$ was direct, and, under these conditions, does not proceed via a disproportionation pathway as proposed earlier by Newcomb.[122] In contrast, when the hydride donor $AcrH_2$ was added to a different $Mn^{IV}(O)$ complex, $Mn^{IV}(O)(TMP)$, a disproportionation mechanism was invoked in which the $Mn^{IV}(O)$ is in equilibrium with Mn^{III} and $Mn^{V}(O)$ (Scheme 32). The $Mn^{V}(O)$ species was proposed to be the active oxidant in the reaction.[143] The reaction of $Mn^{IV}(O)(TMP)$ with ferrocene derivatives, which are one-electron reductants, was proposed to go through a direct electron-transfer mechanism, and did not involve disproportionation. DFT calculations provided

some insight into the different reaction pathways observed for $Mn^{V}(O)$ vs. $Mn^{IV}(O)$ with $AcrH_2$.[144] In the case of $Mn^{IV}(O)$, an H-atom abstraction is more thermodynamically favored than overall hydride transfer, whereas with $Mn^{V}(O)$, hydride abstraction is more favored. The $Mn^{V}(O)$ was described as the more potent oxidant with that substrate. The different reaction pathways of these $Mn^{IV}(O)$ porphyrins were highly controlled by the nature of the substrate.

The reactivity of $Mn^{V}(O)$ porphyrins with substrates is complicated by the possible presence of axial ligands (H_2O, OH^-, or O^{2-}) that are present in buffered aqueous solution. A "naked" 5-coordinate $Mn^{V}(O)$(TPFPP) complex was generated from Mn^{III}(TPFPP) and iodosylbenzene in the gas phase in methanol by electrospray ionization and the reactivity was monitored by Fourier transform ion cyclotron resonance (FT-ICR) mass spectrometry.[145,146] The $Mn^{V}(O)$(TPFPP) was capable of OAT to olefins to give the reduced Mn^{III}(TPFPP) complex. The rate of OAT depended on the ionization energy of the olefin, with the fastest reactions occurring for olefins with lower ionization energies. Furthermore, selectivity of the gaseous $Mn^{V}(O)$(TPFPP) complex for Z isomers over E isomers of the alkene was also observed. In negative ion mode, the gas-phase trans-dioxo $Mn^{V}(O)_2$(TPFPP) complex could be generated, and was found to be completely unreactive towards olefins and sulfides, as found previously in aqueous solution.[138] The $Mn^{V}(O)$(TPFPP) complex was also found to oxidize *p*-substituted thioanisoles and perform N-dealkylation of *N,N*-dialkylamines.[147] The sulfoxidation reaction rates were found to depend on the electronics of the substrate. A negative linear correlation between the Hammett σ-constant of the *p*-substituted thioanisole and the log of the rate constants could be obtained. The reaction rates between $Mn^{V}(O)$(TPFPP) and *p*-substituted dimethylanilines were also linearly correlated with the Hammett σ^+-parameters of the substrates, and the slope of the line had a negative value. In the case of this substrate, an initial electron-transfer mechanism from the dimethylaniline substrate to the $Mn^{V}(O)$ species was proposed. The reaction rates slowed with increasing ionization energy of the dimethylaniline, providing further support for this mechanism.

High-valent Mn-oxo porphyrins are typically generated via O-atom transfer from an appropriate activated O-atom transfer reagent (*m*CPBA, PhIO) to the Mn^{III}(por). However, Fukuzumi and coworkers showed that water can be used as the O-atom source in the presence of a one-electron oxidant, $[Ru(by)_3]^{3+}$.[148] Oxidation of a series of Mn^{III}-porphyrins in acetonitrile with added water generated either $Mn^{IV}(O)$ or $Mn^{V}(O)$ porphyrins, depending on the axial ligands present in the starting Mn^{III}(por). If Cl^- was present, the $Mn^{IV}(O)$ species was formed, whereas if H_2O was the axial ligand, the $Mn^{V}(O)$ species was formed. The Mn^{III}-porphyrin/oxidant/water system could also serve as a catalyst for epoxidation and alkane hydroxylation reactions, in which the $Mn^{V}(O)$(por) species is implicated as the active oxidant (Scheme 33).

Another unique set of oxidants, the mild, single-oxygen atom donors tetra-*n*-butylammonium periodate (*n*-Bu_4NIO_4) and tetra-*n*-butylammonium hydrogen monosulfate (*n*-Bu_4NHSO_5), were found to generate high-valent Mn-oxo porphyrins.[149,150] The stability and formation of the high-valent Mn(O) species in CH_2Cl_2 were found to be highly dependent on the sterics and electronics of an added alcohol co-solvent (Scheme 34). It was

found that the rate of formation of $Mn^{V}(O)$ species was faster for small linear alcohols than for the larger ones. This observation indicated that the hydrogen bonding between the alcohols and the periodate ion coordinated to Mn facilitated the heterolytic cleavage of the I–O bond. Furthermore, the authors found that the stronger the acidity of the alcohol, the better the hydrogen-bonding interaction. The stability of the $Mn^{V}(O)$ species was enhanced generally by the presence of alcohols, but especially in the presence of bulkier alcohols. These results pointed to hydrogen bonding between the Mn=O unit and the H–O of the alcohols.

Manganese(V)-oxo porphyrins have been found to oxygenate chloride ions, leading to a variety of halogenation chemistry with these molecules. A water soluble manganese porphyrin Mn^{III}(TDMImP) was found to catalytically generate chlorine dioxide (ClO_2) from chlorite ion (ClO_2^-).[151] The proposed mechanism (Scheme 35) involved oxygen transfer from ClO^- or ClO_2^- to Mn^{III}(TDMImP) to give $Mn^{V}(O)_2$(TDMImP), which can oxidize a molecule of ClO_2^- to give Mn^{IV}(O)(TDMImP) and one molecule of ClO_2. The Mn^{IV}(O)(TDMImP) intermediate then reacts with ClO_2^- to give another ClO_2 molecule. To provide support for this mechanism, chlorite ion added to authentic Mn^{IV}(O)(TDMImP) underwent facile reaction under the catalytic conditions to produce ClO_2 and the Mn^{III}(TDMImP) catalyst. The rate-determining step was determined to be the initial oxygen atom transfer to Mn^{III}(TDMImP) from the chlorite ion to give the high-valent $Mn^{V}(O)_2$ species.[152] Halogenation of unactivated C–H bonds was observed with a Mn-porphyrin catalyst, and the presence of high-valent Mn^{V}(O) species has been observed in the UV-vis spectra during the reactions, although the direct C–H cleavage step has not been directly observed.[153]

2.2.2 Manganese-Oxo Corroles and Corrolazines—Manganese-oxo corroles have been studied as meta-stable analogues of their reactive porphyrin counterparts. Relatively stable Mn^{V}(O) corroles can be synthesized from the Mn^{III} precursor and an appropriate O-atom donor. These species are low-spin diamagnetic $S = 0$ complexes and the lifetime of the Mn^{V}(O) depends on the corrole ligand and solvent. Manganese-oxo corroles have been found to participate in the catalytic oxidation of substrates, and the reaction pathways depend highly on the electronic nature of the ligand. Some recent reviews have covered the reactivity of these complexes, including a chapter in the Handbook of Porphyrin Science in 2011,[17] which covers high-valent transition metal corroles and corrolazines, and a Coordination Chemistry Review[154] in 2013, which exclusively covers recent advances in manganese corrole chemistry. Since those reviews were published, several reports on the reactivity of Mn-oxo corroles have further advanced the field.

A survey of the reactivity of a series of Mn^{V}(O) corroles with a series of alkene substrates revealed a strong dependence of the rate constant as well as the mechanism of OAT on the solvent.[155,156] The product of decomposition, which typically changes with ligand identity, was also found to be solvent dependent. The more electron-rich Mn^{V}(O)-corroles decomposed to Mn^{IV}(X) species in toluene and dichloromethane, but in dimethylformamide and dimethylacetamide, the product of decomposition was an Mn^{III} corrole. In toluene and dichloromethane, the rate of decomposition was faster for the electron-deficient corroles, but in dimethylformamide and dimethylacetamide the trend was reversed. Addition of alkene to the self-decay reaction of Mn^{V}(O) was found to greatly accelerate them, with the most

electron-rich and least-substituted alkenes giving the fastest rates. The OAT reaction rates between alkene and Mn^{V}(O)corroles in either CH_2Cl_2 or $C_6H_5CH_3$ depended on the electron-donating properties of the corrole, with the most electron-deficient corroles giving the fastest rates. This trend in OAT rates was reversed in dimethylformamide and dimethylacetamide. The authors attributed this reversed trend to a change in mechanism from direct OAT in toluene and dichloromethane to a disproportionation mechanism in dimethylformamide and dimethylacetamide, in which the Mn^{V}(O) disproportionates to an Mn^{IV}(X) and an Mn^{VI}(O) species, which could be the actual oxidizing agent.

The effect of peripheral substituents on the corrole ring on the reactivity of manganese-oxo corroles has been studied. The effect of *β*-bromination on the OAT reactivity of a series of A_3 and A_2B - *meso*-phenyl substituted Mn^{V}(O) corroles was determined by Chang, Liu, and coworkers.[157] It was found that the brominated Mn^{V}(O) corroles performed OAT at rates much higher than their non-brominated analogues. When the *meso* positions contained *ortho*-*ortho′*-dibromophenyl groups, the steric protection of these substituents provided enhanced stability for the Mn^{V}(O) species. DFT calculations provided insight into the mechanism of various β-substituted (with Br, H, or CH_3) high-valent Mn-oxo corrole complexes reacting with dimethylsulfide, an O-atom acceptor. Liu and coworkers studied different oxidation levels of the corroles by DFT including $[Mn^{IV}(O)(tpfc)]^{-}$ (tpfc = 5,10,15-tris(pentafluorophenyl)corrolato^{3-}), Mn^{V}(O)(tpfc), and the one electron-oxidized $[Mn^{V}(O)(tpfc^{\bullet+})]^{+}$ complexes.[158] The calculated barriers suggested that the OAT reactivity followed the order: $[Mn^{V}(O)(tpfc^{\bullet+})]^{+} > Mn^{V}(O)(tpfc) > [Mn^{IV}(O)(tpfc)]^{-}$, indicating that the overall charge on the complex plays an important role in the mechanism. Furthermore, the more electron-deficient corrole ligand gave a more reactive complex, consistent with earlier DFT work[159] as well as experimental studies. Spin states were also important for determining the energies of the barriers for the reaction between Mn^{V}(O)(tpfc) and DMS. The barrier for the triplet state, best described as high-spin Mn^{V}(O), was found to be lower in energy than the singlet state, implicating the possibility of a spin crossover event along the reaction pathway. This result is consistent with earlier calculations from Cao and coworkers that found that while the ground state of the starting Mn^{V}(O) corrole is the singlet, the OAT triplet pathway has a lower barrier and therefore might play a significant role in the reaction.[160]

High-valent manganese-oxo and -imido corroles were shown to participate in the two-electron reduction of O_2 to H_2O_2, serving as precursors to the catalytically active manganese(III) corrole (Scheme 36).[161] The addition of trifluoroacetic acid to a high-valent Mn^{V}-imido complex, Mn^{V}(NAr)(tpfc) (NAr = 2,6,-dichlorophenylimido^{2-}), resulted in hydrolysis by residual water and production of a complex assigned as a protonated Mn-oxo corrole, $[Mn^{V}(OH)(tpfc)]^{+}$. However, direct evidence for the structure of this complex was not obtained. This complex can be reduced rapidly to Mn^{III}(tpfc) by the reductant octamethylferrocene. The reduced Mn^{III}(tpfc) reacts with O_2 to give a putative Mn^{IV}-superoxo species, which can obtain a proton and electron from TFA and octamethylferrocene, respectively, giving an Mn^{IV}-hydroperoxo species. Rather than undergoing O–O bond cleavage, it was suggested that the Mn^{IV}-hydroperoxo species is protonated and hydrogen peroxide is released. Reduction of the resulting Mn^{IV}(tpfc) allows for the catalytic cycle to begin again. Others have observed the formation of Mn^{V}(O)

corroles from Mn^{III}(corroles) during the metallation of free-base corroles with Mn^{II} sources in the presence of O_2, although the mechanism was not elucidated.[162]

The addition of trifluoroacetic acid to Mn^{V}(O)(tpfc) by Fukuzumi, Abu-Omar, and coworkers generated an electronic isomer of this complex, characterized as an Mn^{IV}(OH)($tpfc^{\bullet+}$) species, in which the oxo ligand was protonated.[163] The comparative reactivity of these two valence tautomers was studied (Scheme 37). There was little or no difference for the two complexes in H-atom transfer rates with a substituted phenol as H-atom donor. However, OAT from Mn^{V}(O)(tpfc) to thioanisole was extremely facile, whereas the Mn^{IV}(OH)($tpfc^{\bullet+}$) species was unreactive with thioanisole in the same time frame. In contrast, the electron-transfer reactivity exhibited the opposite trend, with the Mn^{IV}(OH)($tpfc^{\bullet+}$) complex having the faster rates with the reductant ferrocene.

Another method of entry into high-valent Mn-oxo corroles was found by Zhang and coworkers, in which visible light irradiation of $Mn^{IV}(BrO_3^{-})$(tpc) (tpc = triphenylcorrolato^{3-}) and $Mn^{IV}(BrO_3^{-})$(tpfc) complexes resulted in Br–O bond homolysis to give the Mn^{V}(O)-corroles (Scheme 38).[164] This kind of light-induced O–X bond homolysis was used previously by Newcomb and coworkers.[121,122] The reactivity of the photo-generated species was then studied with various organic substrates. The products of the reaction of photo-generated Mn^{V}(O)(tpfc) with organic substrates were highly solvent-dependent, with Mn^{III}(tpfc) as the product in CH_3CN and Mn^{IV} (tpfc) as the product in CH_2Cl_2. In contrast, the reaction of the more electron-rich Mn^{V}(O)(tpc) with organic substrates gave Mn^{IV}(tpc) as the only product regardless of solvent. Despite the complexity of products, the kinetics of the reactions of Mn^{V}(O) species with organic substrates all followed a simple second-order rate law. The reaction of Mn^{V}(O)(tpfc) with *para*-substituted thioanisoles resulted in a linear Hammett plot with a negative slope, which indicated a mechanism in which nucleophilic thioanisole reacted with an electrophilic Mn-oxo complex. When the rates of Mn^{V}(O)(tpfc) and Mn^{V}(O)(tpc) are compared, the Mn^{V}(O)(tpc) was generally the faster oxidant. Because the tpc ligand is more electron-rich than tpfc, and the reactivity of electrophilic metal-oxo species is generally enhanced with a more electron-poor ligand, this result was unexpected. The reactivity was therefore rationalized by the disproportionation of Mn^{V}(O) to Mn^{IV}(X) and Mn^{VI}(O), with Mn^{VI}(O) proposed as the actual oxidant (Scheme 39). This idea also explains the ability of Mn^{V}(O) to promote the facile 2-electron oxidations of alkene and sulfide substrates to give the Mn^{IV}(X) species, which is only one oxidation state below Mn^{V}(O). However, direct experimental evidence of the putative Mn^{VI}(O) oxidant remains elusive.

The effects of axial ligation on high-valent manganese-oxo corroles have been studied by ligands with tethered nitrogenous-bases.[165] The reactivity between the 6-coordinate acetamido-, pyridyl-, and imidazolyl- appended Mn^{V}(O) corroles and alkenes was found to be enhanced relative to the 5-coordinate Mn^{V}(O)corrole analogue. The reaction rates increased with increasing axial donor strength in the order: acetamido < pyridyl < imidazolyl. It was postulated that the coordination of the axial ligand destabilizes the Mn^{V}(O) species, which then increases the rate of OAT. These appended corroles were also capable of catalytic epoxidation, and the turnover frequency (TOF) also increased with the strength of the axial donor, following the same trend as the stoichiometric reactions.

The chemistry of high-valent manganese-oxo corrolazines was reviewed in 2011 in the Handbook of Porphyrin Science[17] and a survey of recent work from Goldberg and coworkers on these complexes appeared in 2015 in an Accounts of Chemical Research article.[166] A summary of work since these previous reviews is given here.

Although a number of spectroscopic methods had been used to characterize a high-valent manganese-oxo corrolazine complex $Mn^{V}(O)(TBP_8Cz)$ (TBP_8Cz = octakis(*p*-*tert*-butylphenyl)corrolazinato^{3-}) since the initial report of this complex in 2001, it was not until 2015 that the structure was determined by single crystal x-ray diffraction (XRD).[136] The structure revealed a short Mn–O bond distance of 1.55 Å and the Mn ion was displaced 0.55 Å relative to the plane of the four pyrrole nitrogens. Importantly, the Mn ion was five-coordinate, in contrast to Mn(O) porphyrin complexes, which typically have a sixth ligand.

The effect of modifying the peripheral aryl substituents at the β-position of the corrolazine ring had subtle but measurable effects on the reactivity of the $Mn^{V}(O)$ complexes.[167] The one-electron reduction potential of $Mn^{V}(O)(MeOP_8Cz)$ ($MeOP_8Cz$ = octakis(*p*-methoxyphenyl)corrolazinato^{3-}) ($E_{1/2}$ = −0.57 V vs Fc^{+}/Fc) was shifted negative compared to $Mn^{V}(O)(TBP_8Cz)$ ($E_{1/2}$ = −0.53 V vs Fc^{+}/Fc), indicating a slightly more electron rich metal center for the methoxy derivative. A Hammett study of the OAT reaction of $Mn^{V}(O)(MeOP_8Cz)$ with various *p*-substituted triarylphosphines to give triarylphosphine oxides revealed a more negative slope than with the $Mn^{V}(O)(TBP_8Cz)$ derivative, consistent with $Mn^{V}(O)(MeOP_8Cz)$ as a less electrophilic oxidant. In H-atom abstraction, the $Mn^{V}(O)(MeOP_8Cz)$ gave slightly faster rates than the $Mn^{V}(O)(TBP_8Cz)$ complex, and this result was rationalized by an enhanced basicity for the putative $[Mn^{IV}(O)(MeOP_8Cz)]^{-}$ species which compensates for the more negative redox potential of the $Mn^{V}(O)$ complex.

The corrolazine scaffold provides additional opportunities for modification through attachment of electrophiles to the *meso*-nitrogen atoms. An $Mn^{III}(TBP_8Cz)$ complex could be singly- or doubly- protonated on the *meso*-nitrogens using triflic acid (HOTf).[168] The mono- protonated $[Mn^{III}(TBP_8CzH)]^{+}$ complex was the resting state of a catalyst capable of oxidizing the benzyl C–H bonds of toluene derivatives. One proposed intermediate in the catalytic cycle was a protonated high-valent $Mn^{V}(OH)(TBP_8Cz)$ complex. Addition of HOTf to independently synthesized $Mn^{V}(O)(TBP_8Cz)$ was found to generate the valence tautomer $Mn^{IV}(OH)(TBP_8Cz^{\bullet+})$. This species oxidized substrates very slowly; however, when excess HOTf was added, it was capable of rapid C–H oxidation by a PCET mechanism consistent with this species being competent during catalysis. From these results, the proposed catalytic cycle is shown in Scheme 40, whereby the photoexcited protonated manganese corrolazine complex $[Mn^{III}(OTf)(TBP_8CzH)]^{+}$ reacts with dioxygen to generate a putative Mn^{IV}-superoxo species, which abstracts an H• from a toluene derivative (hexamethylbenzene) to generate a putative Mn^{IV}-hydroperoxo species and the substrate radical. O–O bond cleavage of the $Mn^{IV}(OOH)$ species occurs in concert with oxygen rebound to the substrate radical to give the high-valent manganese-oxo species, $Mn^{IV}(OH)(TBP_8Cz^{\bullet+})$, and hydroxylated organic product. The $Mn^{IV}(OH)(TBP_8Cz^{\bullet+})$, in the presence of a second H^{+} equivalent, reacts with another equivalent of hexamethylbenzene to give another equivalent of hydroxylated product along with regeneration of the resting state of the catalyst.

Theoretical calculations have been used as insightful tools into the nature of high-valent metal-oxo species. DFT calculations are popular for studying these types of complexes, but pitfalls in these methods remain, especially with respect to describing spin state energetics. Ghosh and coworkers used a higher level of theory to examine the low-lying excited states of $Mn^{V}(O)$ corroles and corrolazines using ab initio methods. The calculations uniformly indicated that a low-spin ($S = 0$) d^2 ground state was favored for these compounds, and confirmed that the corrole and corrolazine macrocycles are unambiguously innocent in the ground states.[169] The next low-lying excited states exhibited a high-spin Mn^{V} configuration, with the $Mn^{IV}(O)$ macrocycle-π-cation-radical states much higher in energy. Furthermore, the authors proposed that the *meso*-nitrogens of the corrolazine do not impart special stability to the ligand, but rather the steric bulk provided by the eight *tert*-butylphenyl β-substituents allow for the enhanced stability of the $Mn^{V}(O)$ species relative to the corrole.

DFT calculations have provided some insight into the reactivity of high-valent Mn-oxo corrolazines. The oxidation of C–H bonds by the low-spin $Mn^{V}(O)(TBP_8Cz)$ showed dramatic rate accelerations in the presence of anionic axial donors.[170] In a separate computational study, Shaik and coworkers proposed that the origin of the rate enhancement was due to a low-energy triplet transition state, as the most likely C–H bond cleavage pathway.[171] Higher-level NEVPT2:CAS calculations have shown that the energetically favored ground state is the singlet state for the same six-coordinate complexes, and showed that the singlet-triplet gap is much larger than predicted by the former DFT calculations. The six-coordinate complexes $[Mn^{V}(O)(X)(TBP_8Cz)]^{-}$ ($X = CN^{-}$, F^{-}) also exhibited dramatically enhanced OAT rates relative to the non-axially ligated $Mn^{V}(O)(TBP_8Cz)$ in reactions with sulfide substrates, including *para*-substituted thioanisole derivatives.[172,173] Calculations on this OAT reaction predicted that the six-coordinate complex $[Mn^{V}(O)(X)(TBP_8Cz)]^{-}$ reacted through the low-spin singlet pathway, avoiding spin-crossover during the reaction mechanism.[174] Experimental data showed a rare V-shaped Hammett plot for OAT, and this result could only be reproduced by calculations on the singlet pathway (Figure 3). When the Hammett plot was calculated for the reaction along the triplet pathway, a linear Hammett plot was obtained. This result provided an experimental test for distinguishing spin state pathways.

3. High-Valent Metal-Hydroxo Complexes

For discrete, isolated synthetic complexes of Mn or Fe, we are not aware of any *high-valent* (oxidation state = +4 or +5) metal-hydroxo porphyrinoid species. The analogous porphyrin and corrole metal(IV)-halogen (chloride, bromide, iodide, fluoride) complexes have been isolated, but have not exhibited biomimetic reactivity.[154,175,176]

4. Metal-Oxygen Complexes

4.1 Iron-Oxygen Complexes

4.1.1 Iron-Oxygen Porphyrins—Many studies of heme-dioxygen chemistry have focused on functional mimics for myoglobin and hemoglobin. Several reviews exist that cover dioxygen binding and activation by synthetic iron porphyrin complexes, including spectroscopic and structural features of the dioxygen adducts as well as their reactivity with

proton/electron sources. A comprehensive review was published in *Chemical Reviews* in 1994 by Momenteau and Reed, covering synthesis and characterization of heme dioxygen adducts and some reactivity.[177] Extensive auto-oxidation reactivity of these species was summarized in a *Coordination Chemistry Reviews* article by Shikama in 1988.[178] In The Porphyrin Handbook (2000), Watanabe described the reactivity of ferric porphyrin peroxo complexes, and Collman et al. summarized the literature of functional synthetic analogues of terminal oxidases.[33,179] In 2004, a *Chemical Review* article by Collman[180] summarized the literature on reversibly-formed synthetic heme-dioxygen adducts as functional analogs of the heme enzymes Cytochrome *c* oxidase, myoglobin, and hemoglobin. The same year, a *Chemical Review* article by Karlin[181] summarized the literature on synthetic heme-copper dioxygen chemistry as models for the active site of Cytochrome *c* oxidase. It is important to note that this review contained information on well-defined mononuclear heme-dioxygen adducts as a starting point for heme-copper dioxygen chemistry. In 2013, a *Coordination Chemistry Reviews* article by Ohta and Naruta described their recent progress in understanding the vibrational properties of mononuclear heme-peroxo complexes with regards to their influence on the reactivity of these species.[182] In this section, we focus on recent progress in the reactivity of well-defined dioxygen adducts of mononuclear iron porphyrins since the latest review (2012-present).

A report by Ivanović-Burmazović and coworkers showed that the formation of iron-O_2 porphyrin adducts in DMSO is reversible (Scheme 41).[183] The addition of excess potassium superoxide to Fe^{II}(tBuTPP) (tBuTPP = *meso*-tetrakis(*p-tert*-butylphenyl)porphyrinato^{2-}) generated the peroxo species $[Fe^{III}(O_2^{2-})(tBuTPP)]^-$. This process could be reversed by addition of a proton source, triflic acid (HOTf). The HOTf attacked excess free superoxide in the solution, which shifted the equilibrium back towards the Fe^{II}(tBuTPP) complex, according to Scheme 41. This result lies in contrast to other reports in which the presence of acid has been found to induce O–O cleavage to give the high-valent Fe-oxo species rather than disproportionation. By calculation, DMSO was found to have a strong influence on the O_2 binding mode and therefore the electronic structure of the Fe-O_2 adduct. However, potassium ion, present in solution from the superoxide source, was found to exert very little influence on these factors.

A study by van Eldik examined the influence of axial ligand and spin state on the O–O bond cleavage and reactivity of Fe-hydroperoxo porphyrin complexes.[184] The proposed five-coordinate, high-spin $[Fe^{III}(TPFPP)(OOH)]$ was observed to give $Fe^{IV}(O)$(TPFPP), a Cpd-II-like species, suggesting homolytic cleavage of the O–O bond, while the proposed six-coordinate, low-spin $[Fe^{III}(TPFPP)(OH)(OOH)]^-$ was observed to give an $Fe^{IV}(O)$ ($TPFPP^{\bullet+}$) species, suggesting heterolytic cleavage of the O–O bond. The authors attributed this difference in reactivity to the spin-states of the reactant and products for each reaction. The reactivity of the $[Fe^{III}(TPFPP)(OH)(OOH)]^-$ complex with various substrates was tested. No reaction was observed upon addition of olefins and sulfides to this complex, and addition of triphenylphosphine resulted only in displacement of the hydroxide ligand rather than oxidation (Scheme 42).

DFT calculations suggest that a doubly-protonated Fe^{III}-(H_2O_2) porphyrin complex could be a competent oxygen-atom donor for sulfide substrates.[185] The reaction was found to proceed

via proton-coupled heterolytic cleavage of the O–O bond in the $Fe^{III}(H_2O_2)$(Por) complex. The mechanism was initiated by nucleophilic attack of the distal oxygen by the sulfur lone pair of dimethyl sulfide, an electron-rich sulfur substrate. In tandem with the heterolytic cleavage, the Fe^{III}(OH)(Por) abstracts the proton from the protonated sulfoxide product to give dimethylsulfoxide and $Fe^{III}(OH_2)$(Por). An alternative mechanism was ruled out, in which the O–O bond of $Fe^{III}(H_2O_2)$(Por) is cleaved homolytically to generate an [Fe^{III} + •OH] and a hydroxyl radical, •OH. The •OH abstracts an H-atom from [Fe^{III} + •OH] to give Fe^{IV}(O)(porphyrin π-cation-radical) (Cpd-I), which can then perform sulfoxidation. However, the homolytic cleavage step was found to have a much higher activation barrier than the heterolytic/sulfur attack mechanism, indicating that the heterolytic mechanism will undergo sulfoxidation much faster than Cpd-I can be generated (Scheme 43). While an $Fe^{III}(H_2O_2)$ species has not been observed in heme enzyme catalysis, the peroxide shunt is often invoked in mechanistic studies where hydrogen peroxide is used to generate the high-valent iron-oxo species.

Spectroscopic detection of a ferrous-superoxo porphyrin could be achieved by cryo-generation (Scheme 44).[186] Irradiation of a ferric-superoxo complex with a γ-ray source at 77 K resulted in one electron reduction to the ferrous superoxo species, which was characterized by EPR and resonance Raman spectroscopies. DFT calculations also confirmed that the reduction of the $Fe^{III}(O_2^{\bullet-})$ species occurred at the iron center rather than the superoxo-ligand. When the ferrous-superoxo species was warmed to 193 K, the ferric-hydroperoxide species was observed, as characterized previously by Naruta and coworkers, [182] indicating that the $Fe^{II}(O_2^{\bullet-})$ species was basic enough to scavenge a proton even in the absence of an exogenous acid source. This work gave insight into the thermodynamics of the transformation between ferric-superoxo and ferric-hydroperoxo, which differ by a hydrogen atom, and both of which are implicated in the catalytic cycles of heme monooxygenase enzymes.

The influence of the secondary coordination sphere on the reactivity of a ferric-superoxo porphyrin was investigated (Scheme 45).[187] An imidazole as an axial ligand and a carboxylic acid group as a proton donor were tethered to the porphyrin ligand. As a control, the secondary coordination sphere effects of a similar ligand containing an ethoxy carbonyl group instead of the carboxylic acid were compared. When the iron-superoxo species was generated by addition of O_2 to the ferrous iron in the ligand without the proton donor, addition of exogenous reductant and acid resulted in controlled formation of the ferric hydroperoxo species. However, when O_2 was added to the ferrous iron porphyrin containing the pendant proton donor, some ferric-hydroperoxide was observed, in addition to the ferric-superoxo species. The presence of ferric-hydroperoxide from the oxygenation reaction, in the absence of added proton and electron donors, implied that the reduced ferrous porphyrin itself could act as an H^+/e^- donor, but only if the carboxylic acid group was present.

4.1.2 Iron-Oxygen Corroles and Corrolazines—

To our knowledge, there are no examples of well defined iron-(hydro)peroxo or iron–superoxo corrole or corrolazine complexes.

4.2 Manganese-Oxygen Complexes

4.2.1 Manganese-Oxygen Porphyrins—In heme enzymes, the binding and activation of dioxygen or hydrogen peroxide at the metal center are typically the initial steps in the catalytic cycles. Cleavage of the O–O bond leads to the generation of high-valent metal-oxo species. There are very few examples of well-defined manganese-superoxo or –(hydro)peroxo porphyrins.[188] This may be due to the relative stability of the O–O bond-cleaved product, a high-valent manganese-oxo species, in these systems. However, those rare Mn–superoxo or – (hydro)peroxo species that have been observed can be generated by either O_2, H_2O_2, or ROOH binding and activation. Some reviews on Mn-superoxo/peroxo porphyrin species include a section of a chapter by Koga and Tabushi in *Biomimetic Chemistry* from the *Advances in Chemistry* (1980) series[37] and a section of a chapter by Groves and coworkers in the book Biomimetic Oxidations Catalyzed by Transition Metal Complexes (2000).[189] In this section, we focus on the reactivity of the Mn–O–O adducts, which is intimately tied to the extent of O–O bond activation.

The first example of a Mn(porphyrin)(O_2) adduct was reported in 1975. Addition of O_2 at −79 °C to Mn^{II}(TPP) resulted in the reversible formation of a five-coordinate dioxygen-bound Mn(O_2)(TPP) species.[190] Debate about the electronic structure and mode of dioxygen binding followed, with some suggesting an $Mn^{IV}(O_2^{2-})$(Por)(O_2^{2-} = peroxide^{2-}) with the peroxide ligand binding to the Mn in a side-on fashion[191-194] and others an $Mn^{III}(O_2^{\bullet-})$(Por) ($O_2^{-\bullet}$ = superoxide^{1-}) with the superoxide ligand binding to Mn in an end-on fashion.[195,196] The one-electron reduced $[Mn(O_2)(Por)]^-$ adduct generated from addition of potassium superoxide to Mn^{II} (generated from outer sphere reduction of Mn^{III}(Por) by another equivalent of potassium superoxide) was subjected to a similar debate regarding geometry and electronic structure.[197,198] Another way to generate the $[Mn(O_2)(Por)]^-$ species was found when O_2 was added to Mn^{III}(por) in the presence of hydroxide.[199] Ultimately, a crystal structure of an $[Mn(O_2)(TPP)]^-$ adduct showed that a peroxide ligand was bound to Mn^{III}(TPP) in the side-on mode, resolving the debate. This binding mode for the reduced complex also served as precedent for the oxidation state assignment of the neutral $Mn^{IV}(O_2^{2-})$(TPP) complex.[200]

The equilibrium constant for the binding of O_2 to Mn(II) porphyrins was found to depend on the electron-donating or electron-withdrawing nature of the porphyrin ligand.[201] The effect of neutral axial ligands (L) bound to Mn^{II}(por) complexes trans to the O_2 binding site was studied and a correlation between the proton affinities of the series of ligands and the equilibrium constants for O_2 binding was found.[202]

The acylation of an oxygenated manganese-porphyrin complex could be achieved at low temperature by addition of acylchloride to Mn(II) or Mn(III) porphyrins in the presence of O_2 or superoxide, respectively.[203] The Mn-acyl-peroxo species was capable of the oxidation of cyclooctene to cyclooctene oxide. Addition of hydroxide ion to the acyl-peroxo species and warming of the reaction solution induced O–O bond cleavage to give the high-valent Mn-oxo species, which was also able to undergo epoxidation of cyclooctene.

Changing the electronics of the peroxyacid allowed for tuning of the O–O bond cleavage reactivity of an acylperoxo-Mn(TMP) adduct, but the relative rates of O–O cleavage to form

the high valent Mn-oxo species were strongly dependent on the presence or absence of hydroxide ion.[204] In the presence of hydroxide, the more electron-rich peroxyacids were more reactive than the electron-poor peroxyacids. In the absence of hydroxide ion, the opposite trend was observed. These differences in reactivity were attributed to a change in mechanism from homolytic to heterolytic O–O cleavage in the presence and absence of hydroxide, respectively.

A manganese(III)peroxycarbonate complex could be formed from the reaction of $[Mn(O_2)(Por)]^-$ adducts with carbon dioxide.[205] Homolytic or heterolytic O–O bond cleavage of the peroxycarbonate adducts was dependent on the solvent, temperature, and porphyrin ligand. Formation of $[Mn(O_2CO_2)(Por)]^-$ adducts was achieved by addition of potassium superoxide to either Mn^{II}(TPP), Mn^{II}(TPFPP), or $Mn^{II}(TP_{iv}P)$ ($TP_{iv}P$ = *meso*-tetrakis(α-pivalamidophenyl)porphyrinato^{2-}), followed by addition of carbon dioxide at − 70 °C. Depending on the solvent, O–O cleavage occurred to give one of two high-valent Mn(O) species. In THF, a ligating solvent, homolytic O–O cleavage to give the Mn^{IV}(O) was favored, whereas in toluene heterolysis to give the Mn^{V}(O) was preferred.

The reactivity of peroxomanganese(III) porphyrins with organic substrates was studied and compared with other metal-peroxo complexes.[206] It was found that $[Mn^{III}(O_2)(Por)]^-$ acted as a nucleophile of moderate strength. The peroxo complex $[Mn^{III}(O_2)(Por)]^-$ was able to oxidize an extremely electron-deficient alkene, tetracyanoethylene, in addition to acyl halides and CO_2. However, $[Mn^{III}(O_2)(Por)]^-$ was unable to oxidize other olefins, including some electron-deficient olefins and all electron-rich olefins tested, as well as triphenylphosphine and butyllithium. It was suggested that the relative stability of this complex was due to strong orbital overlap between the metal and O_2 ligand.

The mechanism of heterolytic O–O bond cleavage of a Mn^{III}(OOH)(TDMImP) was studied.[207] The O–O bond cleavage step was found to be rate determining and followed a concerted “push-pull” mechanism, in which an axial $^-$OH was partially deprotonated and provided the “push”, while the terminal oxygen in the $^-$OOH ligand was partially protonated and acted as a “pull” to release an H_2O molecule into the solvent medium. This “push-pull” model has also been invoked to explain the heterolytic O–O bond cleavage to generate Cpd-I during the catalytic cycle of Cytochrome P450s and other heme enzymes.

4.2.2 Manganese-Oxygen Corroles—Well-defined manganese-peroxo corrole complexes are rare, while manganese-superoxo corrole complexes are unknown. The following examples constitute the only evidence for these species to date, and their reactivity is still not well understood.

In 2009, Åkermark, Sun, and coworkers showed evidence for the formation of O_2 by addition of hydroxide to an Mn^{V}(O) corrole complex (Scheme 46).[208] Nucleophilic attack of hydroxide on Mn^{V}(O)(tnpc) (tnpc = 5,10,15-tris(4-nitrophenyl)corrolato^{3-}) initially generated a putative Mn^{III} hydroperoxy complex, which was not observed. Formal H• abstraction by an unidentified oxidant from this complex gave an Mn^{IV} species, which was assigned as an Mn^{IV}-peroxo complex based on UV-vis and mass spectrometry. Further oxidation through an unknown mechanism results in the Mn^{III} corrole and release of

dioxygen. Formation of O_2 was quantitated by online gas analysis, and addition of $H_2{}^{18}O$ to the hydroxide reaction resulted in mixed-labeled Mn-peroxo complex as well as mixed-label dioxygen ($^{16,18}O_2$), confirming that O–O bond formation occurs in this system.

Following this work, Nam and coworkers provided evidence for the reversible interconversion of an $Mn^V(O)$ corrole and an Mn-peroxo corrole complex (Scheme 47).[209] The addition of H_2O_2 to Mn^{III} (tfmpc) (tfmpc = 5,10,15-tris(trifluoromethylphenyl)corrolato^{3-}) in the presence of hydroxide resulted in an intermediate assigned as an $Mn^{IV}(O_2)^-$ species based on UV-vis, EPR, and mixed labeling mass spectrometry studies using ^{18}O-labeled reagents. The addition of hydroxide to $Mn^V(O)$ (tfmpc) also resulted in the formation of this new species, and could be reversed back to the starting $Mn^V(O)$ complex with the addition of perchloric acid. The mechanism of interconversion is not understood with regard to electron-count, since $Mn^V(O)$ and hydroxide should give an Mn^{III}(peroxo) complex and H_2O_2 addition to Mn^{III} (tfmpc) should give the same Mn^{III} species. The overall pathway is shown in Scheme 47.

5. Conclusions and Final Remarks

In this review, we discussed the biomimetic reactivity of iron and manganese -oxo and -dioxygen intermediates in porphyrinoid systems. The reactivity of these species depends heavily on the identity of the porphyrinoid ligand (either porphyrin, corrole, or corrolazine), the metal identity and oxidation state, as well as the type of substrate. These results are analogous to natural systems that depend on tuning environment to control reactivity. Experimental and theoretical studies both gave crucial insights into the fundamental reaction mechanisms.

While biomimetic reactivity of metal-oxo and metal-dioxygen intermediates has been extensively studied, we still foresee interesting challenges ahead. For example, the direct observation of the combination of an organic radical and a high-valent metal-hydroxide compound has not yet been achieved. Understanding the factors that select for rebound chemistry over other reactions (such as dehydrogenation) could allow for insight into the design of metalloporphyrinoid catalysts that undergo selective hydroxylations with substrates that contain many possible sites of oxidation. The design principles from these studies could also give insight into C–H halogenation performed by heme chloroperoxidase. High-valent iron-oxo corrole complexes and their reactivity are notably absent from the literature. Only one corresponding high-valent iron-oxo corrolazine has been characterized. The field is open for ligand development to access high-valent mononuclear Fe(O) corroles and corrolazines. There is still much to learn about metal-oxygen species and what controls the extent of O_2 activation, the O–O bond formation/cleavage steps, and the mechanism of O–O bond formation/cleavage. Manganese or iron corroles could allow for the study of these species, but there are few examples in the literature showing that they can form stable metal-oxygen complexes. The syntheses of these species would allow for unknown reactivity to be revealed.

Achieving answers to these questions and opening up the field to new reactivity could give valuable insight into the natural systems and provide a foundational basis for the development of new metalloporphyrinoid-mediated reactions.

Acknowledgements

We thank the NIH for financial support (GM101153 to D.P.G.). R.A.B. is grateful for the Harry and Cleio Greer Fellowship. J.P.T.Z. is grateful for The Glen E. Meyer ‘39 Fellowship.

Author Biographies

Regina A. Baglia received her B.S. degree in biochemistry in 2011 from Temple University, in Philadelphia, PA, where she performed undergraduate research as a Diamond Research Scholar in the Department of Chemistry with Prof. Michael J. Zdilla. She received her PhD in chemistry at The Johns Hopkins University in 2016, where she worked with Prof. David P. Goldberg. While at Hopkins, she was awarded the George E. Owens Graduate Fellowship, an E^2SHI fellowship, and the Harry and Cleio Greer fellowship.

Jan Paulo T. Zaragoza was born in Manila, Philippines in 1990. He received his B.S. in Biochemistry from the University of the Philippines—Manila in 2010. He is currently pursuing his doctoral studies under the supervision of Prof. David P. Goldberg at the Johns Hopkins University. His research involves the study of high-valent metal-oxo corroles and corrolazines as synthetic models for heme enzyme active sites.

David P. Goldberg received his B.A. degree from Williams College in 1989, and his Ph.D. degree in Inorganic Chemistry in the research group of Prof. Stephen J. Lippard. Following his Ph.D. in 1995, he was an NIH Postdoctoral Fellow in the group of Prof. Brian Hoffman at Northwestern University. He began his independent career at Johns Hopkins University in the department of Chemistry in 1998, where he is currently a Professor of Chemistry. His research interests include synthetic inorganic chemistry, models of heme and nonheme metalloenzymes, dioxygen and nitric oxide activation, and other fundamental transformations important to synthetic and biological oxidation/reduction catalysis.

References

(1). Sono M; Roach MP; Coulter ED; Dawson JH Heme-Containing Oxygenases Chem. Rev 1996, 96, 2841–2888.11848843

(2). Poulos TL Heme Enzyme Structure and Function Chem. Rev 2014, 114, 3919–3962.24400737

(3). Mansuy D; Battioni P In The Porphyrin Handbook; >Kadish KM, >Smith JM, >Guilard R, Eds.; Academic Press: San Diego, CA, USA, 2000; Vol. 4, p 1–15.

(4). Efimov I; Basran J; Thackray SJ; Handa S; Mowat CG; Raven EL Structure and Reaction Mechanism in the Heme Dioxygenases Biochemistry 2011, 50, 2717–2724.21361337

(5). Claessens CG; González-Rodríguez D; Rodríguez-Morgade MS; Medina A; Torres T Subphthalocyanines, Subporphyrazines, and Subporphyrins: Singular Nonplanar Aromatic Systems Chem. Rev 2014, 114, 2192–2277.24568182

(6). Shimizu S Recent Advances in Subporphyrins and Triphyrin Analogues: Contracted Porphyrins Comprising Three Pyrrole Rings Chem. Rev 2017, 117, 2730–2784.27779851

(7). Jasat A; Dolphin D Expanded Porphyrins and Their Heterologs Chem. Rev 1997, 97, 2267–2340.11848901

(8). Sessler JL; Seidel D Synthetic Expanded Porphyrin Chemistry Angew. Chem., Int. Ed 2003, 42, 5134–5175.

(9). Tanaka T; Osuka A Chemistry of meso-Aryl-Substituted Expanded Porphyrins: Aromaticity and Molecular Twist Chem. Rev 2017, 117, 2584–2640.27537063

(10). Rosenthal J; Nocera DG In Progress in Inorganic Chemistry; John Wiley & Sons, Inc.: 2008, p 483–544.

(11). Anderson JS; Gallagher AT; Mason JA; Harris TD A Five-Coordinate Heme Dioxygen Adduct Isolated within a Metal–Organic Framework J. Am. Chem. Soc 2014, 136, 16489–16492.25380235

(12). Li W-S; Aida T Dendrimer Porphyrins and Phthalocyanines Chem. Rev 2009, 109, 6047–6076.19769361

(13). Lu Y; Berry SM; Pfister TD Engineering Novel Metalloproteins: Design of Metal-Binding Sites into Native Protein Scaffolds Chem. Rev 2001, 101, 3047–3080.11710062

(14). Prier CK; Arnold FH Chemomimetic Biocatalysis: Exploiting the Synthetic Potential of Cofactor-Dependent Enzymes To Create New Catalysts J. Am. Chem. Soc 2015, 137, 13992–14006.26502343

(15). Dydio P; Key HM; Nazarenko A; Rha JY-E; Seyedkazemi V; Clark DS; Hartwig JF An artificial metalloenzyme with the kinetics of native enzymes Science 2016, 354, 102–106.27846500

(16). Bhagi-Damodaran A; Michael MA; Zhu Q; Reed J; Sandoval BA; Mirts EN; Chakraborty S; Moënne-Loccoz P; Zhang Y; Lu Y Why copper is preferred over iron for oxygen activation and reduction in haem-copper oxidases Nat Chem 2017, 9, 257–263.28221360

(17). McGown AJ; Badiei YM; Leeladee P; Prokop KA; DeBeer S; Goldberg DP In Handbook of Porphyrin Science; >Kadish KM, >Smith JM, >Guilard R, Eds.; World Scientific Press: Singapore, 2011; Vol. 14, p 525–599.

(18). Weiss R, Gold A, Trautwein AX, and Terner J In The Porphyrin Handbook; >Kadish KM, >Smith KM and >Guilard R, Ed.; Academic Press: San Diego, CA, USA, 2000; Vol. 4, p 65–96.

(19). Groves JT; Nemo TE; Myers RS Hydroxylation and epoxidation catalyzed by iron-porphine complexes. Oxygen transfer from iodosylbenzene J. Am. Chem. Soc 1979, 101, 1032–1033.

(20). Groves JT; Haushalter RC; Nakamura M; Nemo TE; Evans BJ High-valent iron-porphyrin complexes related to peroxidase and cytochrome P-450 J. Am. Chem. Soc 1981, 103, 2884–2886.

(21). Watanabe Y; Fujii H In Metal-Oxo and Metal-Peroxo Species in Catalytic Oxidations; >Meunier B, Ed.; Springer: Berlin; New York, 2000, p 62.

(22). Fujii H Electronic structure and reactivity of high-valent oxo iron porphyrins Coord. Chem. Rev 2002, 226, 51–60.

(23). Fujii H In Heme Peroxidases; >Raven E, >Dunford B, Eds.; The Royal Society of Chemistry: 2016, p 181–217.

(24). Meunier B; de Visser SP; Shaik S Mechanism of Oxidation Reactions Catalyzed by Cytochrome P450 Enzymes Chem. Rev 2004, 104, 3947–3980.15352783

(25). Groves JT High-valent iron in chemical and biological oxidations J. Inorg. Biochem 2006, 100, 434–447.16516297

(26). Pan Z; Zhang R; Newcomb M Kinetic studies of reactions of iron(IV)-oxo porphyrin radical cations with organic reductants J. Inorg. Biochem 2006, 100, 524–532.16500709

(27). Nam W High-Valent Iron(IV)–Oxo Complexes of Heme and Non-Heme Ligands in Oxygenation Reactions Acc. Chem. Res 2007, 40, 522–531.17469792

(28). Costas M Selective C–H oxidation catalyzed by metalloporphyrins Coord. Chem. Rev 2011, 255, 2912–2932.

(29). Hohenberger J; Ray K; Meyer K The biology and chemistry of high-valent iron-oxo and iron-nitrido complexes Nat Commun 2012, 3, 720.22395611

(30). Rutkowska-Zbik D; Drzewiecka-Matuszek A; Witko M The Influence of Structural Parameters on the Reactivity of Model Complexes for Compound II: A Mini Review Topics in Catalysis 2014, 57, 946–952.

(31). Groves JT; Shalyaev K; Lee J In The Porphyrin Handbook; >Kadish KM, >Smith KM, >Guilard R, Eds.; Academic Press: San Diego, CA, USA, 2000; Vol. 4, p 17–40.

(32). Suslick KS In The Porphyrin Handbook; Kadish KM, Smith KM, Guilard R, Eds.; Academic Press: San Diego, 2000; Vol. 4, p 41–64.

(33). Watanabe Y In The Porphyrin Handbook; Kadish KM, Smith KM, Guilard R, Eds.; Academic Press: San Diego, CA, USA, 2000; Vol. 4, p 97–118.

(34). Meunier B; Robert A; Pratviel G; Bernadou J In The Porphyrin Handbook; Kadish KM, Smith KM, Guilard R, Eds.; Academic Press: San Diego, CA, USA, 2000; Vol. 4, p 119–188.

(35). de Visser SP; Nam W High-valent iron-oxo porphyrins in oxygenation reactions Handbook of Porphyrin Science; Kadish KM, Smith KM, Guilard R, Eds 2010, 85–140.

(36). McLain JL; Lee J; Groves JT In Biomimetic Oxidations Catalyzed by Transition Metal Complexes; Meunier B, Ed.; Imperial College Press: London, 2000, p 91–169.

(37). Tabushi I; Koga N In Biomimetic Chemistry; American Chemical Society: 1980; Vol. 191, p 291–306.

(38). Nam W In Comprehensive Coordination Chemistry II; Meyer TJ, Ed.; Pergamon: Oxford, 2003, p 281–307.

(39). Dolphin D; Traylor TG; Xie LY Polyhaloporphyrins: Unusual Ligands for Metals and Metal-Catalyzed Oxidations Acc. Chem. Res 1997, 30, 251–259.

(40). Bell SR; Groves JT A Highly Reactive P450 Model Compound I J. Am. Chem. Soc 2009, 131, 9640–9641.19552441

(41). Pan Z; Zhang R; Fung LWM; Newcomb M Photochemical Production of a Highly Reactive Porphyrin–Iron–Oxo Species Inorg. Chem 2007, 46, 1517–1519.17284026

(42). Jeong YJ; Kang Y; Han A-R; Lee Y-M; Kotani H; Fukuzumi S; Nam W Hydrogen Atom Abstraction and Hydride Transfer Reactions by Iron(IV)–Oxo Porphyrins Angew. Chem., Int. Ed 2008, 47, 7321–7324.

(43). Pan Z; Wang Q; Sheng X; Horner JH; Newcomb M Highly Reactive Porphyrin–Iron–Oxo Derivatives Produced by Photolyses of Metastable Porphyrin–Iron(IV) Diperchlorates J. Am. Chem. Soc 2009, 131, 2621–2628.19193008

(44). Chen T-H; Asiri N; Kwong KW; Malone J; Zhang R Ligand control in the photochemical generation of high-valent porphyrin-iron-oxo derivatives Chem. Commun 2015, 51, 9949–9952.

(45). Radoń M; Broclawik E; Pierloot K DFT and Ab Initio Study of Iron-Oxo Porphyrins: May They Have a Low-Lying Iron(V)-Oxo Electromer? J. Chem. Theory Comput 2011, 7, 898–908.26606340

(46). Pan Z; Horner JH; Newcomb M Tunneling in C–H Oxidation Reactions by an Oxoiron(IV) Porphyrin Radical Cation: Direct Measurements of Very Large H/D Kinetic Isotope Effects J. Am. Chem. Soc 2008, 130, 7776–7777.18512909

(47). Cong Z; Kinemuchi H; Kurahashi T; Fujii H Factors Affecting Hydrogen-Tunneling Contribution in Hydroxylation Reactions Promoted by Oxoiron(IV) Porphyrin π-Cation Radical Complexes Inorg. Chem 2014, 53, 10632–10641.25222493

(48). Yosca TH; Rittle J; Krest CM; Onderko EL; Silakov A; Calixto JC; Behan RK; Green MT Iron(IV)hydroxide pKa and the Role of Thiolate Ligation in C–H Bond Activation by Cytochrome P450 Science 2013, 342, 825–829.24233717

(49). Tani F; Matsu-ura M; Nakayama S; Naruta Y Synthetic models for the active site of cytochrome P450 Coord. Chem. Rev 2002, 226, 219–226.

(50). Hessenauer-Ilicheva N; Franke A; Wolak M; Higuchi T; van Eldik R Spectroscopic and Mechanistic Studies on Oxidation Reactions Catalyzed by the Functional Model SR Complex for Cytochrome–P450: Influence of Oxidant, Substrate, and Solvent Chem. - Eur. J 2009, 15, 12447–12459.19806618

(51). Hessenauer-Ilicheva N; Franke A; Meyer D; Woggon W-D; van Eldik R Mechanistic Insight into Formation of Oxo-Iron(IV) Porphyrin π-Cation Radicals from Enzyme Mimics of Cytochrome P450 in Organic Solvents Chem. - Eur. J 2009, 15, 2941–2959.19185039

(52). Suzuki N; Higuchi T; Urano Y; Kikuchi K; Uekusa H; Ohashi Y; Uchida T; Kitagawa T; Nagano T Novel Iron Porphyrin–Alkanethiolate Complex with Intramolecular NH¬∑¬∑¬∑S Hydrogen Bond: Synthesis, Spectroscopy, and Reactivity J. Am. Chem. Soc 1999, 121, 11571–11572.

(53). Meyer DN; Woggon W-D Synthesis and Characterization of a New Family of Iron Porphyrins CHIMIA International Journal for Chemistry 2005, 59, 85–87.

(54). Hessenauer-Ilicheva N; Franke A; Meyer D; Woggon W-D; van Eldik R Low-Temperature Rapid-Scan Detection of Reactive Intermediates in Epoxidation Reactions Catalyzed by a New Enzyme Mimic of Cytochrome P450 J. Am. Chem. Soc 2007, 129, 12473–12479.17880072

(55). Han A-R; Jin Jeong Y; Kang Y; Yoon Lee J; Sook Seo M; Nam W Direct evidence for an iron(iv)-oxo porphyrin π-cation radical as an active oxidant in catalytic oxygenation reactions Chem. Commun 2008.

(56). Franke A; Fertinger C; van Eldik R Which Oxidant Is Really Responsible for P450 Model Oxygenation Reactions? A Kinetic Approach Angew. Chem., Int. Ed 2008, 47, 5238–5242.

(57). Takahashi A; Kurahashi T; Fujii H Effect of Imidazole and Phenolate Axial Ligands on the Electronic Structure and Reactivity of Oxoiron(IV) Porphyrin π-Cation Radical Complexes: Drastic Increase in Oxo-Transfer and Hydrogen Abstraction Reactivities Inorg. Chem 2009, 48, 2614–2625.19216512

(58). Takahashi A; Kurahashi T; Fujii H Redox Potentials of Oxoiron(IV) Porphyrin π-Cation Radical Complexes: Participation of Electron Transfer Process in Oxygenation Reactions Inorg. Chem 2011, 50, 6922–6928.21714484

(59). Takahashi A; Yamaki D; Ikemura K; Kurahashi T; Ogura T; Hada M; Fujii H Effect of the Axial Ligand on the Reactivity of the Oxoiron(IV) Porphyrin π-Cation Radical Complex: Higher Stabilization of the Product State Relative to the Reactant State Inorg. Chem 2012, 51, 7296–7305.22716193

(60). Kang Y; Chen H; Jeong YJ; Lai W; Bae EH; Shaik S; Nam W Enhanced Reactivities of Iron(IV)-Oxo Porphyrin π-Cation Radicals in Oxygenation Reactions by Electron-Donating Axial Ligands Chemistry - A European Journal 2009, 15, 10039–10046.

(61). Kumar D; Sastry GN; de Visser SP Axial Ligand Effect On The Rate Constant of Aromatic Hydroxylation By Iron(IV)–Oxo Complexes Mimicking Cytochrome P450 Enzymes J. Phys. Chem. B 2012, 116, 718–730.22132821

(62). de Visser SP Trends in Substrate Hydroxylation Reactions by Heme and Nonheme Iron(IV)-Oxo Oxidants Give Correlations between Intrinsic Properties of the Oxidant with Barrier Height J. Am. Chem. Soc 2010, 132, 1087–1097.20041691

(63). Kumar D; Sastry GN; de Visser SP Effect of the Axial Ligand on Substrate Sulfoxidation Mediated by Iron(IV)–Oxo Porphyrin Cation Radical Oxidants Chem. - Eur. J 2011, 17, 6196–6205.21469227

(64). Kumar D; Latifi R; Kumar S; Rybak-Akimova EV; Sainna MA; de Visser SP Rationalization of the Barrier Height for p-Z-styrene Epoxidation by Iron(IV)-Oxo Porphyrin Cation Radicals with Variable Axial Ligands Inorg. Chem 2013, 52, 7968–7979.23822112

(65). Kumar D; Karamzadeh B; Sastry GN; de Visser SP What Factors Influence the Rate Constant of Substrate Epoxidation by Compound I of Cytochrome P450 and Analogous Iron(IV)-Oxo Oxidants? J. Am. Chem. Soc 2010, 132, 7656–7667.20481499

(66). de Visser SP; Tahsini L; Nam W How Does the Axial Ligand of Cytochrome P450 Biomimetics Influence the Regioselectivity of Aliphatic versus Aromatic Hydroxylation? Chem. - Eur. J 2009, 15, 5577–5587.19347895

(67). Kudrik EV; Afanasiev P; Alvarez LX; Dubourdeaux P; Clémancey M; Latour J-M; Blondin G; Bouchu D; Albrieux F; Nefedov SE; Sorokin AB An N-bridged high-valent diiron–oxo species on a porphyrin platform that can oxidize methane Nat Chem 2012, 4, 1024–1029.23174983

(68). Dunford HB; Lambeir A-M; Kashem MA; Pickard M On the mechanism of chlorination by chloroperoxidase Arch. Biochem. Biophys 1987, 252, 292–302.3028259

(69). Harrison JE; Schultz J Studies on the chlorinating activity of myeloperoxidase J. Biol. Chem 1976, 251, 1371–1374.176150

(70). Cong Z; Kurahashi T; Fujii H Oxidation of Chloride and Subsequent Chlorination of Organic Compounds by Oxoiron(IV) Porphyrin π-Cation Radicals Angew. Chem., Int. Ed 2011, 50, 9935–9939.

(71). Du J; Chen Z; Chen C; Meyer TJ A Half-Reaction Alternative to Water Oxidation: Chloride Oxidation to Chlorine Catalyzed by Silver Ion J. Am. Chem. Soc 2015, 137, 3193–3196.25700124

(72). Cong Z; Kurahashi T; Fujii H Formation of Iron(III) meso-Chloro-isoporphyrin as a Reactive Chlorinating Agent from Oxoiron(IV) Porphyrin π-Cation Radical J. Am. Chem. Soc 2012, 134, 4469–4472.22375905

(73). Cong Z; Yanagisawa S; Kurahashi T; Ogura T; Nakashima S; Fujii H Synthesis, Characterization, and Reactivity of Hypochloritoiron(III) Porphyrin Complexes J. Am. Chem. Soc 2012, 134, 20617–20620.23214510

(74). Abu-Omar MM High-valent iron and manganese complexes of corrole and porphyrin in atom transfer and dioxygen evolving catalysis Dalton Trans 2011, 40, 3435–3444.21279237

(75). Lee AQ; Streit BR; Zdilla MJ; Abu-Omar MM; DuBois JL Mechanism of and exquisite selectivity for O–O bond formation by the heme-dependent chlorite dismutase Proc. Natl. Acad. Sci 2008, 105, 15654–15659.18840691

(76). Zdilla MJ; Lee AQ; Abu-Omar MM Concerted Dismutation of Chlorite Ion: Water-Soluble Iron-Porphyrins As First Generation Model Complexes for Chlorite Dismutase Inorg. Chem 2009, 48, 2260–2268.19138154

(77). Zdilla MJ; Lee AQ; Abu-Omar MM Bioinspired Dismutation of Chlorite to Dioxygen and Chloride Catalyzed by a Water-Soluble Iron Porphyrin Angew. Chem., Int. Ed 2008, 47, 7697–7700.

(78). Kang M-J; Song WJ; Han A-R; Choi YS; Jang HG; Nam W Mechanistic Insight into the Aromatic Hydroxylation by High-Valent Iron(IV)-oxo Porphyrin π-Cation Radical Complexes J. Org. Chem 2007, 72, 6301–6304.17622172

(79). Asaka M; Fujii H Participation of Electron Transfer Process in Rate-Limiting Step of Aromatic Hydroxylation Reactions by Compound I Models of Heme Enzymes J. Am. Chem. Soc 2016, 138, 8048–8051.27327623

(80). Li C; Wu W; Cho K-B; Shaik S Oxidation of Tertiary Amines by Cytochrome P450—Kinetic Isotope Effect as a Spin-State Reactivity Probe Chem. - Eur. J 2009, 15, 8492–8503.19322770

(81). Garcia-Bosch I; Sharma SK; Karlin KD A Selective Stepwise Heme Oxygenase Model System: An Iron(IV)-Oxo Porphyrin π-Cation Radical Leads to a Verdoheme-Type Compound via an Isoporphyrin Intermediate J. Am. Chem. Soc 2013, 135, 16248–16251.24147457

(82). Chin D-H; Balch AL; La Mar GN Formation of porphyrin ferryl (FeO^{2+}) complexes through the addition of nitrogen bases to peroxo-bridged iron(III) porphyrins J. Am. Chem. Soc 1980, 102, 1446–1448.

(83). Chin D-H; La Mar GN; Balch AL Role of ferryl (FeO^{2+}) complexes in oxygen atom transfer reactions. Mechanism of iron(II) porphyrin catalyzed oxygenation of triphenylphosphine J. Am. Chem. Soc 1980, 102, 5945–5947.

(84). Groves JT; Gross Z; Stern MK Preparation and Reactivity of Oxoiron(IV) Porphyrins Inorg. Chem 1994, 33, 5065–5072.

(85). Tahsini L; Bagherzadeh M; Nam W; de Visser SP Fundamental Differences of Substrate Hydroxylation by High-Valent Iron(IV)-Oxo Models of Cytochrome P450 Inorg. Chem 2009, 48, 6661–6669.19469505

(86). Fertinger C; Hessenauer-Ilicheva N; Franke A; van Eldik R Direct Comparison of the Reactivity of Model Complexes for Compounds 0, I, and II in Oxygenation, Hydrogen-Abstraction, and Hydride-Transfer Processes Chem. - Eur. J 2009, 15, 13435–13440.19876973

(87). Ji L; Franke A; Brindell M; Oszajca M; Zahl A; van Eldik R Combined Experimental and Theoretical Study on the Reactivity of Compounds I and II in Horseradish Peroxidase Biomimetics Chem. - Eur. J 2014, 20, 14437–14450.25220399

(88). Oszajca M; Franke A; Drzewiecka-Matuszek A; Brindell M; Stochel G; van Eldik R Temperature and Pressure Effects on C–H Abstraction Reactions Involving Compound I and II Mimics in Aqueous Solution Inorg. Chem 2014, 53, 2848–2857.24392857

(89). Nehru K; Seo MS; Kim J; Nam W Oxidative N-Dealkylation Reactions by Oxoiron(IV) Complexes of Nonheme and Heme Ligands Inorg. Chem 2007, 46, 293–298.17198439

(90). Kitagishi H; Kurosawa S; Kano K Intramolecular Oxidative O-Demethylation of an Oxoferryl Porphyrin Complexed with a Per-O-methylated β-Cyclodextrin Dimer Chem. Asian J 2016, 11, 3213–3219.27616336

(91). Ueda T; Kitagishi H; Kano K Intramolecular Direct Oxygen Transfer from Oxoferryl Porphyrin to a Sulfide Bond Inorg. Chem 2014, 53, 543–551.24328175

(92). Rosa A; Ricciardi G Reactivity of Compound II: Electronic Structure Analysis of Methane Hydroxylation by Oxoiron(IV) Porphyrin Complexes Inorg. Chem 2012, 51, 9833–9845.22946694

(93). Boaz NC; Bell SR; Groves JT Ferryl Protonation in Oxoiron(IV) Porphyrins and Its Role in Oxygen Transfer J. Am. Chem. Soc 2015, 137, 2875–2885.25651467

(94). McGown AJ; Badiei YM; Leeladee P; Prokop KA; DeBeer S; Goldberg DP In The Handbook of Porphyrin Science; Kadish KM, Smith KM, Guilard R, Eds.; World Scientific: New Jersey, 2011; Vol. 14, p 525–600.

(95). Vogel E; Will S; Tilling AS; Neumann L; Lex J; Bill E; Trautwein AX; Wieghardt K Metallocorroles with Formally Tetravalent Iron Angew. Chem., Int. Ed. Engl 1994, 33, 731–735.

(96). Gross Z High-valent corrole metal complexes J. Biol. Inorg. Chem 2001, 6, 733–738.11681707

(97). Simkhovich L; Mahammed A; Goldberg I; Gross Z Synthesis and Characterization of Germanium, Tin, Phosphorus, Iron, and Rhodium Complexes of Tris(pentafluorophenyl)corrole, and the Utilization of the Iron and Rhodium Corroles as Cyclopropanation Catalysts Chem. - Eur. J 2001, 7, 1041–1055.11303864

(98). Ye S; Tuttle T; Bill E; Simkhovich L; Gross Z; Thiel W; Neese F The Electronic Structure of Iron Corroles: A Combined Experimental and Quantum Chemical Study Chem. - Eur. J 2008, 14, 10839–10851.18956397

(99). Walker FA; Licoccia S; Paolesse R Iron corrolates: Unambiguous chloroiron(III) (corrolate)$2^{-\bullet}$ π-cation radicals J. Inorg. Biochem 2006, 100, 810–837.16519943

(100). Harischandra DN; Zhang R; Newcomb M Photochemical Generation of a Highly Reactive Iron–Oxo Intermediate. A True Iron(V)–Oxo Species? J. Am. Chem. Soc 2005, 127, 13776–13777.16201783

(101). Harischandra DN; Lowery G; Zhang R; Newcomb M Production of a Putative Iron(V)–Oxocorrole Species by Photo-Disproportionation of a Bis-Corrole–Diiron(IV)–μ-Oxo Dimer: Implication for a Green Oxidation Catalyst Organic Letters 2009, 11, 2089–2092.19361171

(102). Zhang R; Vanover E; Chen T-H; Thompson H Visible light-driven aerobic oxidation catalyzed by a diiron(IV) μ-oxo biscorrole complex Applied Catalysis A: General 2013, 464–465, 95–100.

(103). Wasbotten I; Ghosh A Theoretical Evidence Favoring True Iron(V)-Oxo Corrole and Corrolazine Intermediates Inorg. Chem 2006, 45, 4910–4913.16780311

(104). Latifi R; Valentine JS; Nam W; de Visser SP Predictive studies of H-atom abstraction reactions by an iron(iv)–oxo corrole cation radical oxidant Chem. Commun 2012, 48, 3491–3493.

(105). Avidan-Shlomovich S; Gross Z Reaction mechanism for the highly efficient catalytic decomposition of peroxynitrite by the amphipolar iron(iii) corrole 1-Fe Dalton Trans 2015, 44, 12234–12243.25747957

(106). Biswas AN; Pariyar A; Bose S; Das P; Bandyopadhyay P Mild oxidation of hydrocarbons catalyzed by iron corrole with tert-butylhydroperoxide Catal. Commun 2010, 11, 1008–1011.

(107). Schwalbe M; Dogutan DK; Stoian SA; Teets TS; Nocera DG Xanthene-Modified and Hangman Iron Corroles Inorg. Chem 2011, 50, 1368–1377.21244031

(108). Zyska B; Schwalbe M Synthesis of sterically hindered xanthene-modified iron corroles with catalase-like activity Chem. Commun 2013, 49, 3799–3801.

(109). McGown AJ; Kerber WD; Fujii H; Goldberg DP Catalytic Reactivity of a *Meso*-N-Substituted Corrole and Evidence for a High-Valent Iron–Oxo Species J. Am. Chem. Soc 2009, 131, 8040–8048.19462977

(110). Kerber WD; Ramdhanie B; Goldberg DP H2O2 Oxidations Catalyzed by an Iron(III) Corrolazine: Avoiding High-Valent Iron–Oxido Species? Angew. Chem., Int. Ed 2007, 46, 3718–3721.

(111). Kurahashi S; Ikeue T; Sugimori T; Takahashi M; Mikuriya M; Handa M; Ikezaki A; Nakamura M Formation and characterization of five- and six-coordinate iron(III) corrolazine complexes J. Porphyrins Phthalocyanines 2012, 16, 518–529.

(112). Cho K; Leeladee P; McGown AJ; DeBeer S; Goldberg DP A High-Valent Iron–Oxo Corrolazine Activates C–H Bonds via Hydrogen-Atom Transfer J. Am. Chem. Soc 2012, 134, 7392–7399.22489757

(113). Charnock JM; Garner CD; Trautwein AX; Bill E; Winkler H; Ayougou K; Mandon D; Weiss R Characterization of an Oxo(porphyrinato)manganese(IV) Complex by X-ray Absorption Spectroscopy Angew. Chem., Int. Ed. Engl 1995, 34, 343–346.

(114). Groves JT; Lee J; Marla SS Detection and Characterization of an Oxomanganese(V) Porphyrin Complex by Rapid-Mixing Stopped-Flow Spectrophotometry J. Am. Chem. Soc 1997, 119, 6269–6273.

(115). Jin N; Groves JT Unusual Kinetic Stability of a Ground-State Singlet Oxomanganese(V) Porphyrin. Evidence for a Spin State Crossing Effect J. Am. Chem. Soc 1999, 121, 2923–2924.

(116). Meunier B; de Visser S. l. P.; Shaik S Mechanism of Oxidation Reactions Catalyzed by Cytochrome P450 Enzymes Chem. Rev 2004, 104, 3947–3980.15352783

(117). Meunier B Metalloporphyrins as versatile catalysts for oxidation reactions and oxidative DNA cleavage Chem. Rev 1992, 92, 1411–1456.

(118). Nam W; Kim I; Lim MH; Choi HJ; Lee JS; Jang HG Isolation of an Oxomanganese(V) Porphyrin Intermediate in the Reaction of a Manganese(III) Porphyrin Complex and H2O2 in Aqueous Solution Chem. - Eur. J 2002, 8, 2067–2071.11981891

(119). Albin V; Bedioui F First electrochemical evidence of existence of an oxomanganese(V) porphyrin intermediate in the reaction of manganese(III) porphyrin and hydrogen peroxide as a model of enzyme mimetics Electrochem. Commun 2003, 5, 129–132.

(120). Shimazaki Y; Nagano T; Takesue H; Ye B-H; Tani F; Naruta Y Characterization of a Dinuclear Mn^{V}=O Complex and Its Efficient Evolution of O_2 in the Presence of Water Angew. Chem., Int. Ed 2004, 43, 98–100.

(121). Zhang R; Newcomb M Laser Flash Photolysis Formation and Direct Kinetic Studies of Manganese(V)-Oxo Porphyrin Intermediates J. Am. Chem. Soc 2003, 125, 12418–12419.14531679

(122). Zhang R; Horner JH; Newcomb M Laser Flash Photolysis Generation and Kinetic Studies of Porphyrin–Manganese–Oxo Intermediates. Rate Constants for Oxidations Effected by Porphyrin–MnV–Oxo Species and Apparent Disproportionation Equilibrium Constants for Porphyrin–MnIV–Oxo Species J. Am. Chem. Soc 2005, 127, 6573–6582.15869278

(123). Kwong KW; Winchester CM; Zhang R Photochemical generation of manganese(IV)-oxo porphyrins by visible light photolysis of dimanganese(III) μ-oxo bis-porphyrins Inorg. Chim. Acta 2016, 451, 202–206.

(124). De Angelis F; Jin N; Car R; Groves JT Electronic Structure and Reactivity of Isomeric Oxo-Mn(V) Porphyrins: Effects of Spin-State Crossing and pKa Modulation Inorg. Chem 2006, 45, 4268–4276.16676990

(125). Balcells D; Raynaud C; Crabtree RH; Eisenstein O The rebound mechanism in catalytic C-H oxidation by MnO(tpp)Cl from DFT studies: electronic nature of the active species Chem. Commun 2008, 744–746.

(126). Sameera WMC; McGrady JE The role of substrate in unmasking oxyl character in oxomanganese complexes: the key to selectivity? Dalton Trans. 2008, 6141–6149.18985246

(127). Li H-B; Tian SX; Yang J Theoretical Study of the Stepwise Protonation of the Dioxo Manganese(V) Porphyrin J. Phys. Chem. B 2008, 112, 15807–15812.19367950

(128). Balcells D; Raynaud C; Crabtree RH; Eisenstein O A Rational Basis for the Axial Ligand Effect in C–H Oxidation by [MnO(porphyrin)(X)]+ (X = H_2O, OH^-, O^{2-}) from a DFT Study Inorg. Chem 2008, 47, 10090–10099.18788735

(129). Balcells D; Raynaud C; Crabtree RH; Eisenstein O C-H oxidation by hydroxo manganese(v) porphyrins: a DFT study Chem. Commun 2009, 1772–1774.

(130). Silaghi-Dumitrescu R High-valent metalloporphyrins in hydrocarbon activation: metal(v)-oxo or metal(v)-hydroxo? New J. Chem 2010, 34, 1830–1833.

(131). Venturinelli Jannuzzi SA; Phung QM; Domingo A; Formiga ALB; Pierloot K Spin State Energetics and Oxyl Character of Mn-Oxo Porphyrins by Multiconfigurational ab Initio Calculations: Implications on Reactivity Inorg. Chem 2016, 55, 5168–5179.26901395

(132). Kavousi H; Rezaeifard A; Raissi H; Jafarpour M A DFT investigation of axial N-donor ligands effects on the high valent manganese-oxo meso-tetraphenyl porphyrin J. Porphyrins Phthalocyanines 2015, 19, 651–662.

(133). Rezaeifard A; Kavousi H; Raissi H; Jafarpour M Significant hydrogen-bonding effect on the reactivity of high-valent manganese(V)–oxo porphyrins in C–H bond activation: A DFT study J. Porphyrins Phthalocyanines 2015, 19, 1197–1203.

(134). Lahaye D; Groves JT Modeling the haloperoxidases: Reversible oxygen atom transfer between bromide ion and an oxo-Mn(V) porphyrin J. Inorg. Biochem 2007, 101, 1786–1797.17825916

(135). Song WJ; Seo MS; DeBeer George S; Ohta T; Song R; Kang M-J; Tosha T; Kitagawa T; Solomon EI; Nam W Synthesis, Characterization, and Reactivities of Manganese(V)–Oxo Porphyrin Complexes J. Am. Chem. Soc 2007, 129, 1268–1277.17263410

(136). Baglia RA; Prokop-Prigge KA; Neu HM; Siegler MA; Goldberg DP Mn(V)(O) versus Cr(V)(O) Porphyrinoid Complexes: Structural Characterization and Implications for Basicity Controlling H-Atom Abstraction J. Am. Chem. Soc 2015, 137, 10874–10877.26295412

(137). Gross Z The Groves–Spiro Dioxomanganese(V) Story Angew. Chem., Int. Ed 2008, 47, 2737–2739.

(138). Jin N; Ibrahim M; Spiro TG; Groves JT Trans-dioxo Manganese(V) Porphyrins J. Am. Chem. Soc 2007, 129, 12416–12417.17887684

(139). Lee JY; Lee Y-M; Kotani H; Nam W; Fukuzumi S High-valent manganese(v)-oxo porphyrin complexes in hydride transfer reactions Chem. Commun 2009, 704–706.

(140). Jung J; Ohkubo K; Goldberg DP; Fukuzumi S Photocatalytic Oxygenation of 10-Methyl-9,10-dihydroacridine by O2 with Manganese Porphyrins J. Phys. Chem. A 2014, 118, 6223–6229.25079061

(141). Arunkumar C; Lee Y-M; Lee JY; Fukuzumi S; Nam W Hydrogen-Atom Abstraction Reactions by Manganese(V)–and Manganese(IV)–Oxo Porphyrin Complexes in Aqueous Solution Chem. - Eur. J 2009, 15, 11482–11489.19810056

(142). Cho K-B; Nam W A theoretical study into a trans-dioxo MnV porphyrin complex that does not follow the oxygen rebound mechanism in C-H bond activation reactions Chem. Commun 2016, 52, 904–907.

(143). Fukuzumi S; Fujioka N; Kotani H; Ohkubo K; Lee Y-M; Nam W Mechanistic Insights into Hydride-Transfer and Electron-Transfer Reactions by a Manganese(IV)–Oxo Porphyrin Complex J. Am. Chem. Soc 2009, 131, 17127–17134.19888722

(144). Latifi R; Tahsini L; Karamzadeh B; Safari N; Nam W; de Visser SP Manganese substituted Compound I of cytochrome P450 biomimetics: A comparative reactivity study of MnV-oxo versus MnIV-oxo species Arch. Biochem. Biophys 2011, 507, 4–13.21216220

(145). Crestoni ME; Fornarini S; Lanucara F Oxygen-Atom Transfer by a Naked Manganese(V)–Oxo–Porphyrin Complex Reveals Axial Ligand Effect Chem. - Eur. J 2009, 15, 7863–7866.19610004

(146). Chiavarino B; Crestoni ME; Fornarini S; Lanucara F Probing bare high-valent transition oxo-metal complexes: an electrospray ionization Fourier transform ion cyclotron resonance study of reactive intermediates Eur J Mass Spectrom (Chichester, Eng) 2010, 16, 407–414.

(147). Lanucara F; Crestoni ME Biomimetic Oxidation Reactions of a Naked Manganese(V)–Oxo Porphyrin Complex Chem. - Eur. J 2011, 17, 12092–12100.21905135

(148). Fukuzumi S; Mizuno T; Ojiri T Catalytic Electron-Transfer Oxygenation of Substrates with Water as an Oxygen Source Using Manganese Porphyrins Chem. - Eur. J 2012, 18, 15794–15804.23129350

(149). Mohajer D; Abbasi M Solvent Effects on Catalytic Epoxidation of Alkenes by Tetra-n-butylammonium Periodate and (Tetraarylporphyrinato)manganese(III) Eur. J. Inorg. Chem 2008, 2008, 3218–3224.

(150). Mohajer D; Jahanbani M A UV–vis study of the effects of alcohols on formation and stability of Mn(por)(O)(OAc) complexes Spectrochim. Acta, Part A 2012, 91, 360–364.

(151). Umile TP; Groves JT Catalytic Generation of Chlorine Dioxide from Chlorite Using a Water-Soluble Manganese Porphyrin Angew. Chem., Int. Ed 2011, 50, 695–698.

(152). Umile TP; Wang D; Groves JT Dissection of the Mechanism of Manganese Porphyrin-Catalyzed Chlorine Dioxide Generation Inorg. Chem 2011, 50, 10353–10362.21936530

(153). Liu W; Groves JT Manganese Catalyzed C–H Halogenation Acc. Chem. Res 2015, 48, 1727–1735.26042637

(154). Liu H-Y; Mahmood MHR; Qiu S-X; Chang CK Recent developments in manganese corrole chemistry Coord. Chem. Rev 2013, 257, 1306–1333.

(155). Yu L; Wang Q; Dai L; Li W-Y; Chen R; Mahmood MHR; Liu H-Y; Chang C-K Solvent effects on oxygen atom transfer reaction between manganese(V)-oxo corrole and alkene Chin. Chem. Lett 2013, 24, 447–449.

(156). Wang Q; Zhang Y; Yu L; Yang H; Mahmood MH; Liu H-Y Solvent effects on the catalytic activity of manganese(III) corroles J. Porphyrins Phthalocyanines 2014, 18, 316–325.

(157). Mahmood MH; Wang H-H; Liu H-Y; Chang C-K Oxygen atom transfer reactions from sterically encumbered brominated (oxo)manganese(V) corroles to styrene J. Porphyrins Phthalocyanines 2015, 19, 1238–1250.

(158). He J; Xu Z-G; Xu X; Gong L-Z; Mahmood MH; Liu H-Y Reactivity of (oxo)manganese(V) corroles in one-electron redox state: insights from conceptual DFT and transition state calculations J. Porphyrins Phthalocyanines 2013, 17, 1196–1203.

(159). He Jing, X. Z-G, Zeng Yun-Xiu, Xu Xuan, Yu Lan, Wang Qi, Liu Hai-Yang Effect of Substituents on Mn–O Bond in Oxo-Manganese(V) Corrole Complexes Acta Phys. -Chim. Sin 2012, 28, 1658–1664.

(160). Zhu C; Liang J; Wang B; Zhu J; Cao Z Significant effect of spin flip on the oxygen atom transfer reaction from (oxo)manganese(v) corroles to thioanisole: insights from density functional calculations Phys. Chem. Chem. Phys 2012, 14, 12800–12806.22874974

(161). Jung J; Liu S; Ohkubo K; Abu-Omar MM; Fukuzumi S Catalytic Two-Electron Reduction of Dioxygen by Ferrocene Derivatives with Manganese(V) Corroles Inorg. Chem 2015, 54, 4285–4291.25867007

(162). Guntner A; Faschinger F; Aichhorn S; Müllegger S; Schöfberger W Observation of High-Valent Manganese(V)–Corrole Complexes During Metalation of meso-Functionalized A3-Corroles under Aerobic Conditions Synlett 2015, 26, 2180–2184.

(163). Bougher CJ; Liu S; Hicks SD; Abu-Omar MM Valence Tautomerization of High-Valent Manganese(V)-Oxo Corrole Induced by Protonation of the Oxo Ligand J. Am. Chem. Soc 2015, 137, 14481–14487.26517943

(164). Ka WK; Ngo FL; Ranburger D; Malone J; Zhang R Visible light-induced formation of corrole-manganese(V)-oxo complexes: Observation of multiple oxidation pathways J. Inorg. Biochem 2016, 163, 39–44.27513949

(165). Ng N-C; Mahmood MHR; Liu H-Y; Yam F; Yeung L-L; Chang C-K Appended corrole manganese complexes: Catalysis and axial-ligand effect Chin. Chem. Lett 2014, 25, 571–574.

(166). Neu HM; Baglia RA; Goldberg DP A Balancing Act: Stability versus Reactivity of Mn(O) Complexes Acc. Chem. Res 2015, 48, 2754–2764.26352344

(167). Joslin EE; Zaragoza JPT; Baglia RA; Siegler MA; Goldberg DP The Influence of Peripheral Substituent Modification on PV, MnIII, and MnV(O) Corrolazines: X-ray Crystallography, Electrochemical and Spectroscopic Properties, and HAT and OAT Reactivities Inorg. Chem 2016, Article ASAP.

(168). Jung J; Neu HM; Leeladee P; Siegler MA; Ohkubo K; Goldberg DP; Fukuzumi S Photocatalytic Oxygenation of Substrates by Dioxygen with Protonated Manganese(III) Corrolazine Inorg. Chem 2016, 55, 3218–3228.26974004

(169). Zhao H; Pierloot K; Langner EHG; Swarts JC; Conradie J; Ghosh A Low-Energy States of Manganese–Oxo Corrole and Corrolazine: Multiconfiguration Reference ab Initio Calculations Inorg. Chem 2012, 51, 4002–4006.22432719

(170). Prokop KA; de Visser SP; Goldberg DP Unprecedented Rate Enhancements of Hydrogen-Atom Transfer to a Manganese(V)–Oxo Corrolazine Complex Angew. Chem., Int. Ed 2010, 49, 5091–5095.

(171). Janardanan D; Usharani D; Shaik S The Origins of Dramatic Axial Ligand Effects: Closed-Shell MnVO Complexes Use Exchange-Enhanced Open-Shell States to Mediate Efficient H Abstraction Reactions Angew. Chem., Int. Ed 2012, 51, 4421–4425.

(172). Neu HM; Yang T; Baglia RA; Yosca TH; Green MT; Quesne MG; de Visser SP; Goldberg DP Oxygen-Atom Transfer Reactivity of Axially Ligated Mn(V)–Oxo Complexes: Evidence for Enhanced Electrophilic and Nucleophilic Pathways J. Am. Chem. Soc 2014, 136, 13845–13852.25238495

(173). Neu HM; Quesne MG; Yang T; Prokop-Prigge KA; Lancaster KM; Donohoe J; DeBeer S; de Visser SP; Goldberg DP Dramatic Influence of an Anionic Donor on the Oxygen-Atom Transfer Reactivity of a MnV–Oxo Complex Chem. - Eur. J 2014, 20, 14584–14588.25256417

(174). Yang T; Quesne MG; Neu HM; Cantú Reinhard FG; Goldberg DP; de Visser SP Singlet versus Triplet Reactivity in an Mn(V)–Oxo Species: Testing Theoretical Predictions Against Experimental Evidence J. Am. Chem. Soc 2016, 138, 12375–12386.27545752

(175). Liu W; Huang X; Cheng M-J; Nielsen RJ; Goddard WA; Groves JT Oxidative Aliphatic C-H Fluorination with Fluoride Ion Catalyzed by a Manganese Porphyrin Science 2012, 337, 1322–1325.22984066

(176). Simkhovich L; Gross Z Halogeno-Coordinated Iron Corroles Inorg. Chem 2004, 43, 6136–6138.15446854

(177). Momenteau M; Reed CA Synthetic Heme-Dioxygen Complexes Chem. Rev 1994, 94, 659–698.

(178). Shikama K Stability properties of dioxygen-iron(II) porphyrins: an overview from simple complexes to myoglobin Coord. Chem. Rev 1988, 83, 73–91.

(179). Collman JP; Boulatov R; Sunderland CJ In The Porphyrin Handbook; Kadish KM, Smith KM, Guilard R, Eds.; Academic Press: San Diego, CA, USA, 2003; Vol. 11, p 1–49.

(180). Collman JP; Boulatov R; Sunderland CJ; Fu L Functional Analogues of Cytochrome c Oxidase, Myoglobin, and Hemoglobin Chem. Rev 2004, 104, 561–588.14871135

(181). Kim E; Chufán EE; Kamaraj K; Karlin KD Synthetic Models for Heme– Copper Oxidases Chem. Rev 2004, 104, 1077–1134.14871150

(182). Ohta T; Liu J-G; Naruta Y Resonance Raman characterization of mononuclear heme-peroxo intermediate models Coord. Chem. Rev 2013, 257, 407–413.

(183). Duerr K; Troeppner O; Olah J; Li J; Zahl A; Drewello T; Jux N; Harvey JN; Ivanovic-Burmazovic I Solution behavior of iron(iii) and iron(ii) porphyrins in DMSO and reaction with superoxide. Effect of neighboring positive charge on thermodynamics, kinetics and nature of iron-(su)peroxo product Dalton Trans. 2012, 41, 546–557.22045167

(184). Franke A; Fertinger C; van Eldik R Axial Ligand and Spin-State Influence on the Formation and Reactivity of Hydroperoxo–Iron(III) Porphyrin Complexes Chem. - Eur. J 2012, 18, 6935–6949.22532376

(185). Wang B; Li C; Cho K-B; Nam W; Shaik S The FeIII(H2O2) Complex as a Highly Efficient Oxidant in Sulfoxidation Reactions: Revival of an Underrated Oxidant in Cytochrome P450 J. Chem. Theory Comput 2013, 9, 2519–2525.26583848

(186). Ohta T; Liu J-G; Nagaraju P; Ogura T; Naruta Y A cryo-generated ferrous-superoxo porphyrin: EPR, resonance Raman and DFT studies Chem. Commun 2015, 51, 12407–12410.

(187). Nagaraju P; Ohta T; Liu J-G; Ogura T; Naruta Y The secondary coordination sphere controlled reactivity of a ferric-superoxo heme: unexpected conversion to a ferric hydroperoxo intermediate by reaction with a high-spin ferrous heme Chem. Commun 2016, 52, 7213–7216.

(188). Sahu S; Goldberg DP Activation of Dioxygen by Iron and Manganese Complexes: A Heme and Nonheme Perspective J. Am. Chem. Soc 2016, 138, 11410–11428.27576170

(189). McLain JL; Lee J; Groves JT In Biomimetic Oxidations Catalyzed by Transition Metal Complexes; Published by Imperial College Press and distributed by World Scientific Publishing Co.: 2011, p 91–169.

(190). Weschler CJ; Hoffman BM; Basolo F Synthetic oxygen carrier. Dioxygen adduct of a manganese porphyrin J. Am. Chem. Soc 1975, 97, 5278–5280.170324

(191). Hoffman BM; Weschler CJ; Basolo F The dioxygen adduct of meso-tetraphenylporphyrinmanganese(II), a synthetic oxygen carrier J. Am. Chem. Soc 1976, 98, 5473–5482.956568

(192). Hoffman BM; Szymanski T; Brown TG; Basolo F The dioxygen adducts of several manganese(II) porphyrins. Electron paramagnetic resonance studies J. Am. Chem. Soc 1978, 100, 7253–7259.

(193). Hanson LK Axial ligand effects on iron and manganese porphyrins: Extended hückel calculations of cyt p450 analogs and of O2 binding to iron and manganese Int. J. Quantum Chem 1979, 16, 73–87.

(194). Urban MW; Nakamoto K; Basolo F Infrared spectra of molecular oxygen adducts of (tetraphenylporphyrinato)manganese(II) in argon matrixes Inorg. Chem 1982, 21, 3406–3408.

(195). Dedieu A; Rohmer MM Oxygen binding to manganese porphyrin. An ab initio calculation J. Am. Chem. Soc 1977, 99, 8050–8051.

(196). Newton JE; Hall MB Generalized molecular orbital calculations on transition-metal dioxygen complexes: model for manganese porphyrin Inorg. Chem 1985, 24, 2573–2577.

(197). Valentine JS; Quinn AE Reaction of superoxide with the manganese(III) tetraphenylporphine cation Inorg. Chem 1976, 15, 1997–1999.

(198). Shirazi A; Goff HM Characterization of superoxide-metalloporphyrin reaction products: effective use of deuterium NMR spectroscopy J. Am. Chem. Soc 1982, 104, 6318–6322.

(199). Nakagaki PC; Calderwood TS; Bruice TC Relevance of the reaction of a manganese(III) chelate with hydroxide ion to photosynthesis: Reaction of hydroxide ion with 5,10,15,20-tetrakis(2,4,6-trimethylphenyl)porphinatomanganese(III) in ligating and nonligating solvents Proc. Natl. Acad. Sci 1988, 85, 5424–5428.16593963

(200). VanAtta RB; Strouse CE; Hanson LK; Valentine JS Peroxo(tetraphenylporphinato)manganese(III) and chloro(tetraphenylporphinato)manganese(II) anions. Synthesis, crystal structures, and electronic structures J. Am. Chem. Soc 1987, 109, 1425–1434.

(201). Jones RD; Summerville DA; Basolo F Manganese(II) porphyrin oxygen carriers. Equilibrium constants for the reaction of dioxygen with para-substituted meso-tetraphenylporphinatomanganese(II) complexes J. Am. Chem. Soc 1978, 100, 4416–4424.

(202). Basolo F; Jones RD; Summerville DA Equilibrium Constants for the Axial Coordination of meso-Tetraphenylporphinatomanganese(II) and -chromium(III) Complexes. Acta Chemica Scandinavica 1978, 32A, 771–780.

(203). Groves JT; Watanabe Y; McMurry TJ Oxygen activation by metalloporphyrins. Formation and decomposition of an acylperoxymanganese(III) complex J. Am. Chem. Soc 1983, 105, 4489–4490.

(204). Groves JT; Watanabe Y Heterolytic and homolytic oxygen-oxygen bond cleavage reactions of acylperoxomanganese(III) porphyrins Inorg. Chem 1986, 25, 4808–4810.

(205). Schappacher M; Weiss R Formation of manganese(IV)-oxo-porphyrin derivatives by decomposition of peroxycarbonate complexes Inorg. Chem 1987, 26, 1189–1190.

(206). Sisemore MF; Selke M; Burstyn JN; Valentine JS Metalloporphyrin Peroxo Complexes of Iron(III), Manganese(III), and Titanium(IV). Comparative Studies Demonstrating That the Iron(III) Complex Is Extremely Nucleophilic Inorg. Chem 1997, 36, 979–984.11669659

(207). Jin N; Lahaye DE; Groves JT A “Push–Pull” Mechanism for Heterolytic O–O Bond Cleavage in Hydroperoxo Manganese Porphyrins Inorg. Chem 2010, 49, 11516–11524.21080695

(208). Gao Y; Åkermark T; Liu J; Sun L; Åkermark B Nucleophilic Attack of Hydroxide on a MnV Oxo Complex: A Model of the O–O Bond Formation in the Oxygen Evolving Complex of Photosystem II J. Am. Chem. Soc 2009, 131, 8726–8727.19496534

(209). Kim SH; Park H; Seo MS; Kubo M; Ogura T; Klajn J; Gryko DT; Valentine JS; Nam W Reversible O–O Bond Cleavage and Formation between Mn(IV)-Peroxo and Mn(V)-Oxo Corroles J. Am. Chem. Soc 2010, 132, 14030–14032.20845972

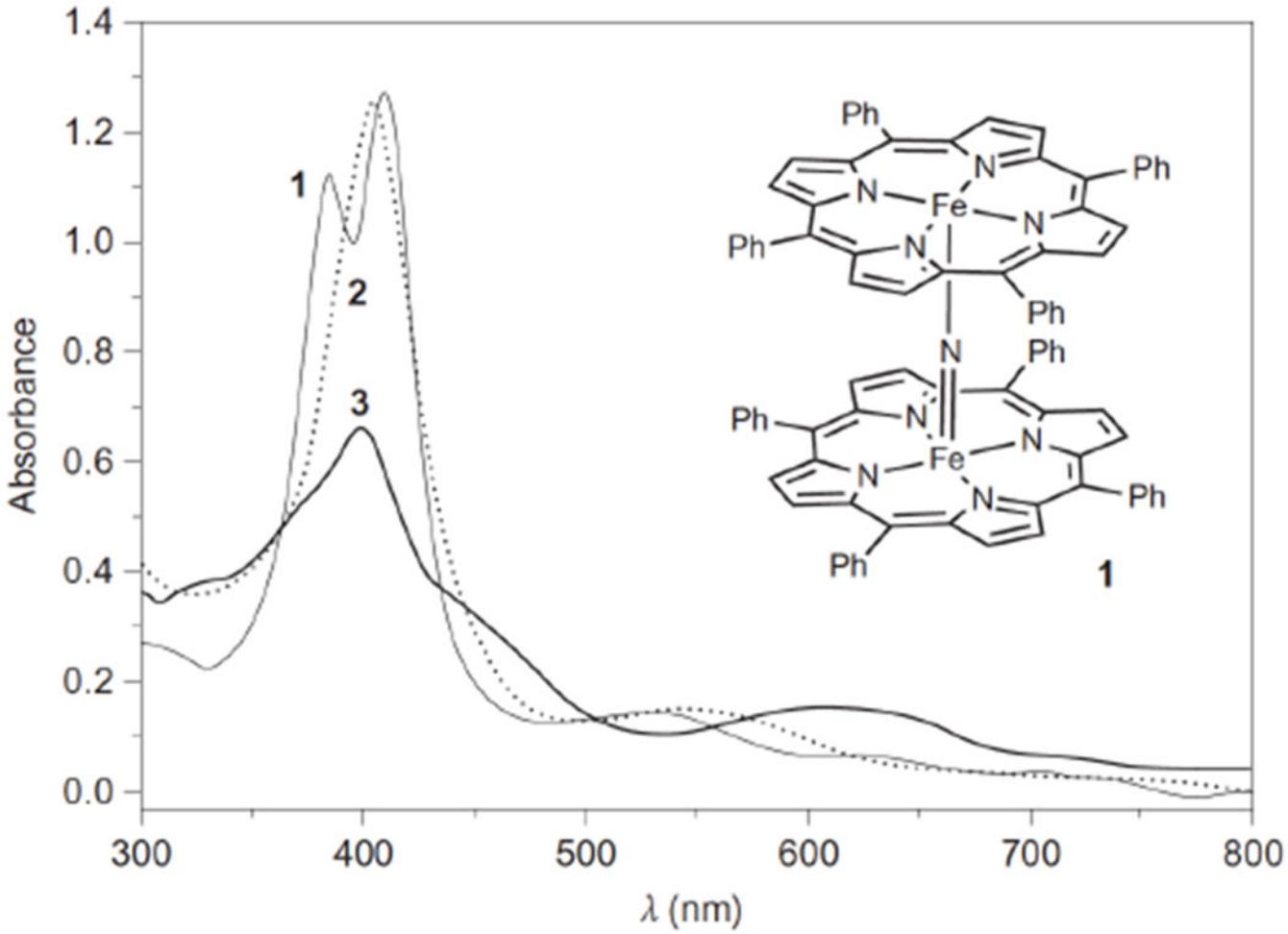

Figure 1.

UV-vis spectral changes from the starting [(TPP)Fe^{III}(N)Fe^{IV}(TPP)] (1), formation of the mcpba adduct (2), and [(TPP)(*m*-CBA)Fe^{IV}(N)Fe^{IV}(O)($TPP^{\bullet+}$)]$^{-}$ (3) in CH_2Cl_2 at −80 °C. Reprinted by permission from Macmillan Publishers Ltd: Nature Chemistry, *Nature Chemistry* 4, 1024–1029 (2012), copyright 2012.

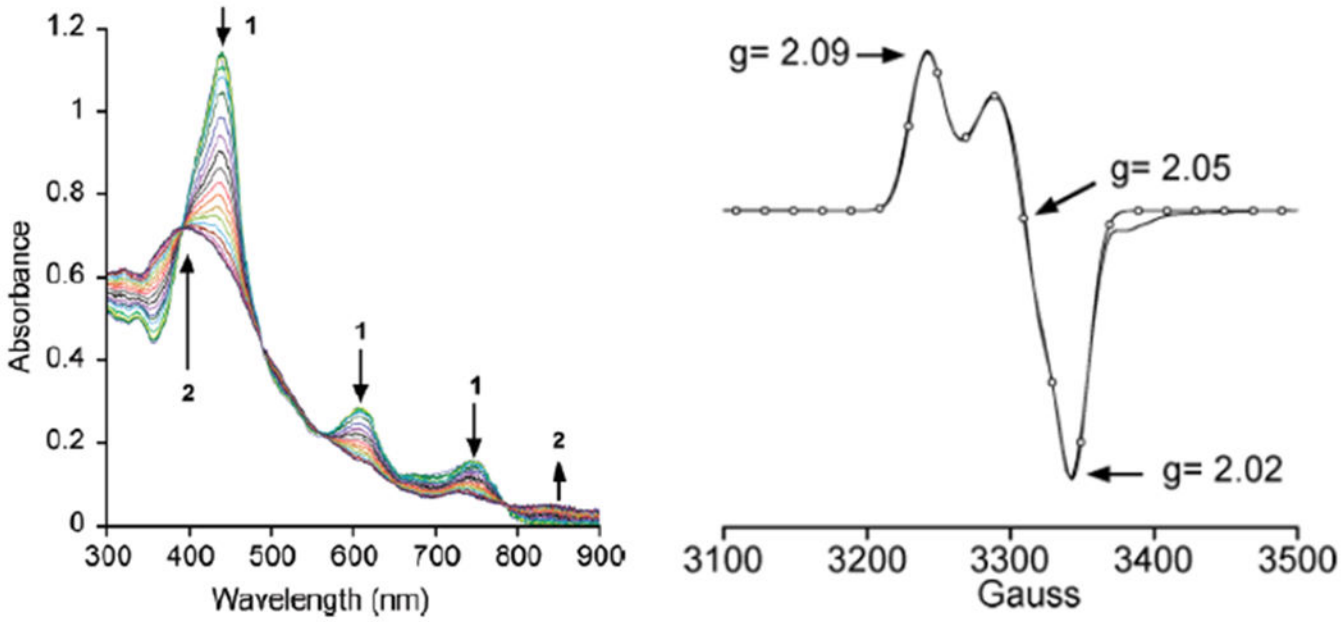

Figure 2.

Left: Time-resolved UV-vis spectrum upon addition of PFIB to $Fe^{III}(TBP_8Cz)$ in CH_2Cl_2/CH_3OH at −78 °C. Right: X-band EPR spectrum of $Fe^{IV}(O)(TBP_8Cz^{\bullet+})$ at 15 K. Reprinted with permission from *J. Am. Chem. Soc.*, 2009, *131* (23), pp 8040–8048. Copyright 2009 American Chemical Society.

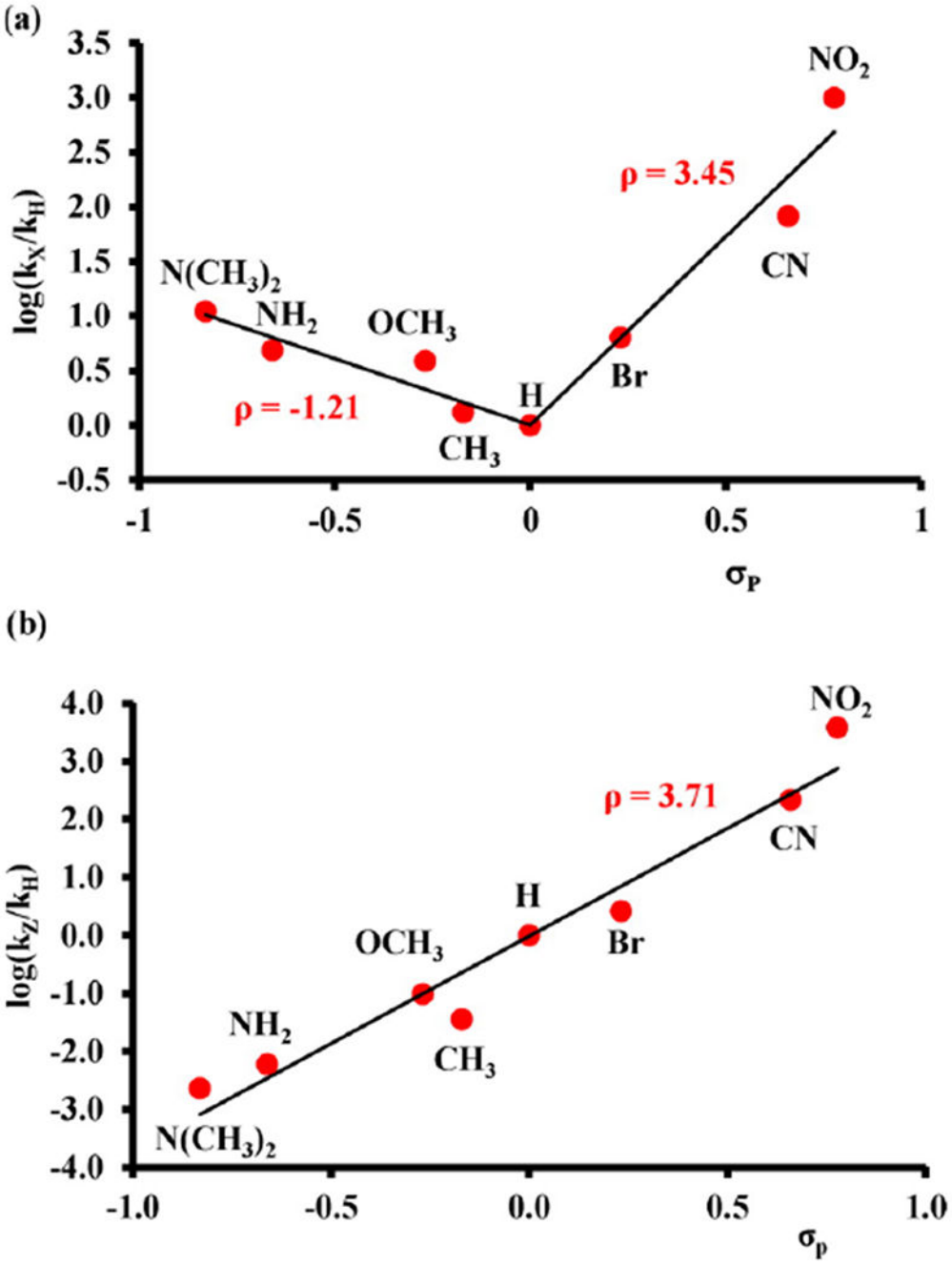

Figure 3.

Computational Hammett plot for the reaction of singlet and triplet $[Mn(O)(H_8Cz)(CN)]^-$ with para-Z-substituted thioanisole derivatives. Data calculated at RIJCOSX-TPSSh-D3/def2-QZVPP/ZORA//RIJCOSX-B3LYP-D3/SDD/BS2 and includes zero-point, thermal, and solvent corrections. (a) Correlation for singlet spin barriers. (b) Correlation for triplet spin barriers. Reproduced with permission from reference [174]. Copyright 2016 American Chemical Society.

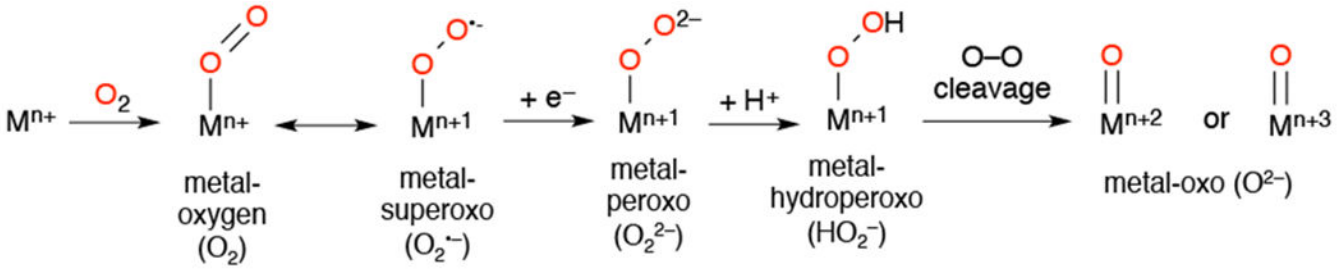

Scheme 1.
Common Metal-Oxygen Intermediates Utilized by Metalloproteins

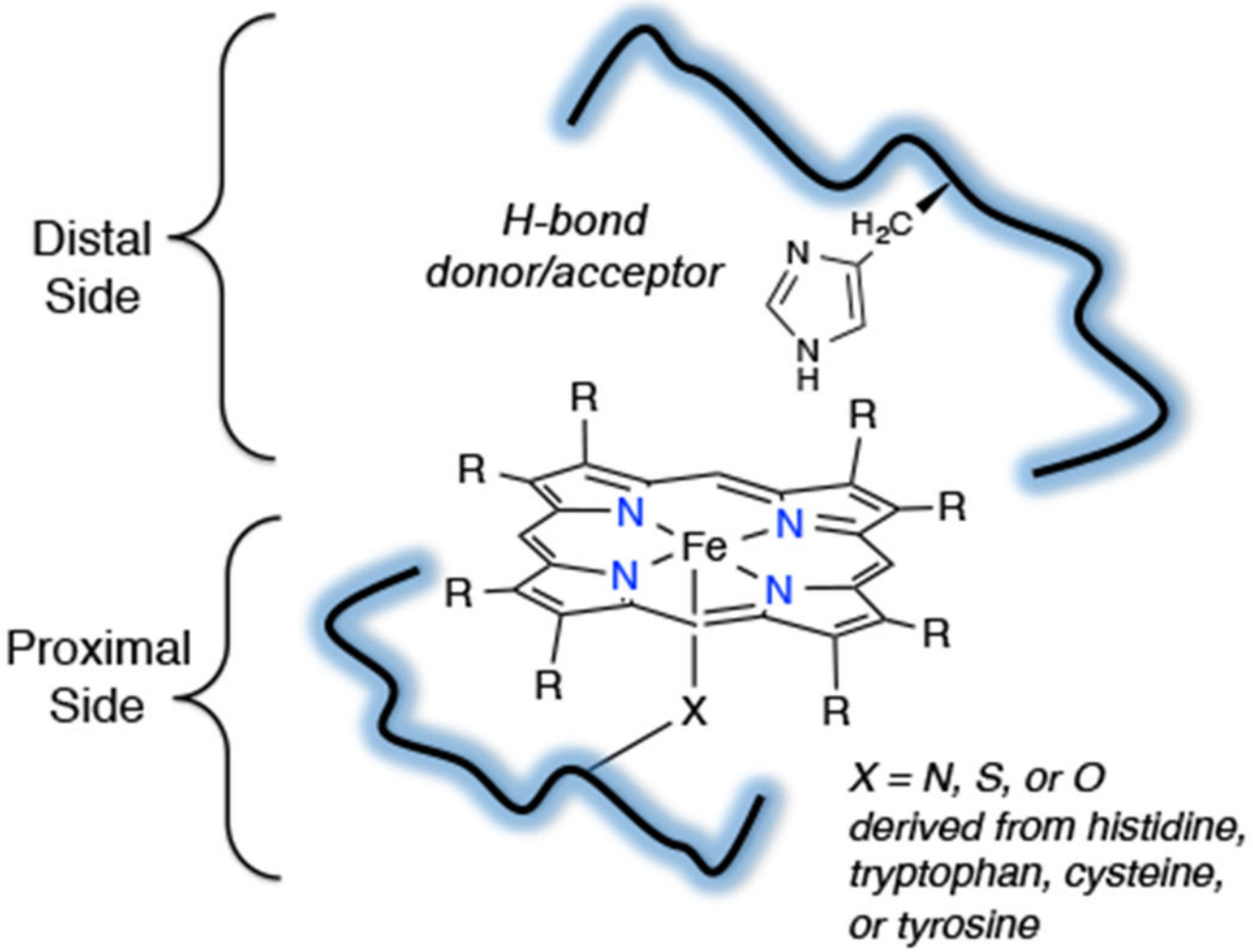

Scheme 2.
Structural Factors that Affect Reactivity in Heme Proteins

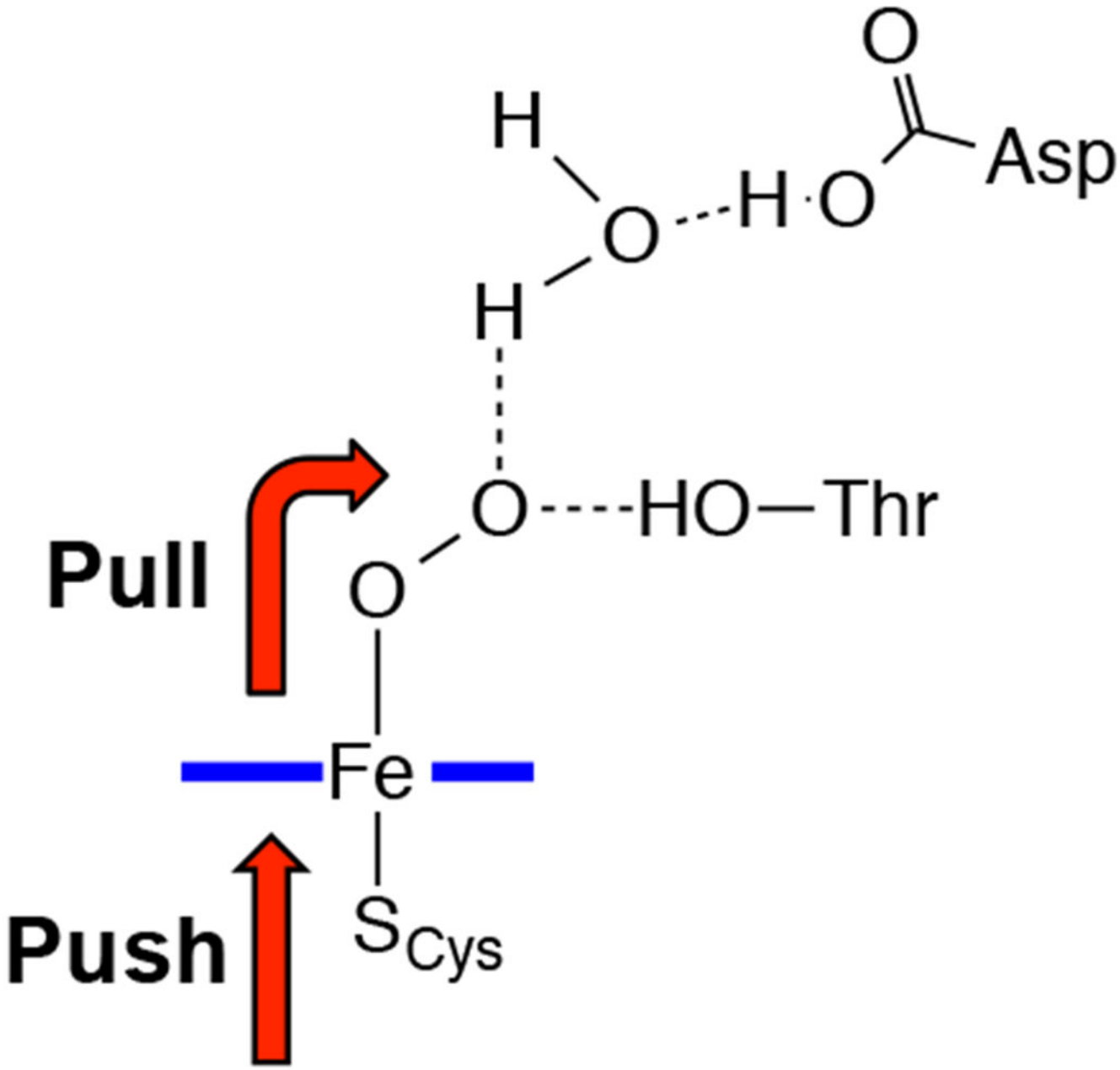

Scheme 3.

Push/Pull Effects of Axial Ligand and Distal Residues on O–O Bond Cleavage in Cytochrome P450

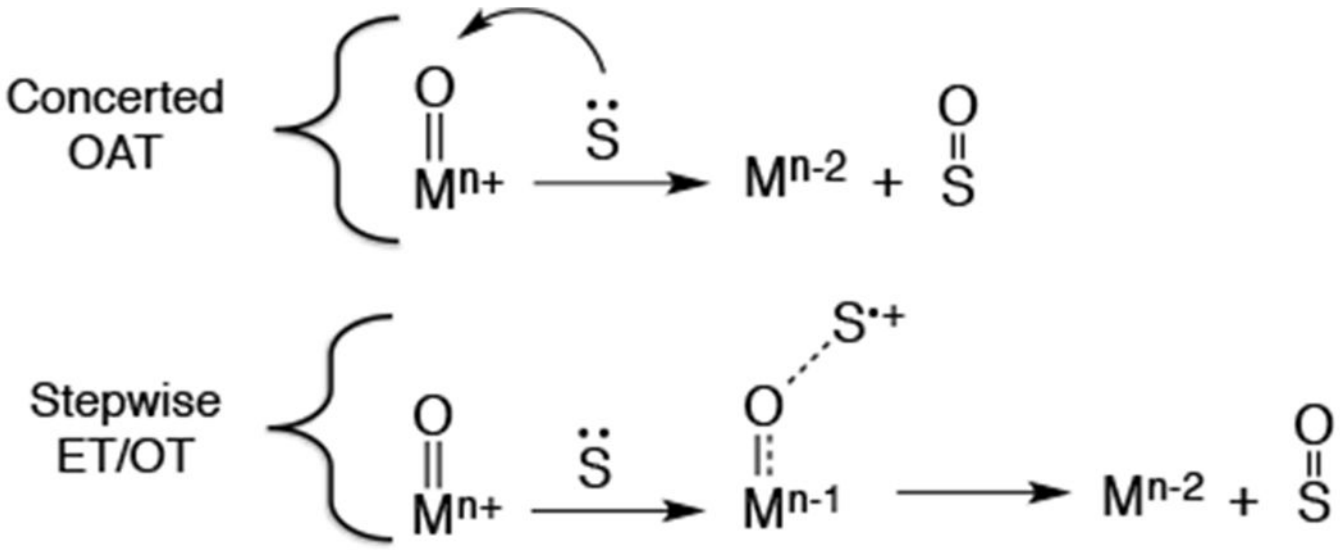

Scheme 4.
Possible Mechanisms for Oxygen Atom Transfer from a Metal-Oxo Complex

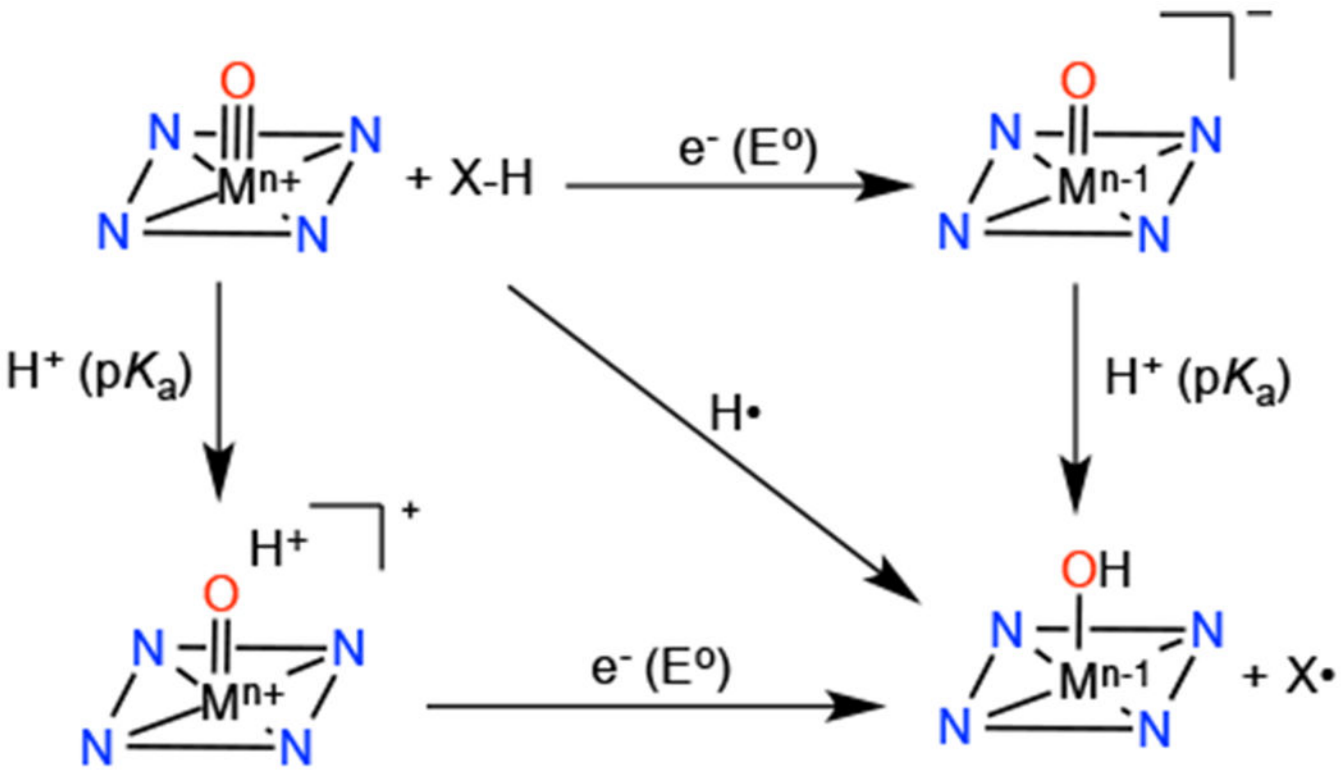

Scheme 5.
Square Scheme Depicting H-atom Transfer to a Metal-Oxo Complex

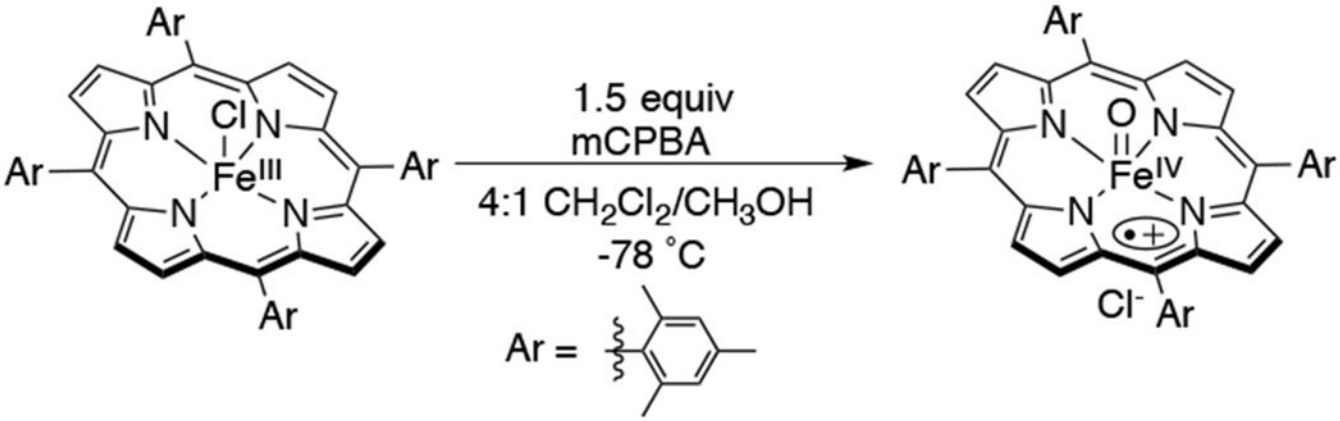

Scheme 6.
Synthesis of $Fe^{IV}(O)(TMP^{\bullet+})$, an Early Compound I Analog

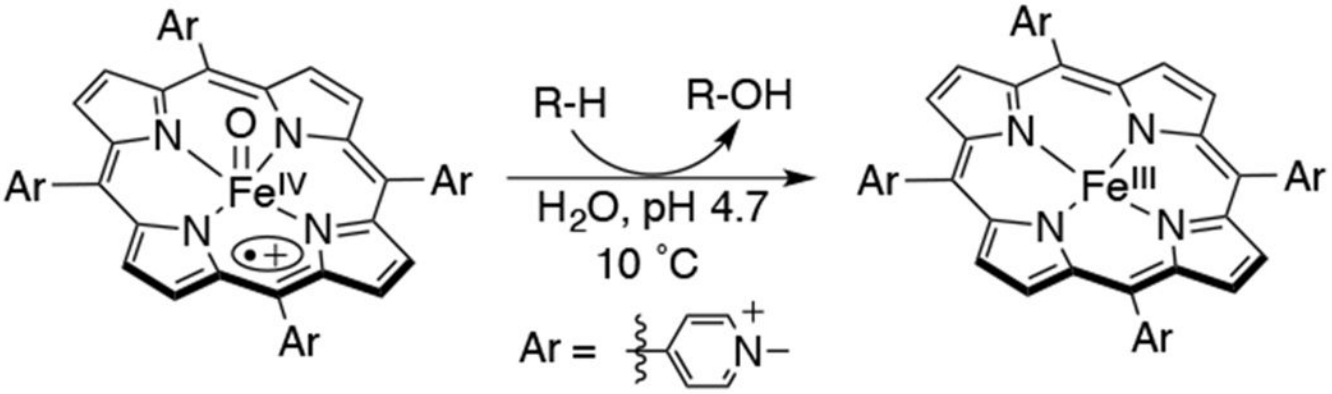

Scheme 7.

Reactivity of $Fe^{IV}(O)(TMPyP^{\bullet+})$, a Highly Reactive Compound I Model Complex

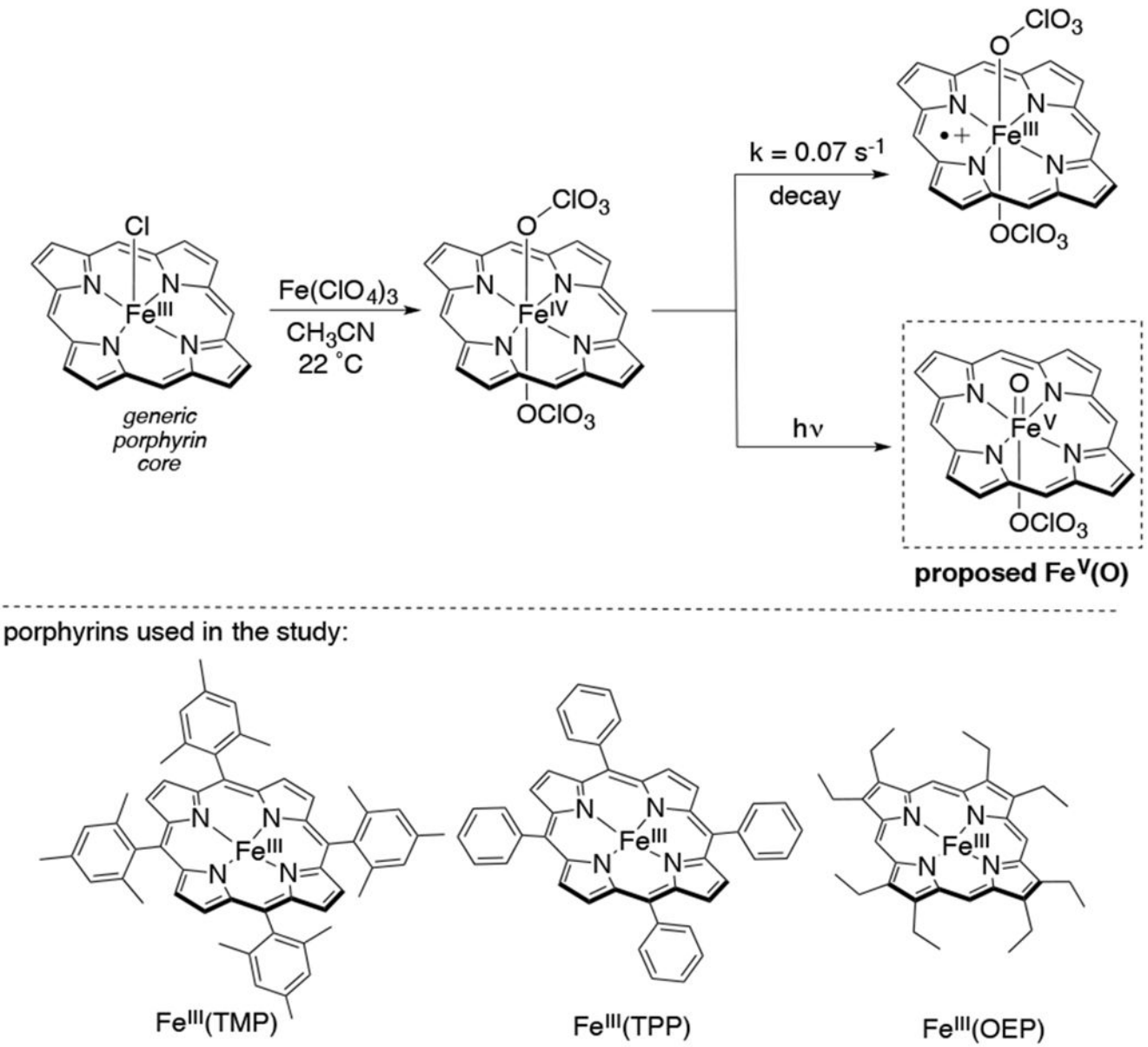

Scheme 8.

Synthesis of a Proposed $Fe^{V}(O)$ Intermediate by Laser-Flash Photolysis, and Different Porphyrin Ligands Used in the Study

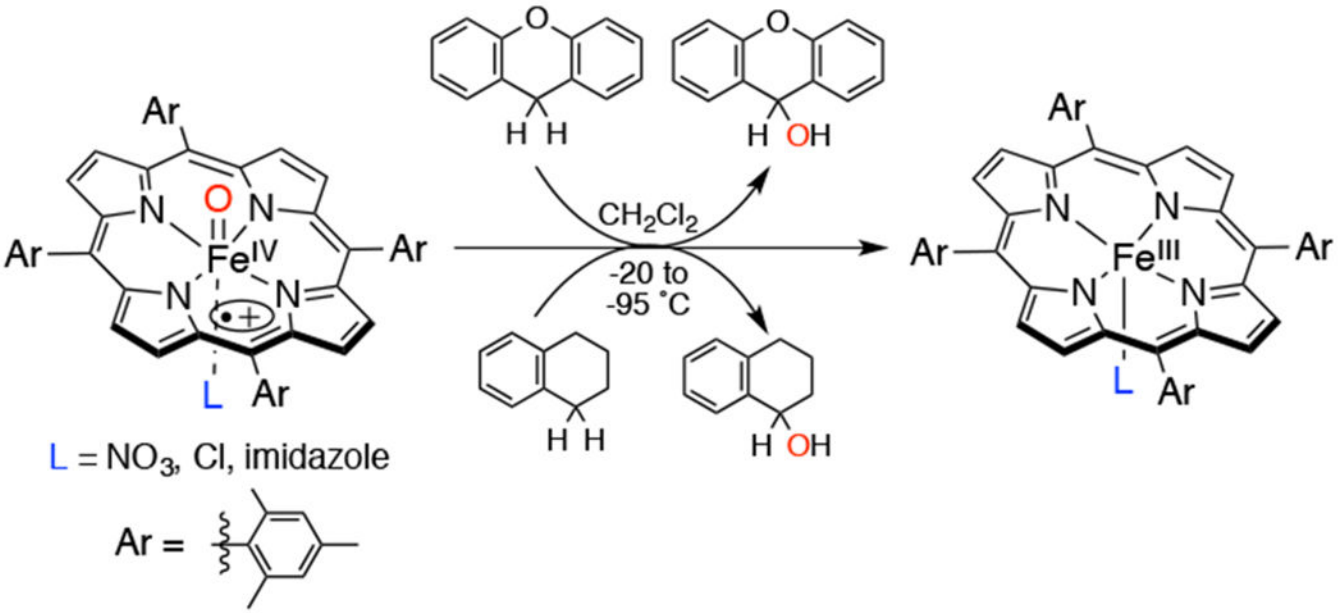

Scheme 9.

Reactivity of a Series of $Fe^{IV}(O)(TMP^{\bullet+})(L)$ Complexes with Benzylic C-H Substrates Xanthene and Tetralin

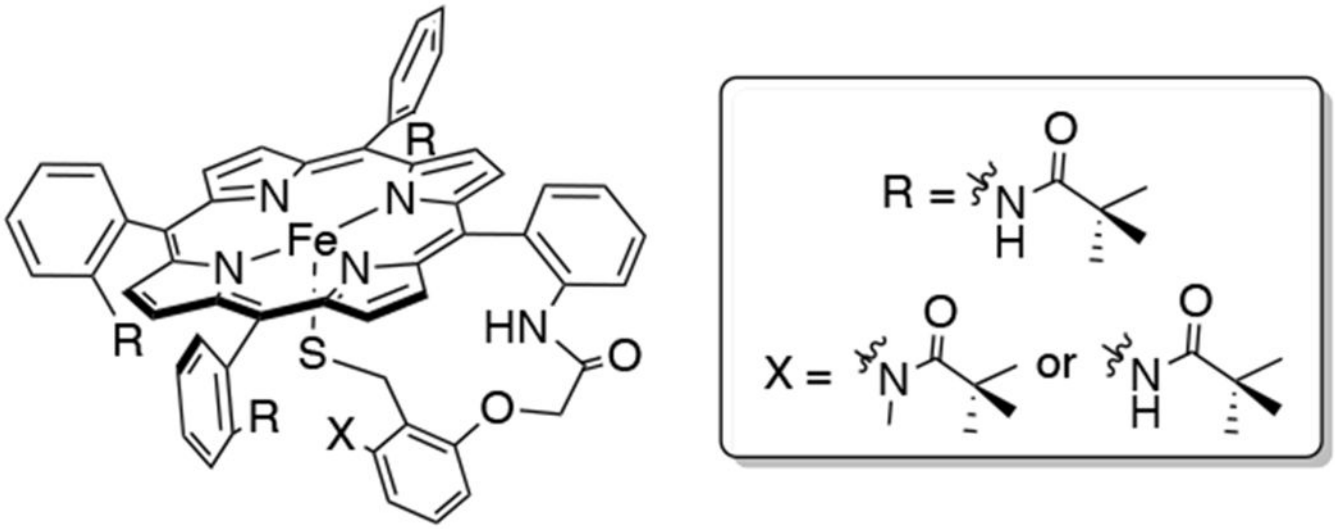

Scheme 10.

Swan Resting (SR) Complex, an Example of a Thiolate-Ligated Heme Model Complex, and its Derivatives

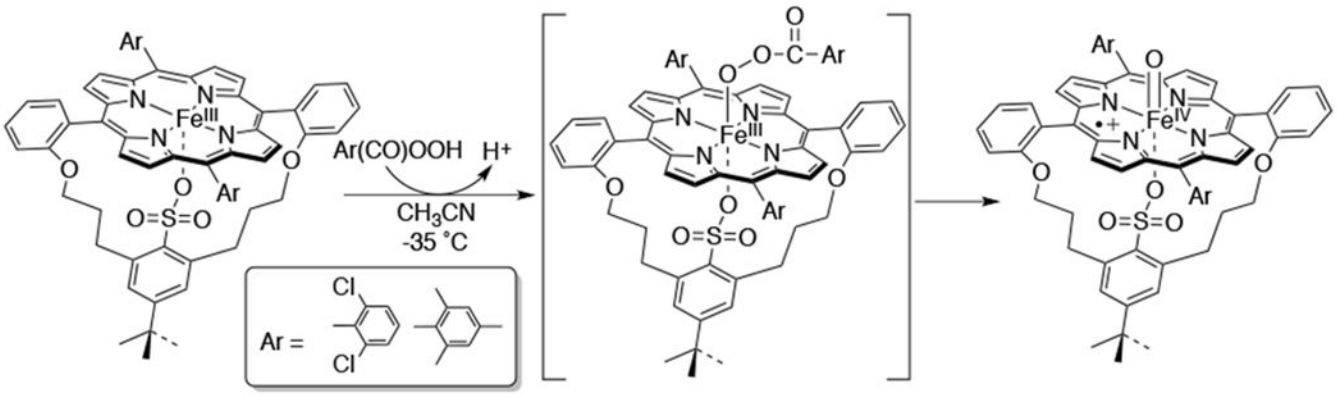

Scheme 11.

Conversion of an RSO_3-ligated Fe^{III}(acylperoxo)(porphyrin) Intermediate into a Cpd I Analog $Fe^{IV}(O)(RSO_3)(porpyrin^{\bullet+})$

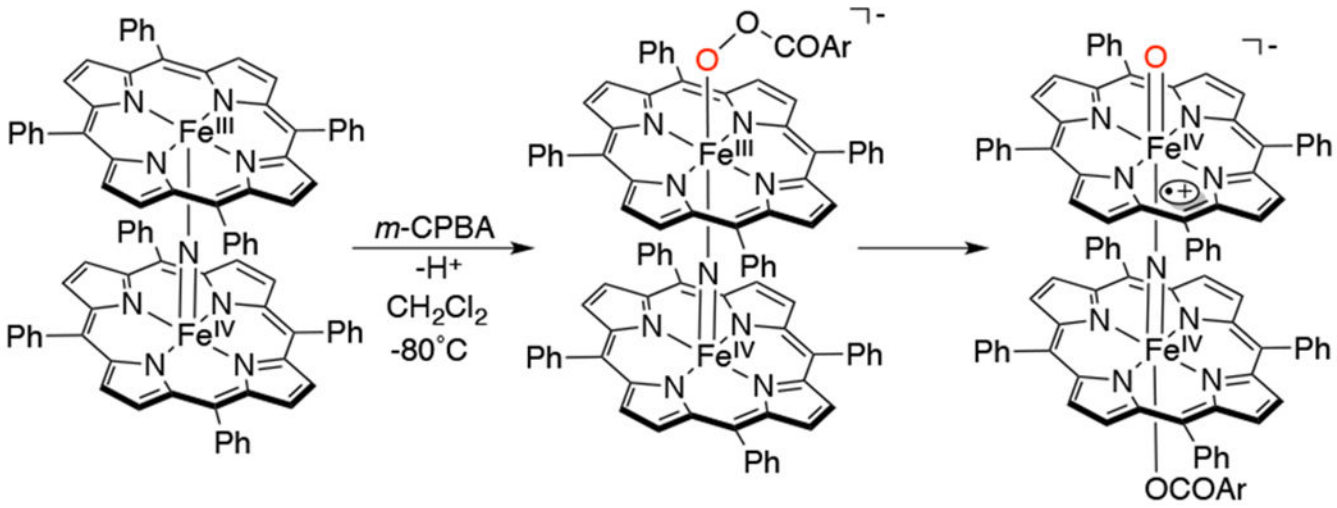

Scheme 12.

Proposed Mechanism for the Formation of $[(TPP)(m\text{-CBA})Fe^{IV}(N)Fe^{IV}(O)(TPP^{\bullet+})]^{-}$

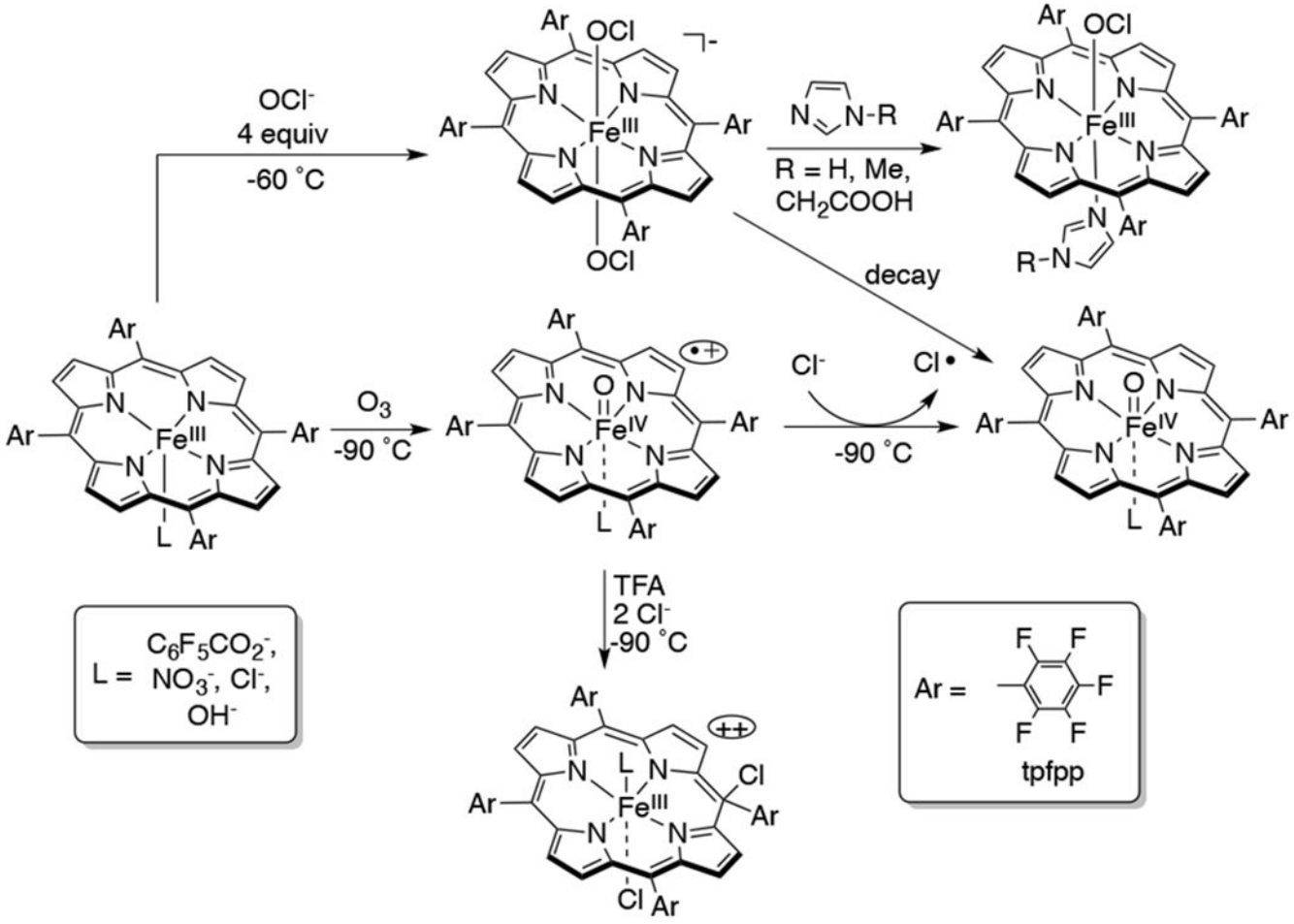

Scheme 13.

Generation of $Fe^{III}(OCl)_2(porph)^-$, $Fe^{IV}(O)(porph^{\bullet+})$, and $Fe^{IV}(O)(porph)$ Species and Their Interconversions

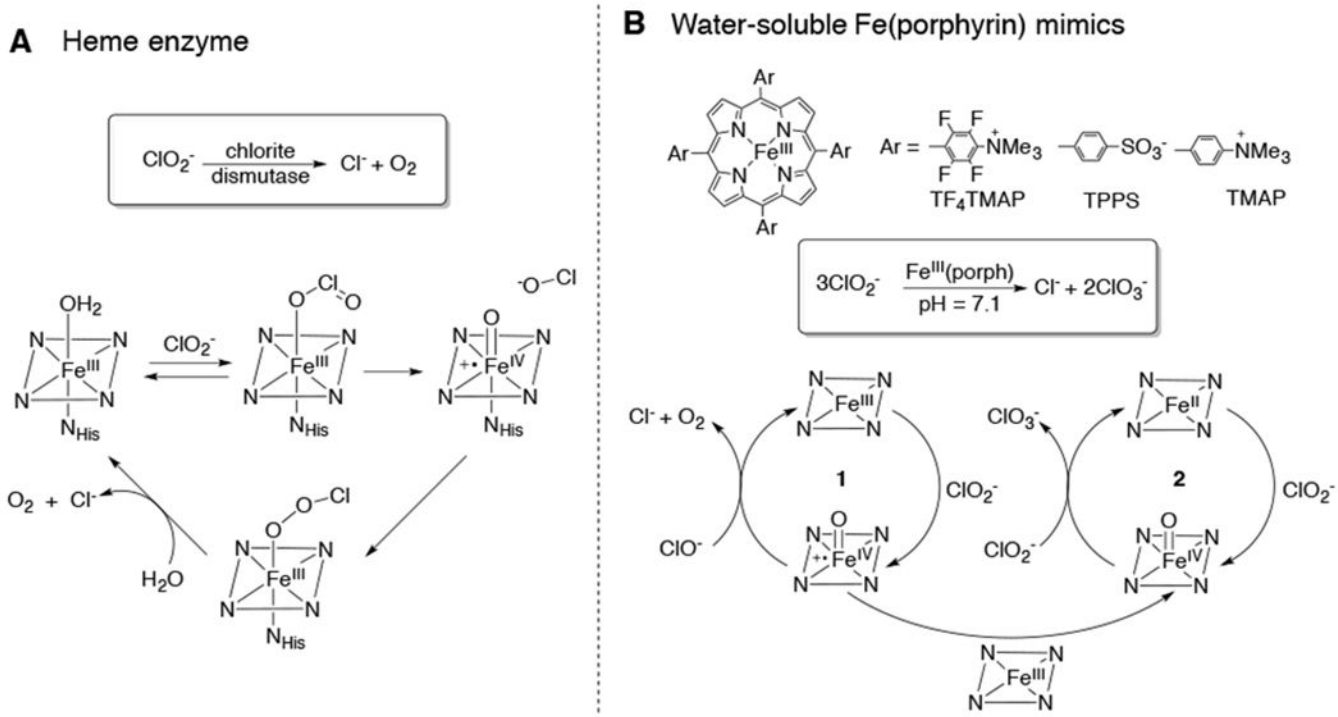

Scheme 14.

Proposed Mechanisms for Chlorite Dismutase and Water-Soluble Porphyrins

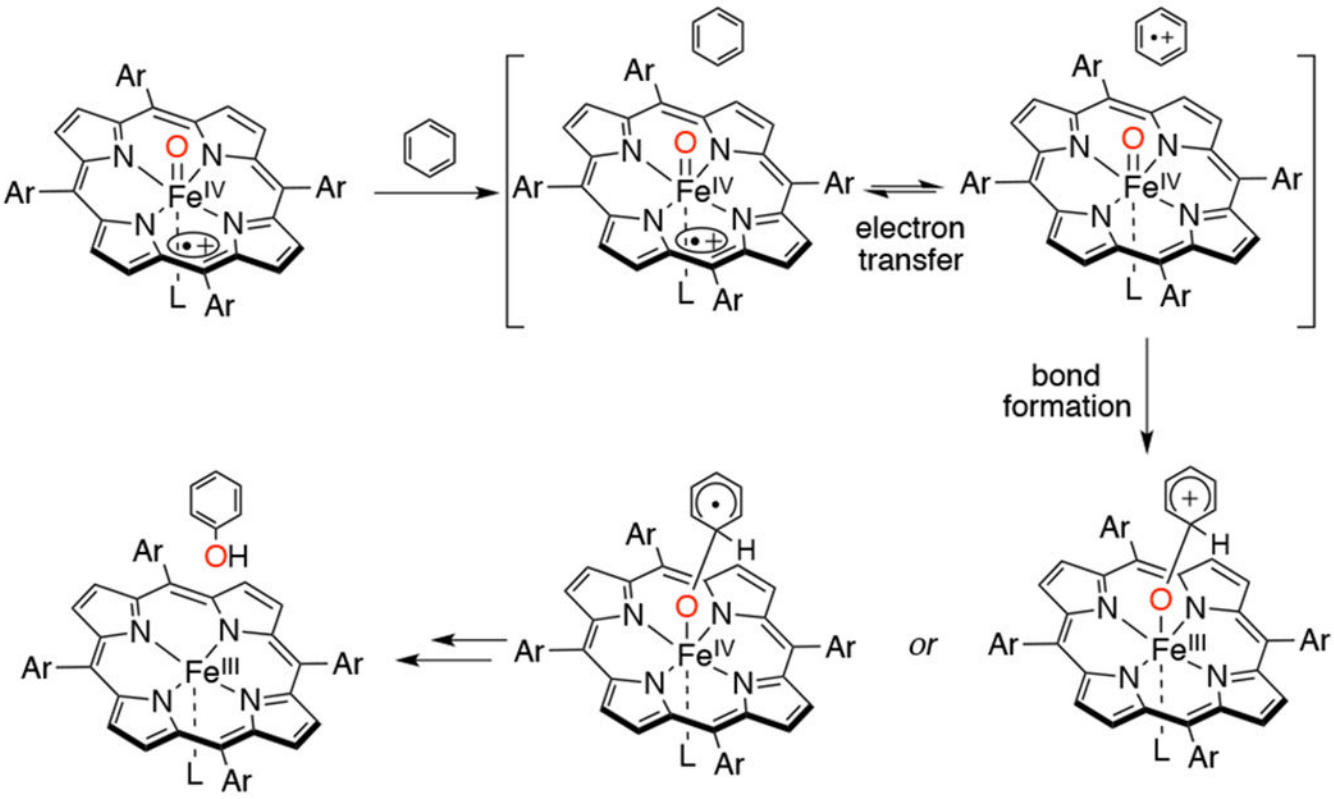

Scheme 15.

Proposed Mechanism of Aromatic Hydroxylation with $Fe^{IV}(O)(porphyrin^{\bullet+})$ Complexes Showing an Electron Transfer Process Coupled to the Subsequent Bond Formation Step

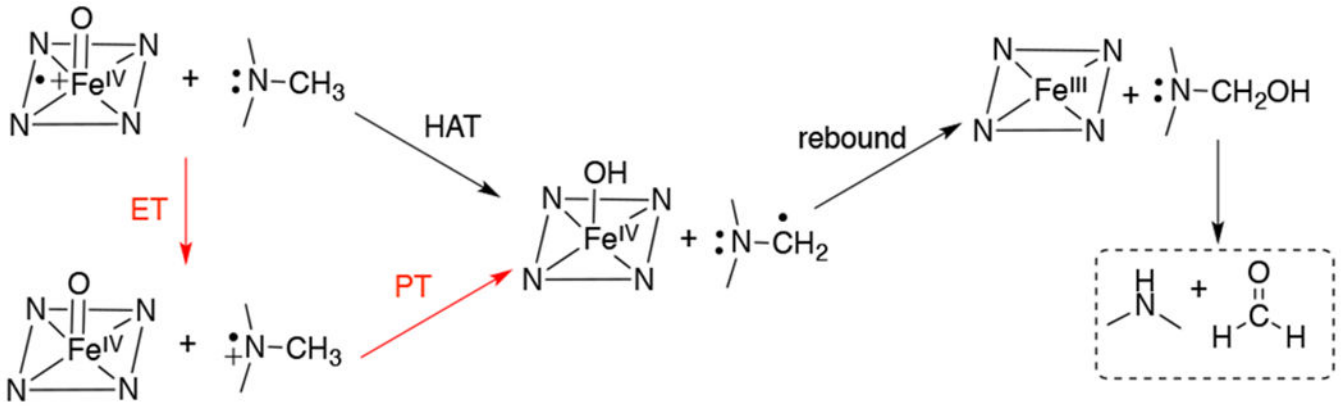

Scheme 16.

Proposed Mechanisms for Oxidative N-demethylation by Compound I, Fe^{IV}(O)(porphyrin$^{\bullet+}$)

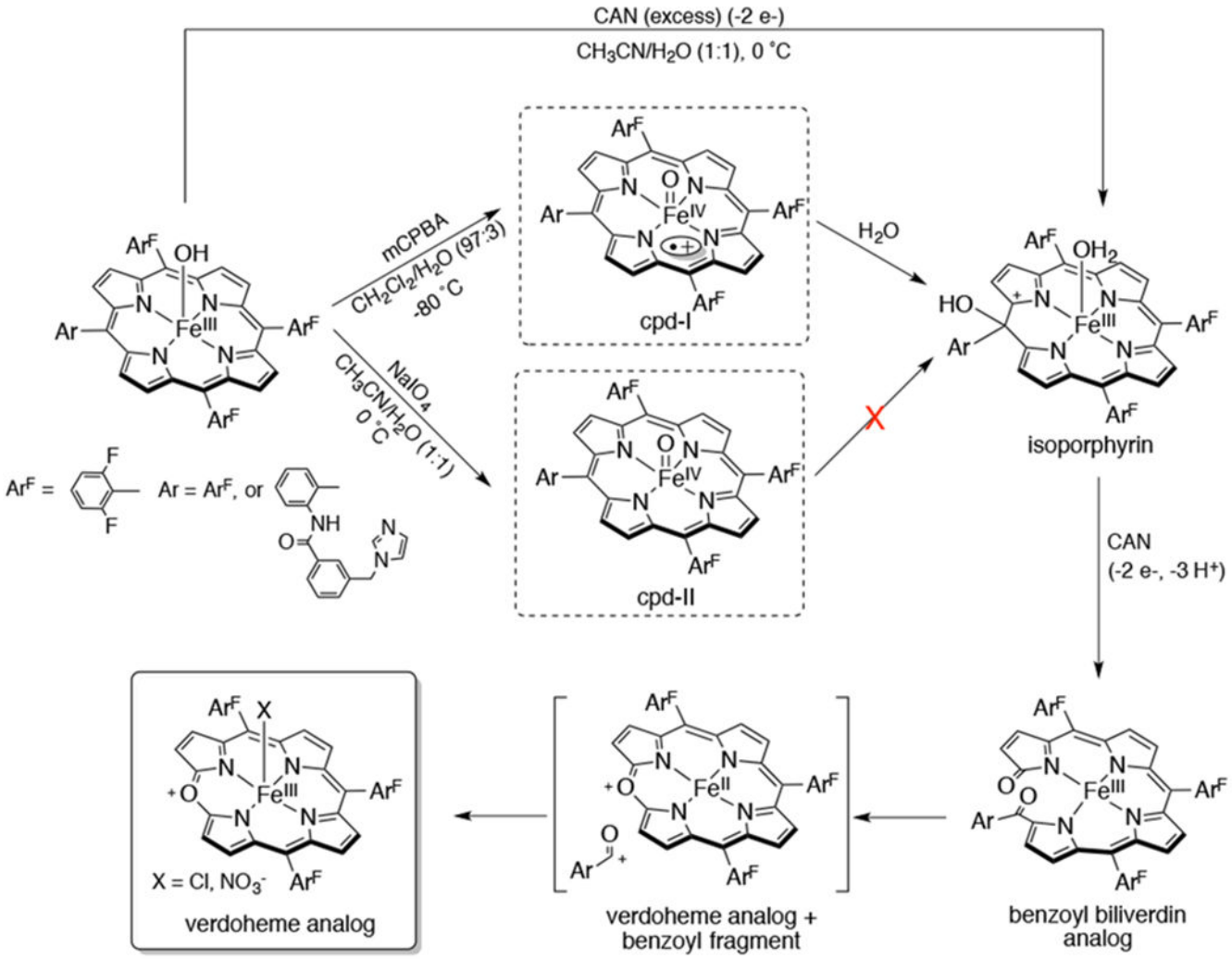

Scheme 17.

Proposed Mechanism for the Selective Oxidation of Fe^{III}(OH)(porphyrin) with CAN to a Verdoheme-like Complex via Formation of Intermediates Resembling Cpd-I, Isoporphyrin, and Benzoyl Biliverdin

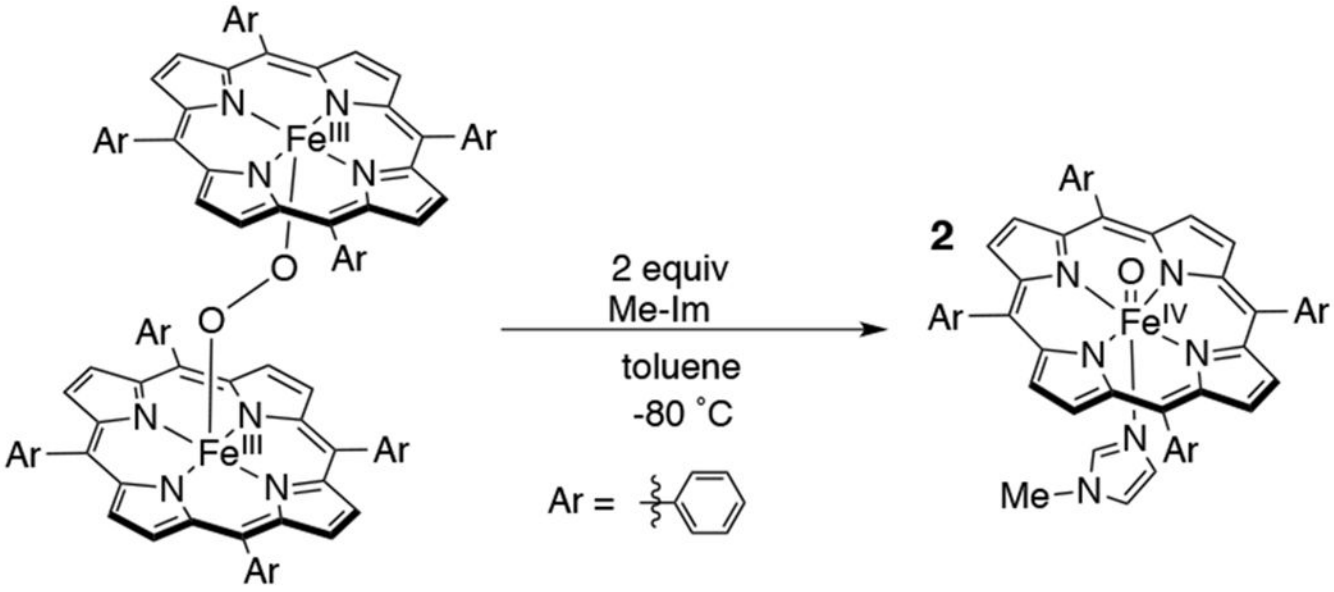

Scheme 18.
Synthesis of Fe^{IV}(O)(TPP), an Early Compound II Analog

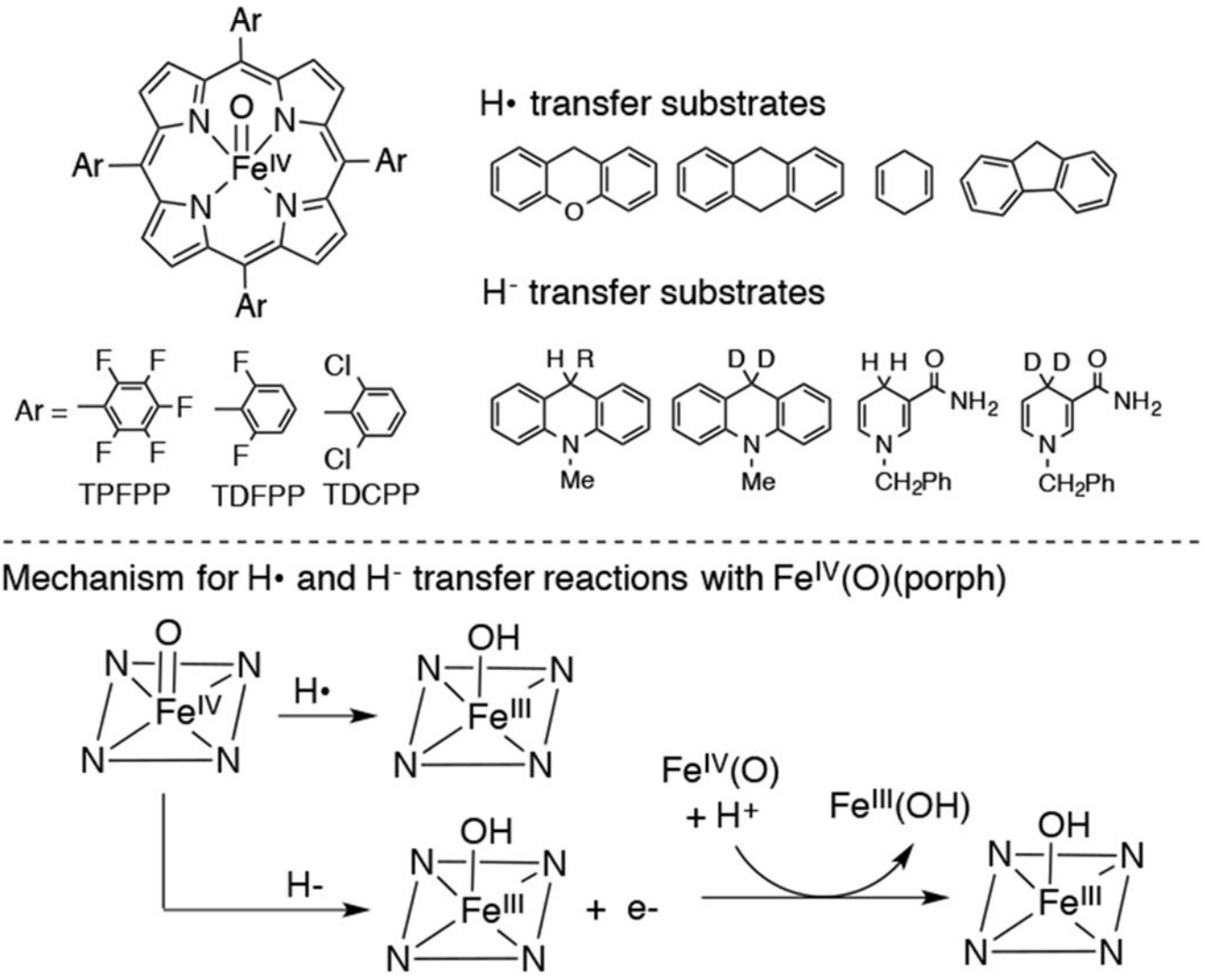

Scheme 19.

Reactivity of a Series of Iron(IV)-Oxo Porphyrins with H-atom and Hydride Donors

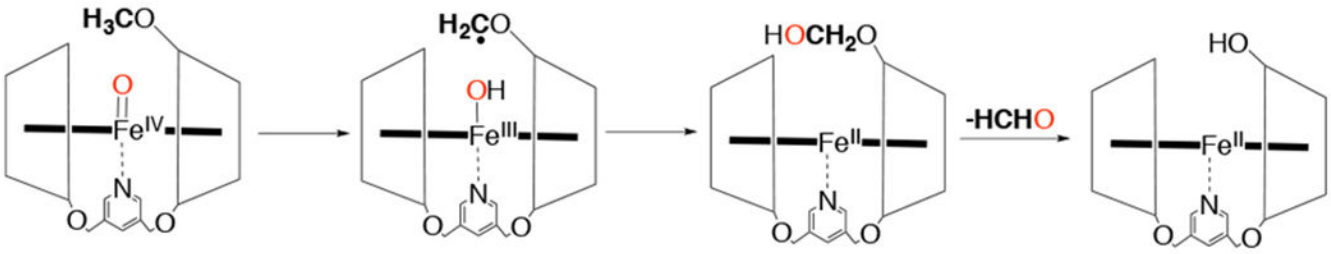

Scheme 20.

Proposed Mechanism for Intramolecular O-demethylation Mediated by an $Fe^{IV}(O)$ Complex Encapsulated in a Per-O-methylated Cyclodextrin Dimer

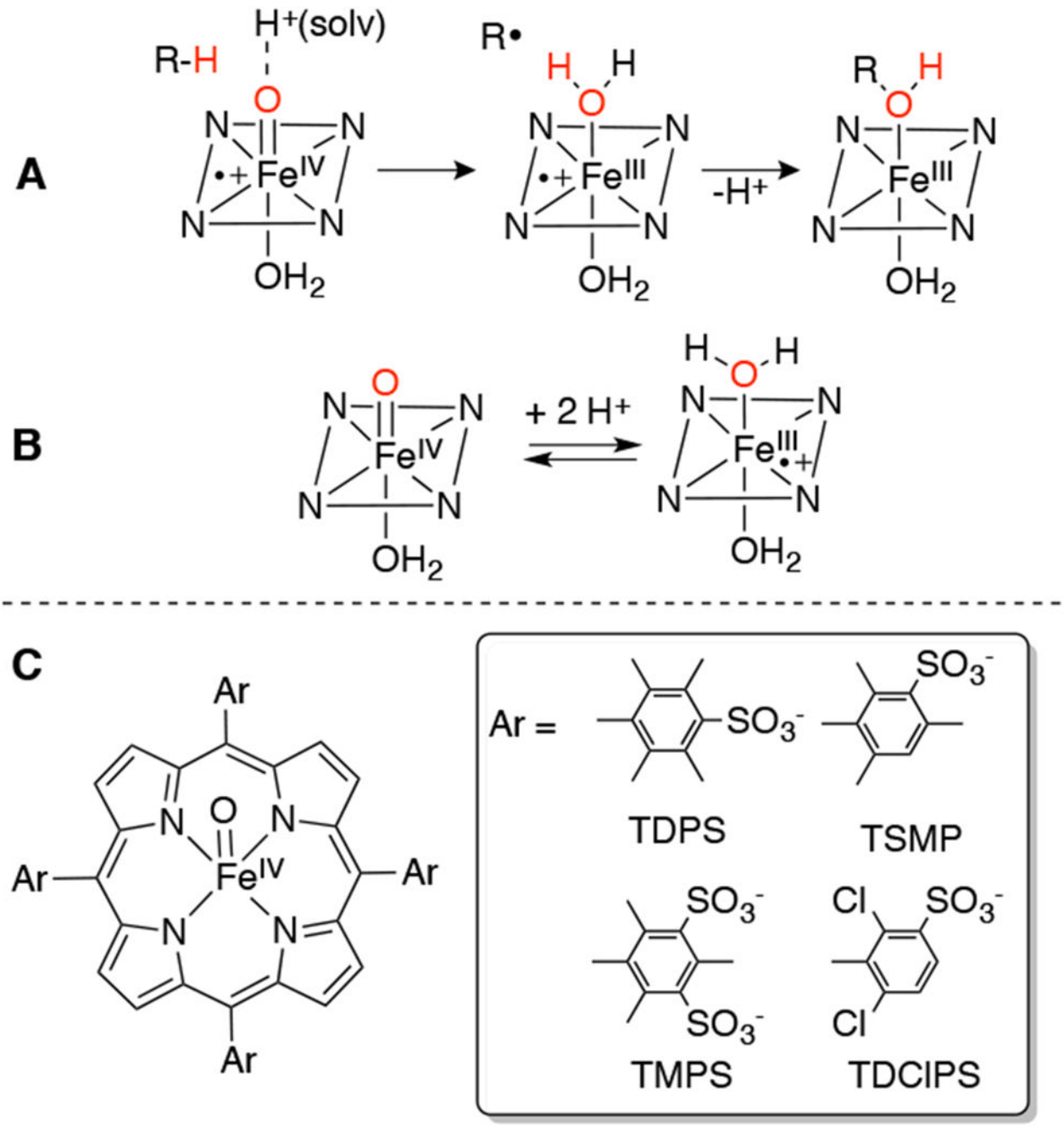

Scheme 21.

A) Proposed Mechanism for Solvent-Proton Assisted C-H Bond Cleavage by a Sulfonated, Water-soluble Iron(IV)-Oxo Porphyrin π-Radical Cation Complex in the Presence of an Exogenous Proton Source B) Valence Tautomer Equilibrium Observed upon Protonation of Iron(IV)-Oxo Porphyrins C) Water-soluble Porphyrins Used in the Study

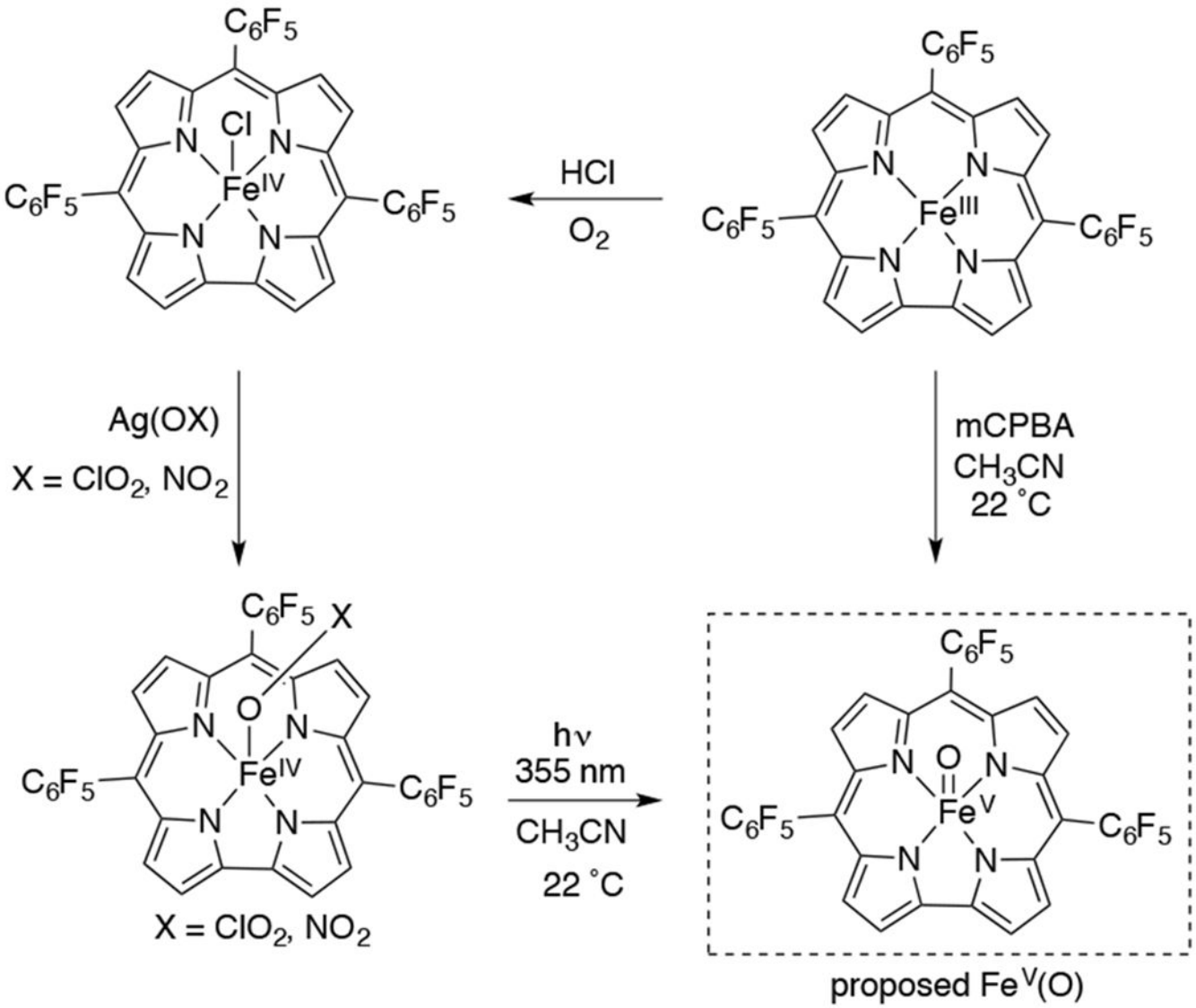

Scheme 22.
Formation of a Proposed $Fe^{V}(O)$ Corrole

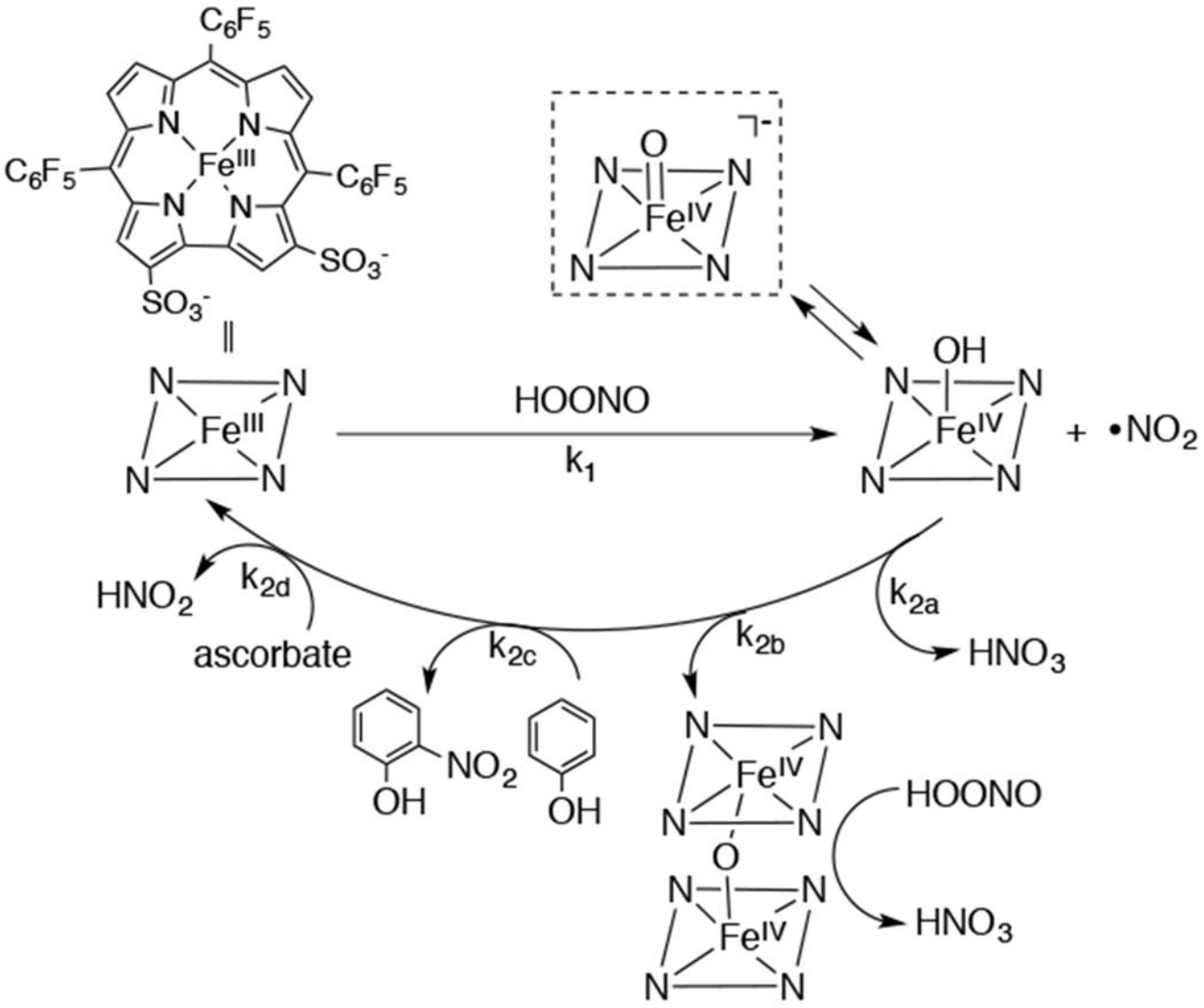

Scheme 23.

Proposed Mechanism for the Catalytic Decomposition of Peroxynitrite with a Water-soluble Fe^{III} Corrole, Showing an $[Fe^{IV}(O)(corrole)]^{-}$ Intermediate

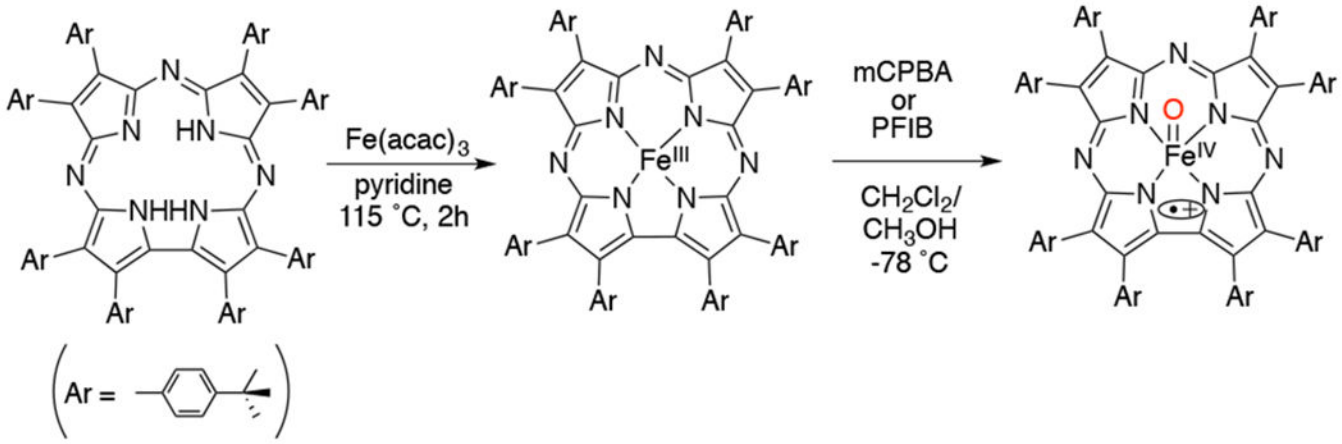

Scheme 24.

Synthesis of $Fe^{III}(TBP_8Cz)$ and $Fe^{IV}(O)(TBP_8Cz^{\bullet+})$

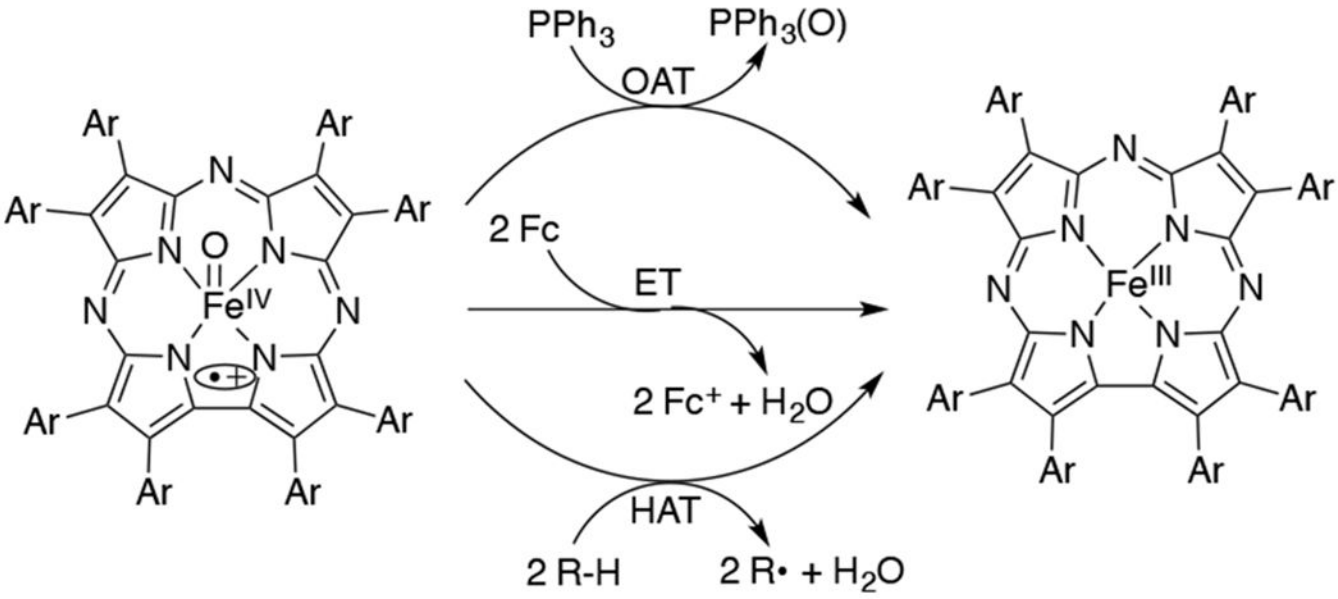

Scheme 25.

O-atom Transfer, H-atom Abstraction, and Electron Transfer Reactions of $Fe^{IV}(O)$ (corrolazine$^{\bullet+}$)

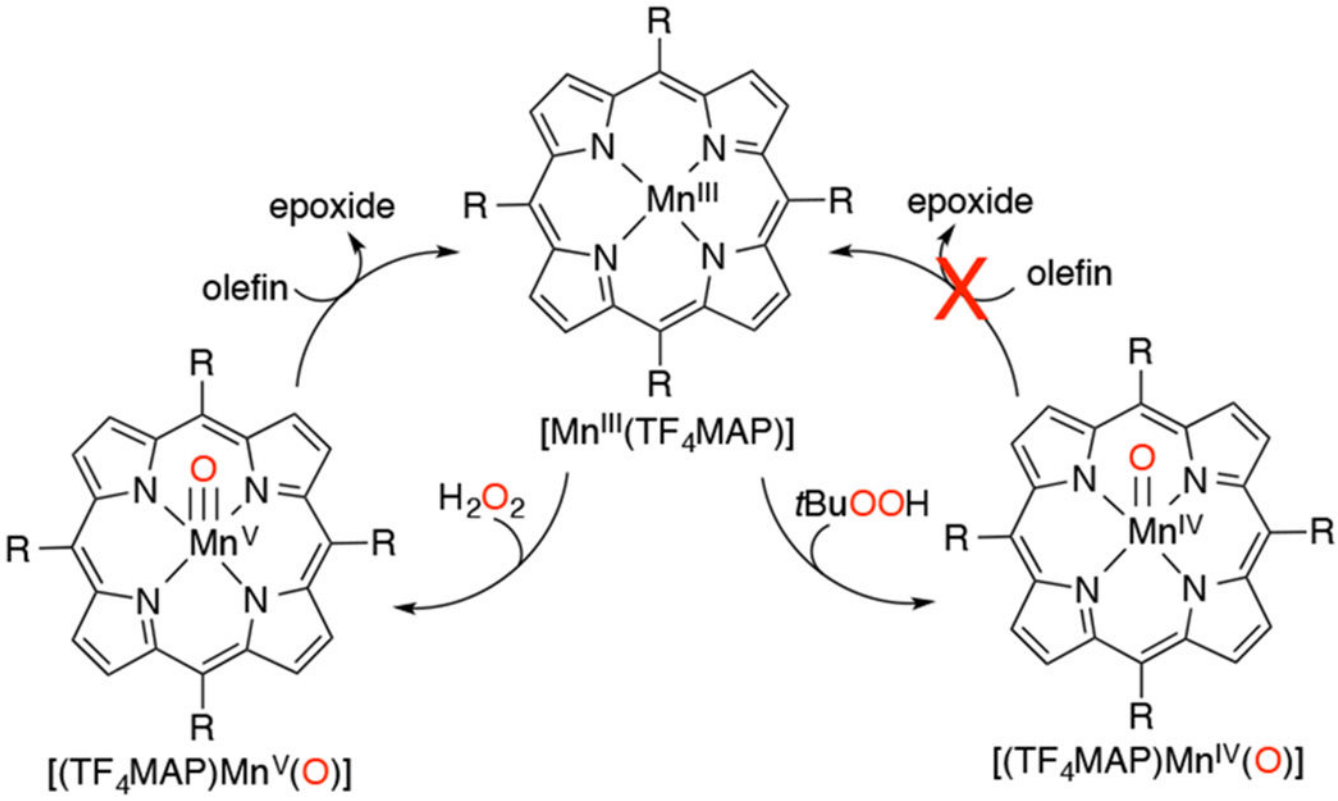

Scheme 26.
Synthesis of High-Valent Manganese-Oxo Species Depends on the Identity of the Oxidant

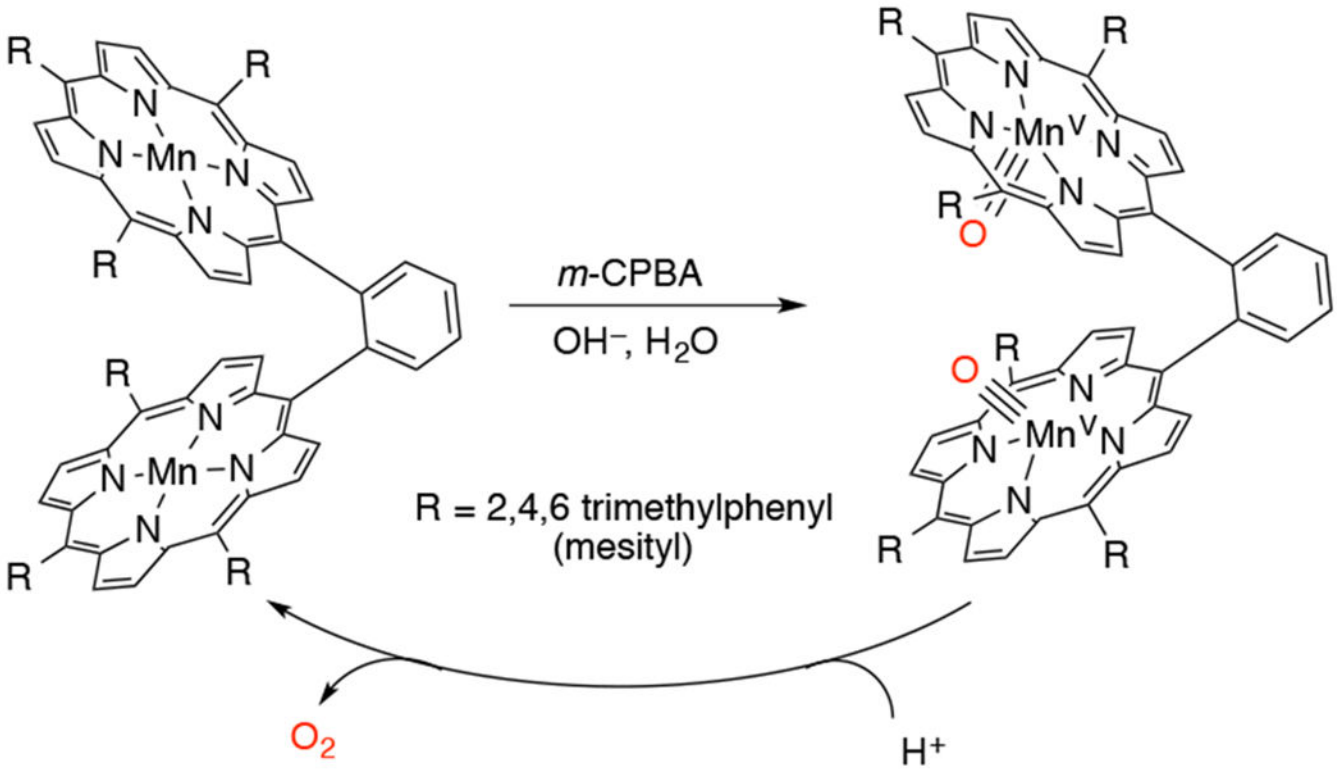

Scheme 27.
Oxygen Evolution from a Dimanganese-oxo Porphyrin Complex

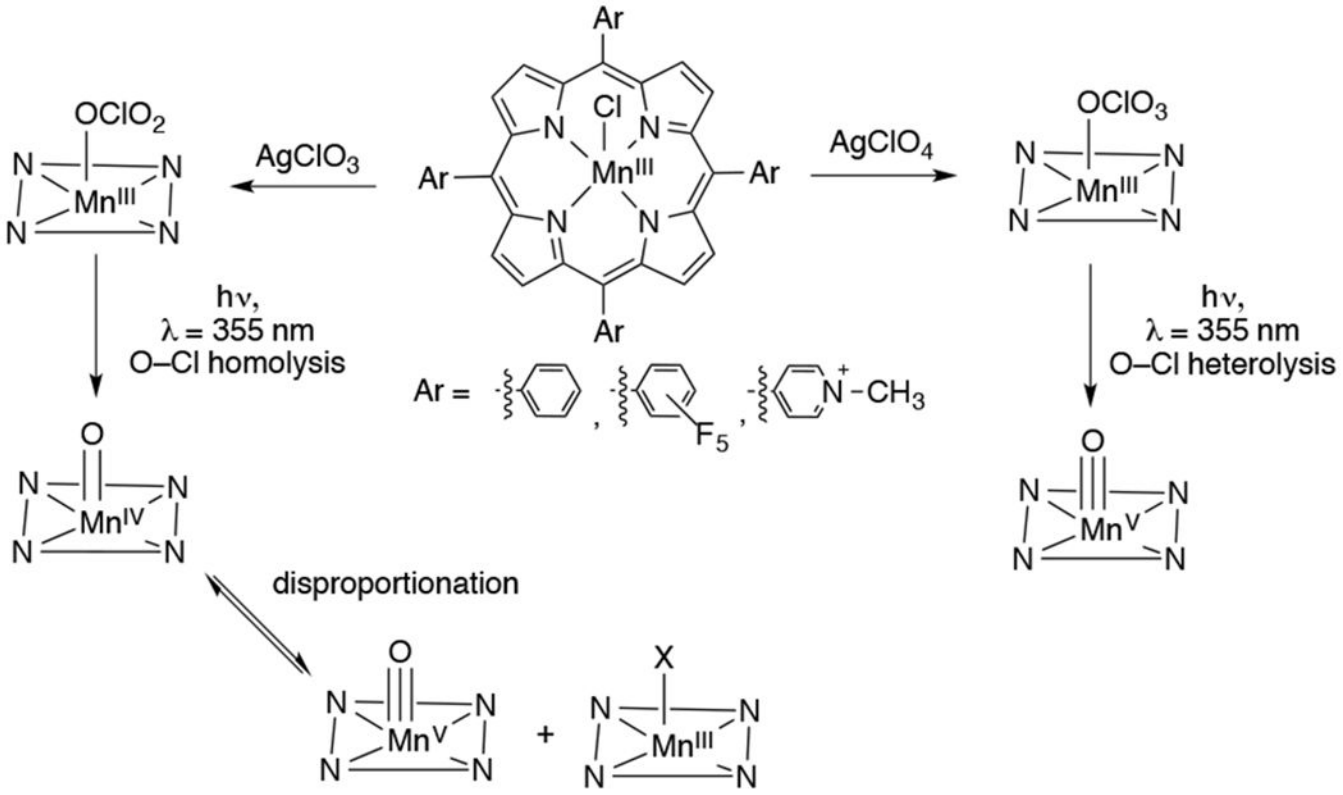

Scheme 28.

Dependence of O–Cl Bond Cleavage on Starting Manganese Porphyrin Axial Ligand

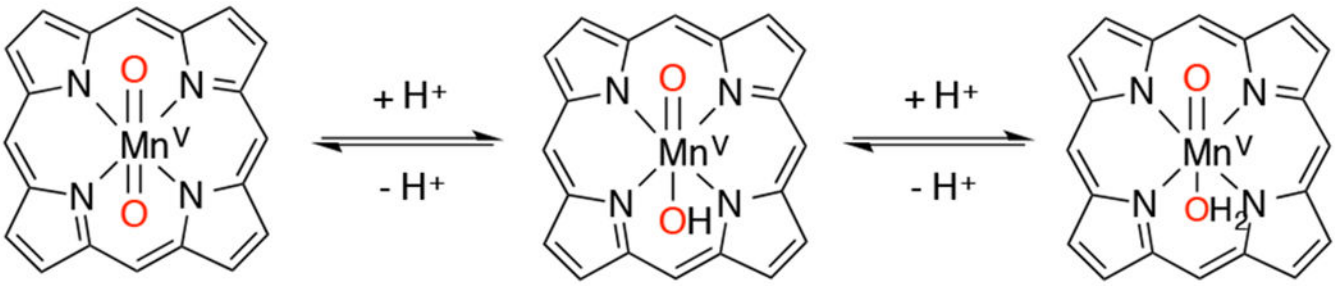

Scheme 29.
pH-Dependent Oxo-Hydroxo Tautomerism in High-Valent Manganese-Oxo Porphyrins

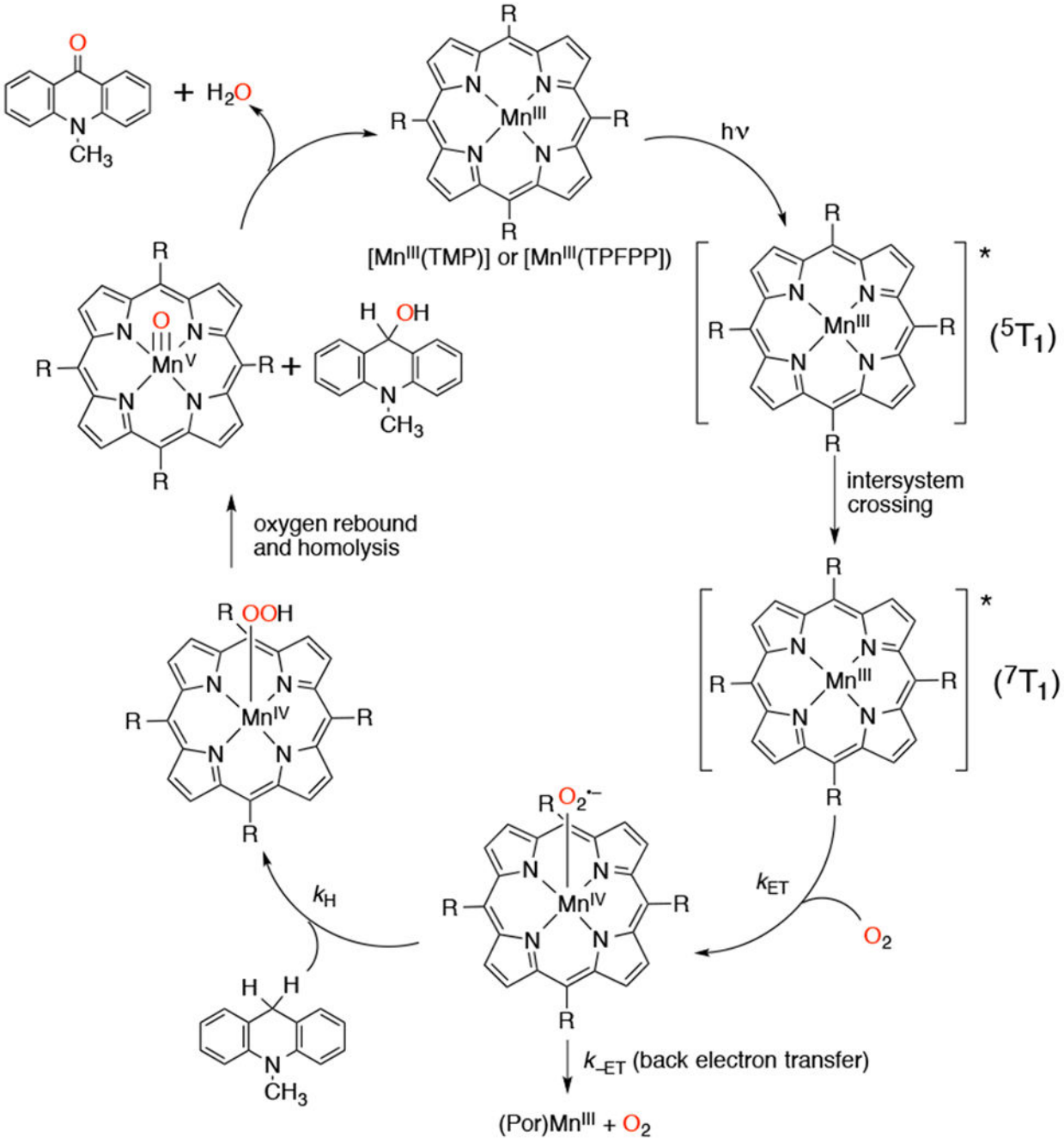

Scheme 30.

Proposed Mechanism of Photocatalytic Oxygenation of $AcrH_2$ by Manganese Porphyrins

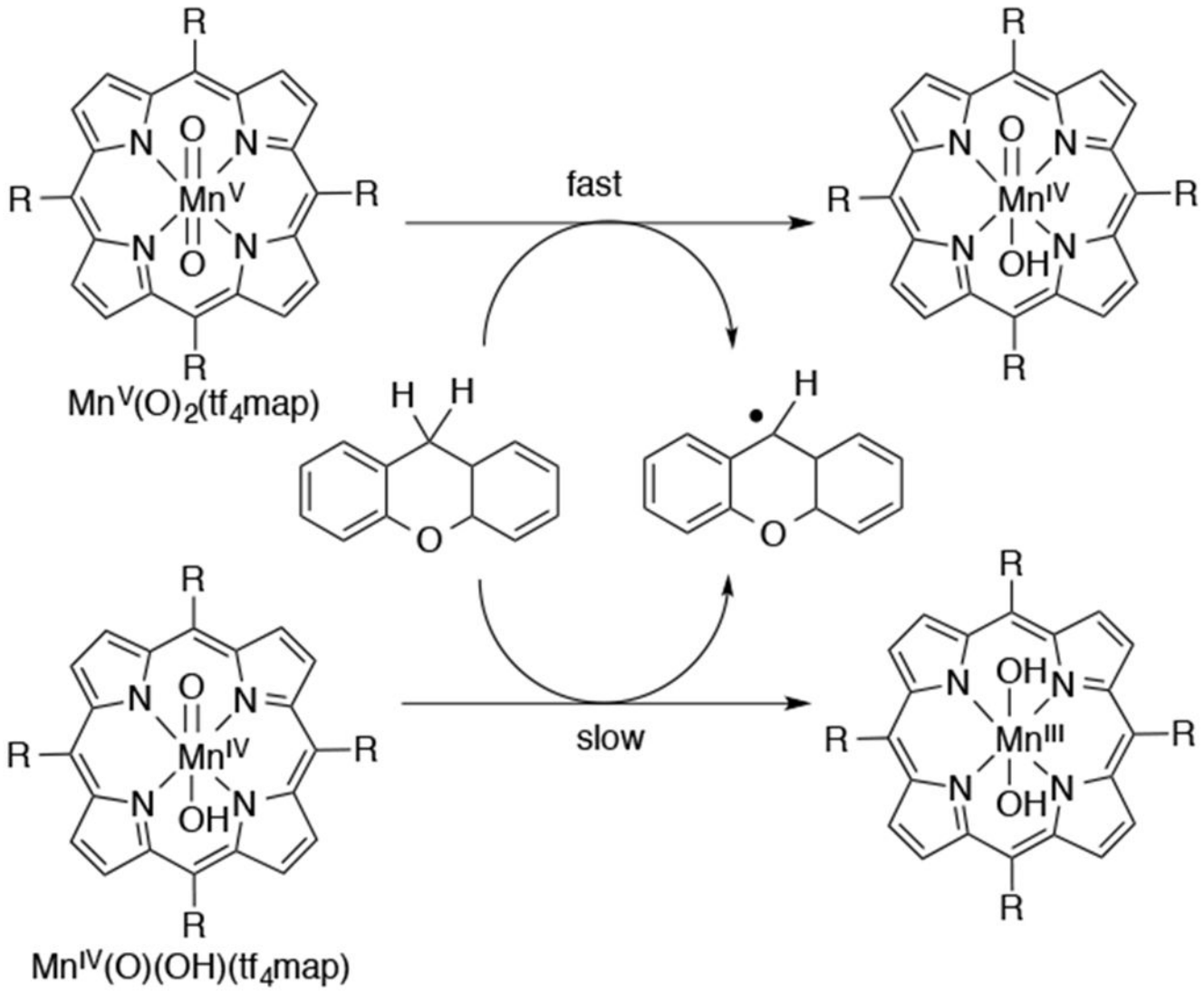

Scheme 31.
Reactivity Comparison of $Mn^{V}(O)$ and $Mn^{IV}(O)$ Porphyrins

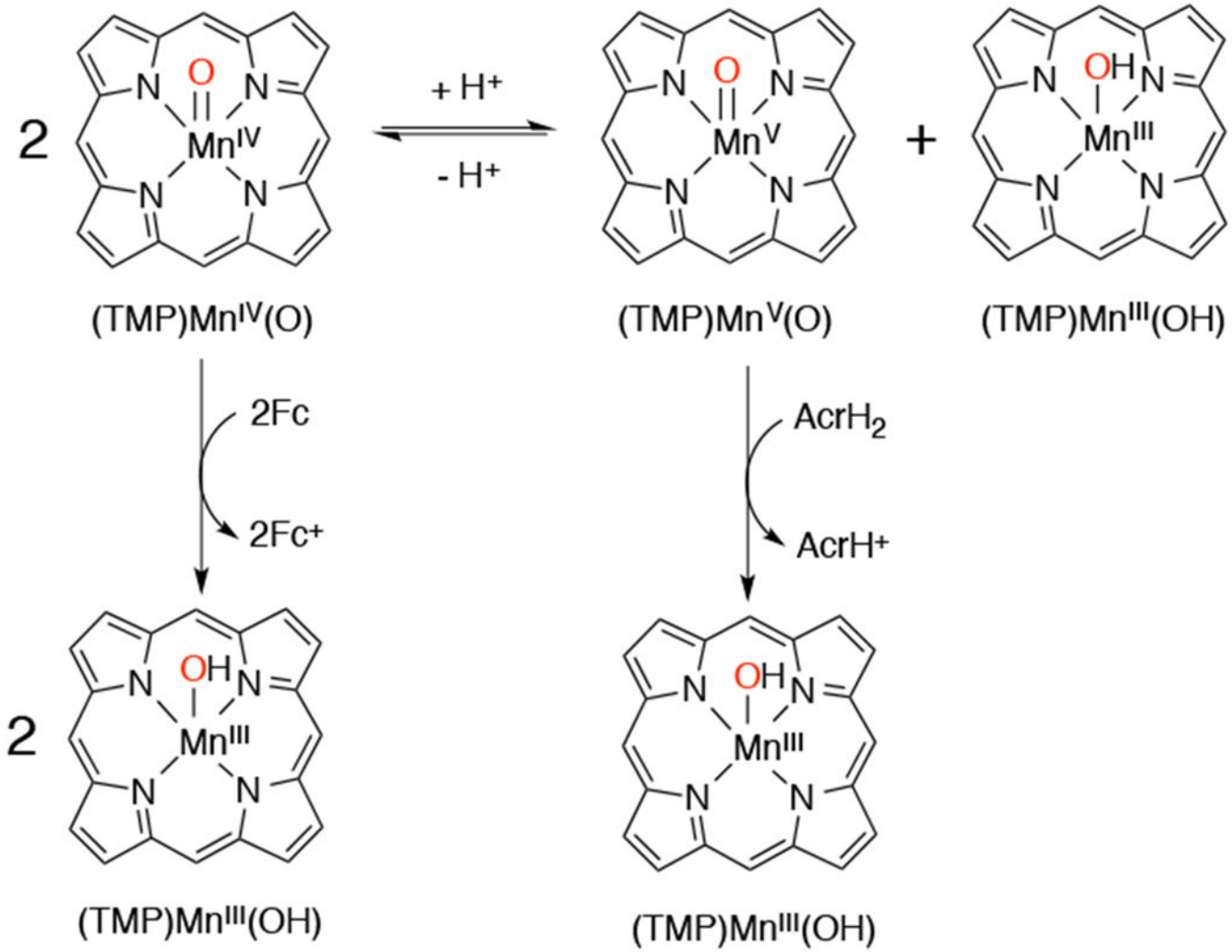

Scheme 32.
Substrate Dependence on Reactivity of a $Mn^{IV}(O)$ Porphyrin

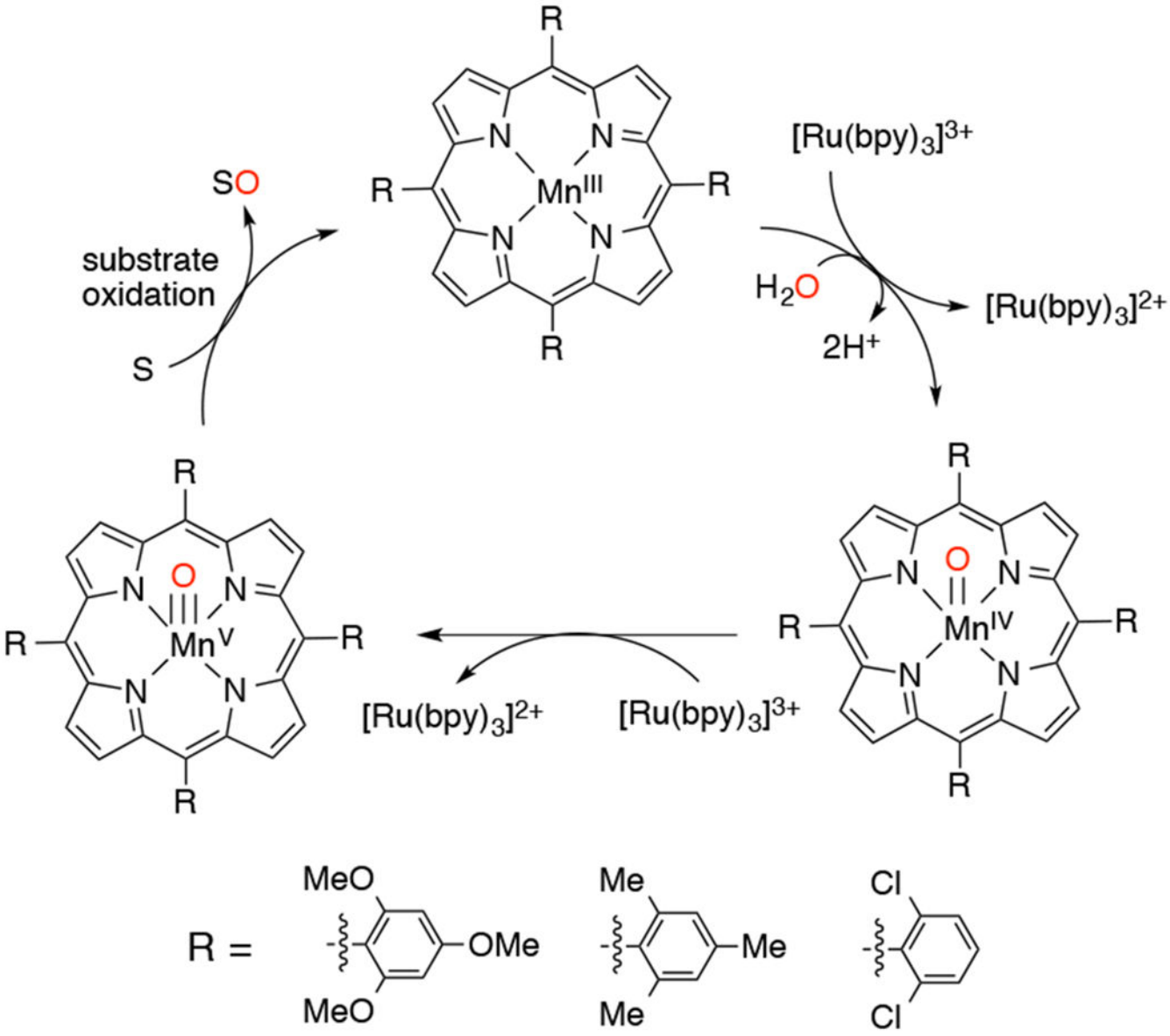

Scheme 33.
Water as the O-atom Source in Manganese Porphyrin-Catalyzed Oxidations

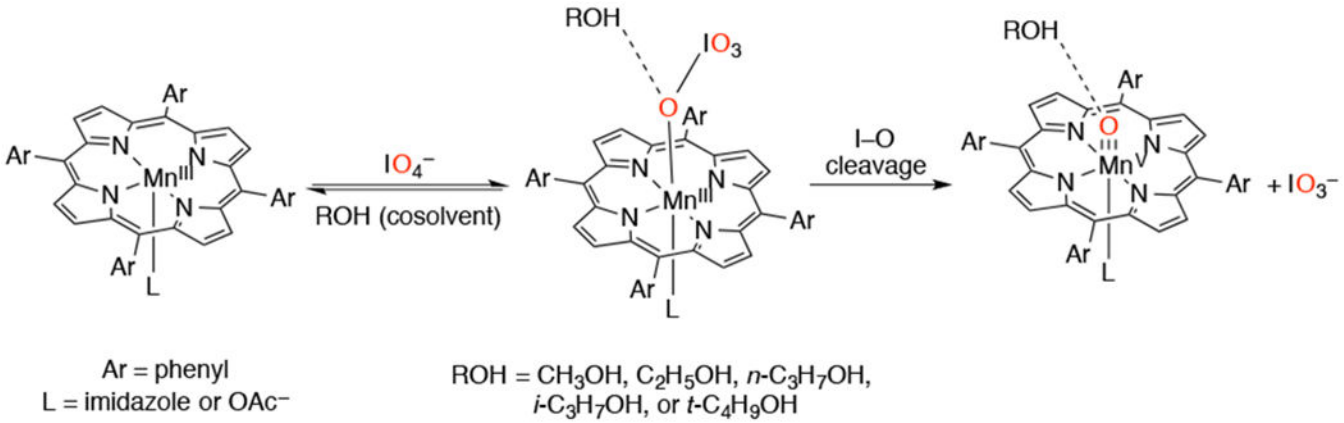

Scheme 34.

Synthesis of an $Mn^{V}(O)$ Porphyrin Complex with Periodate as Oxygen Atom Donor in the Presence of Alcohol Cosolvents

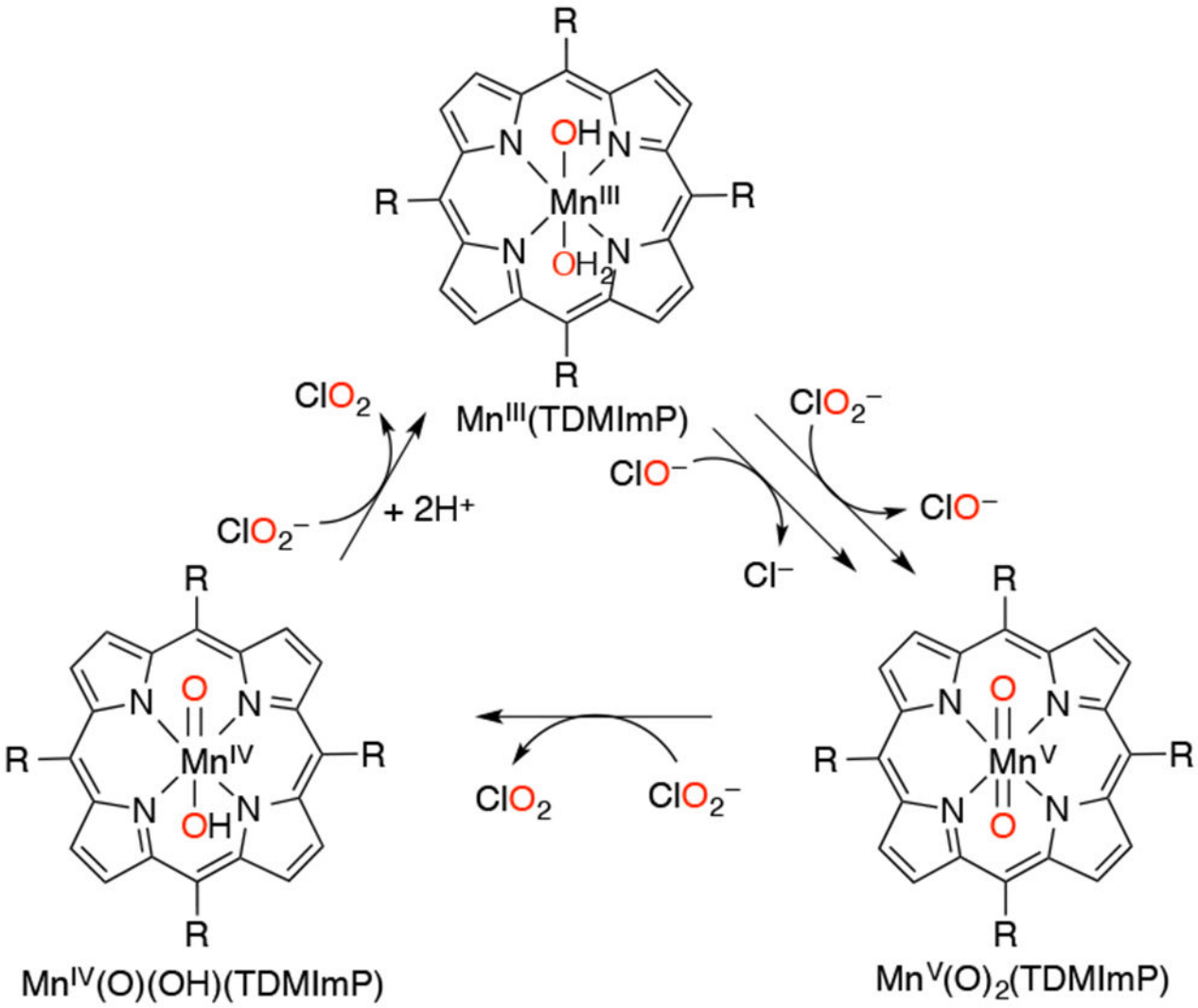

Scheme 35.
Catalytic Chlorite Oxidation by a Mn(III) Porphyrin

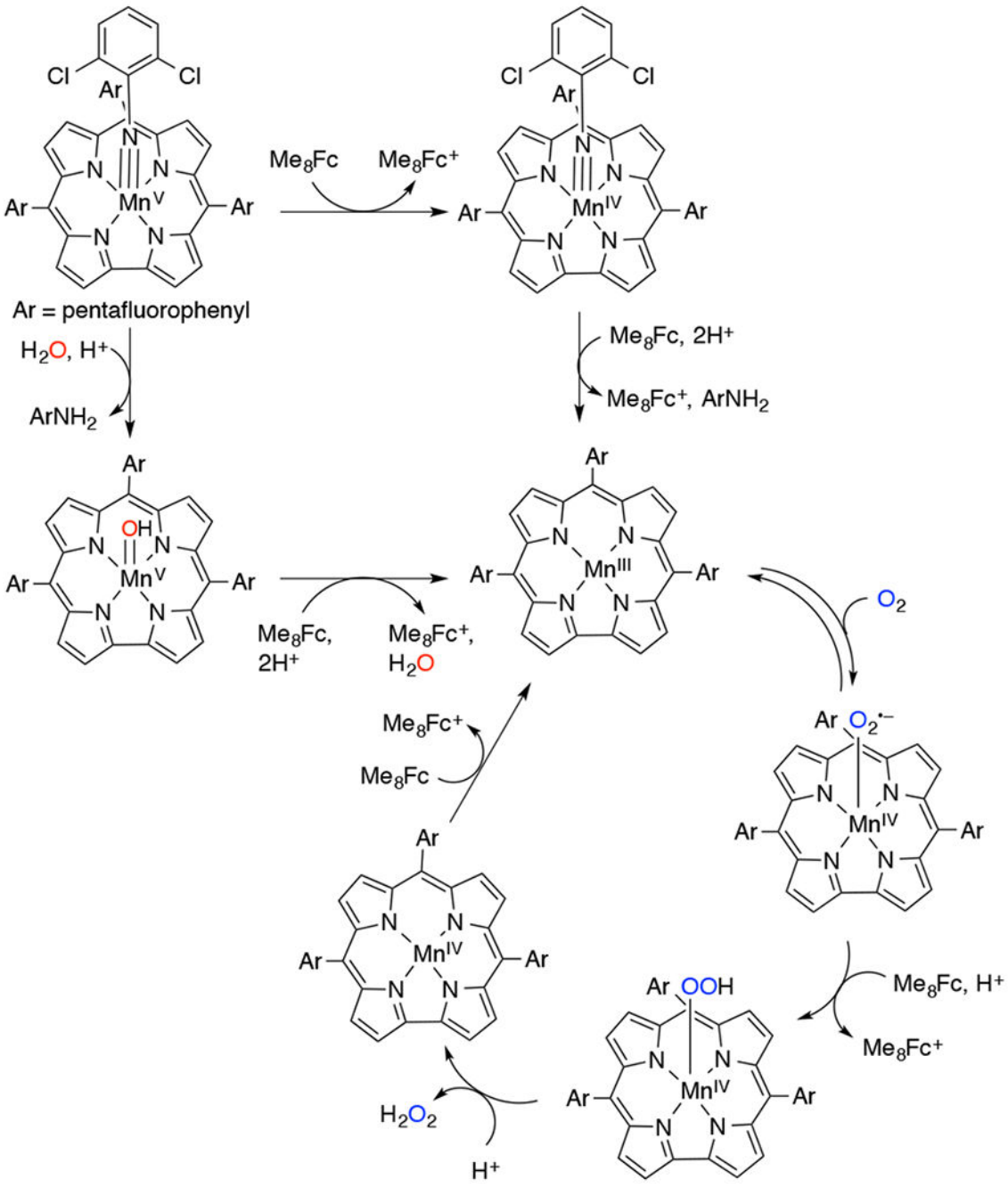

Scheme 36.

Proton-Coupled Reduction of Mn^{V}-imido Corrole to Give a Mn^{III} Corrole

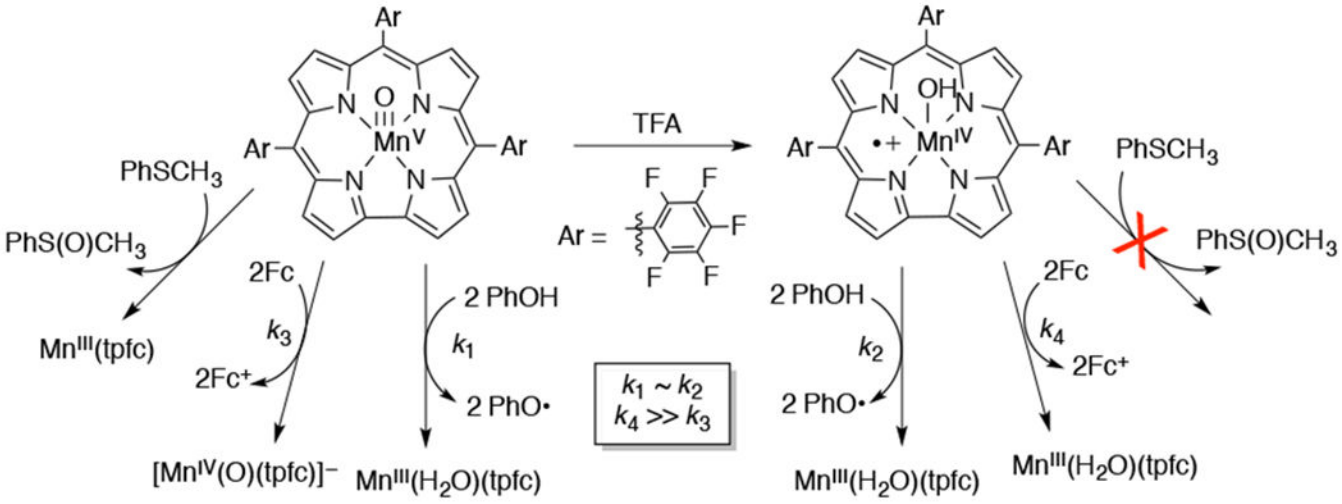

Scheme 37.

Comparison of Reactivity for Two High-Valent Manganese-Oxo Corrole Valence Tautomers

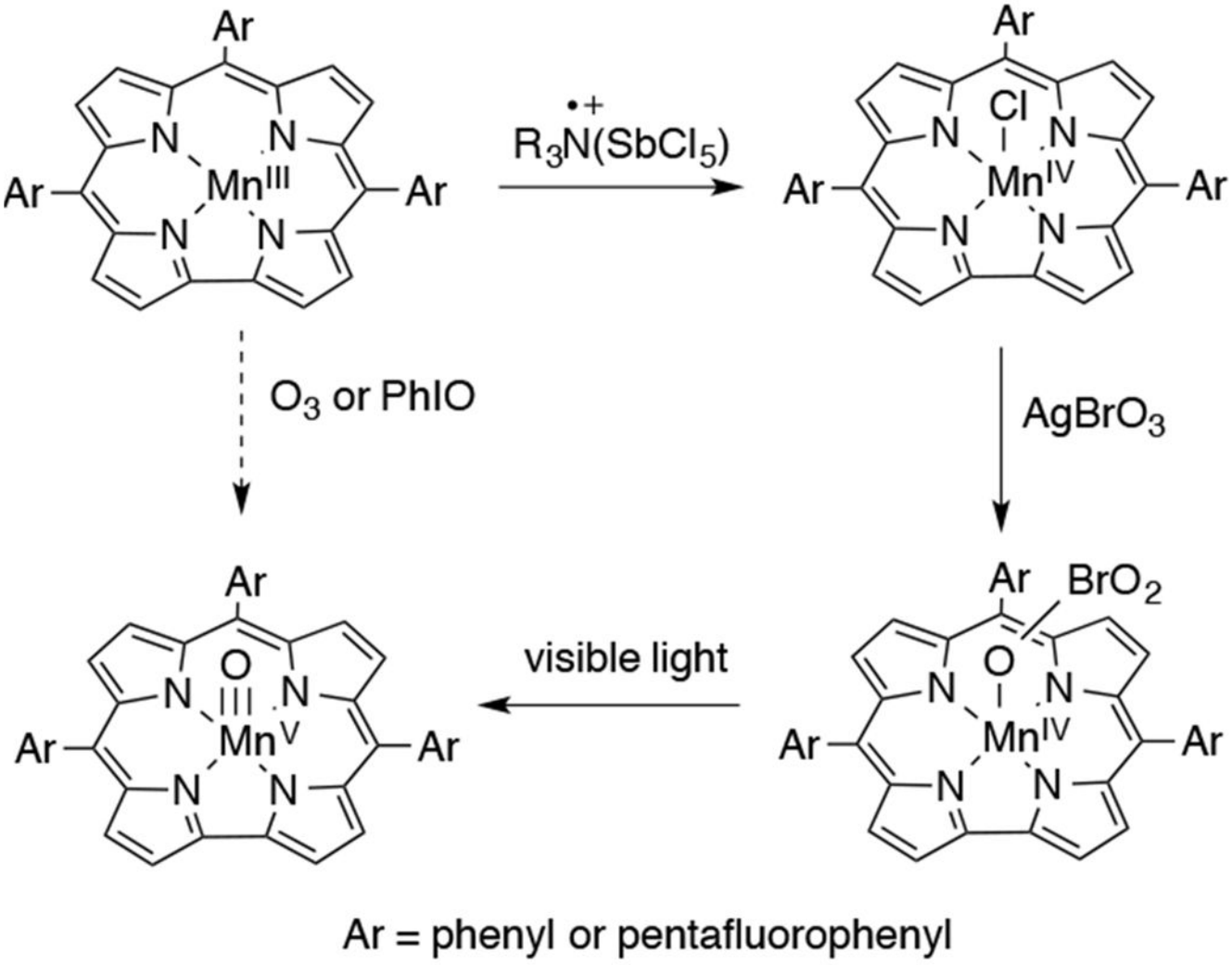

Scheme 38.
Generation of $Mn^{V}(O)$ Corroles by Br–O Bond Homolysis of Mn-Bromate Complexes

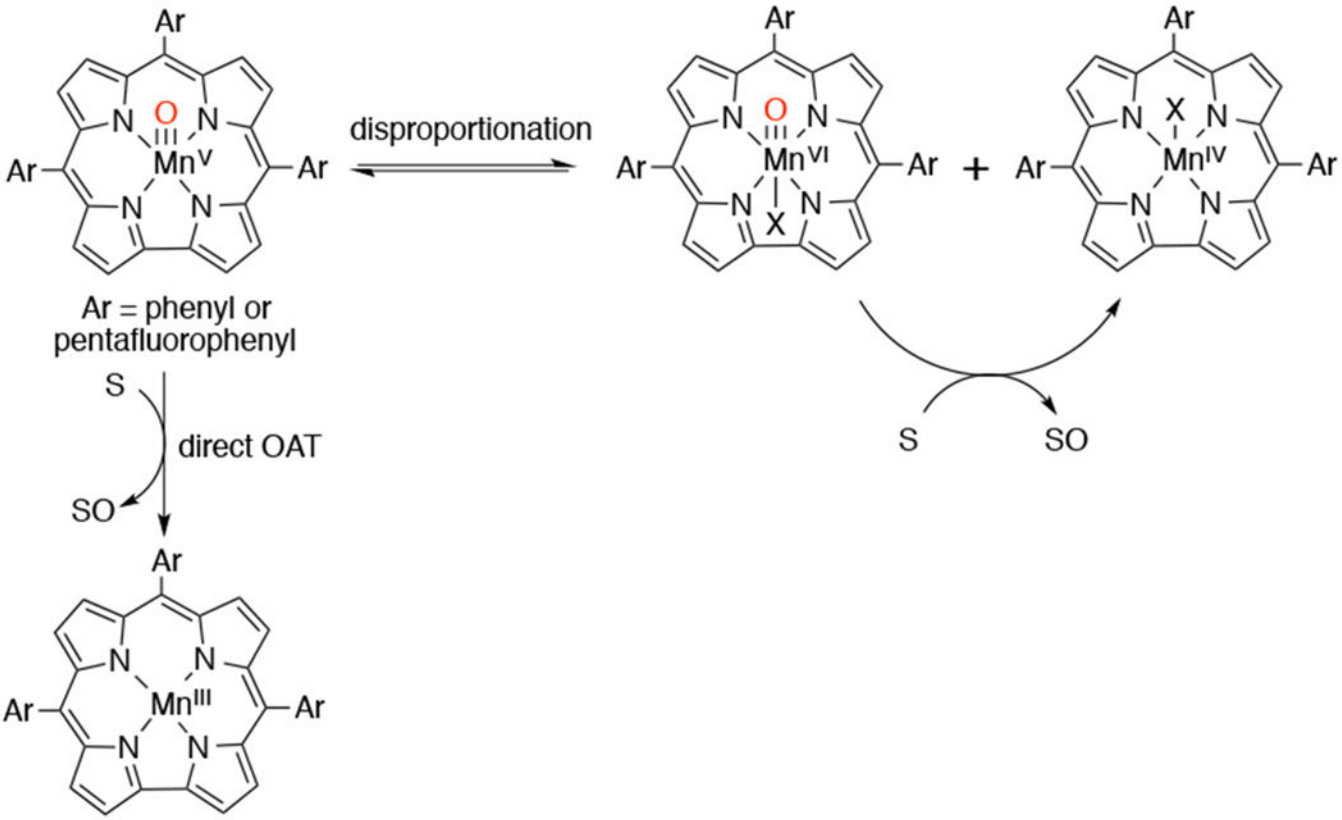

Scheme 39.

Disproportionation of Mn^{V}(O) Corrole to Give Mn^{IV}(X) and Mn^{VI}(O) Corrole Complexes

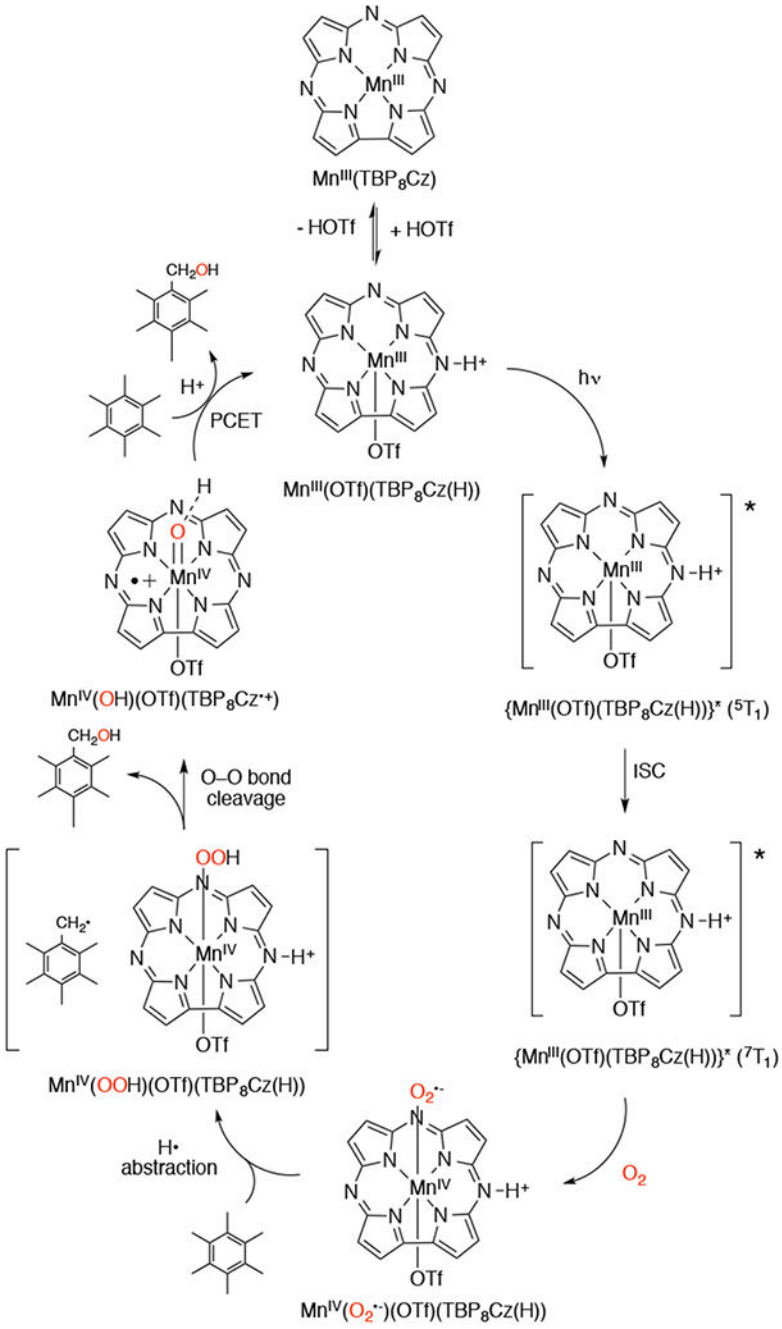

Scheme 40.

Mechanism for Photocatalytic Oxygenation of the Toluene Derivative Hexamethylbenzene by a Protonated Manganese Corrolazine Complex with Dioxygen

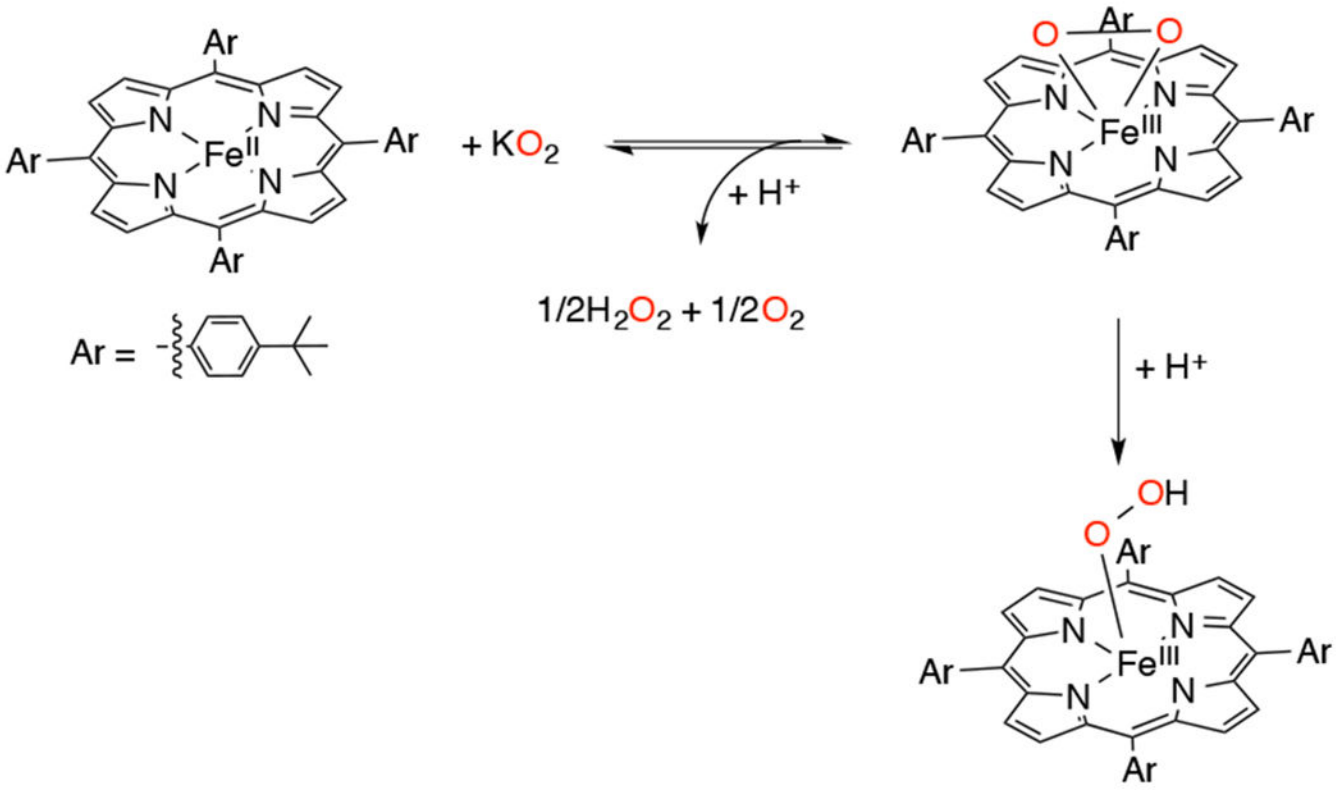

Scheme 41.
Effect of Acid Addition on a Peroxo Adduct of an Iron-Porphyrin

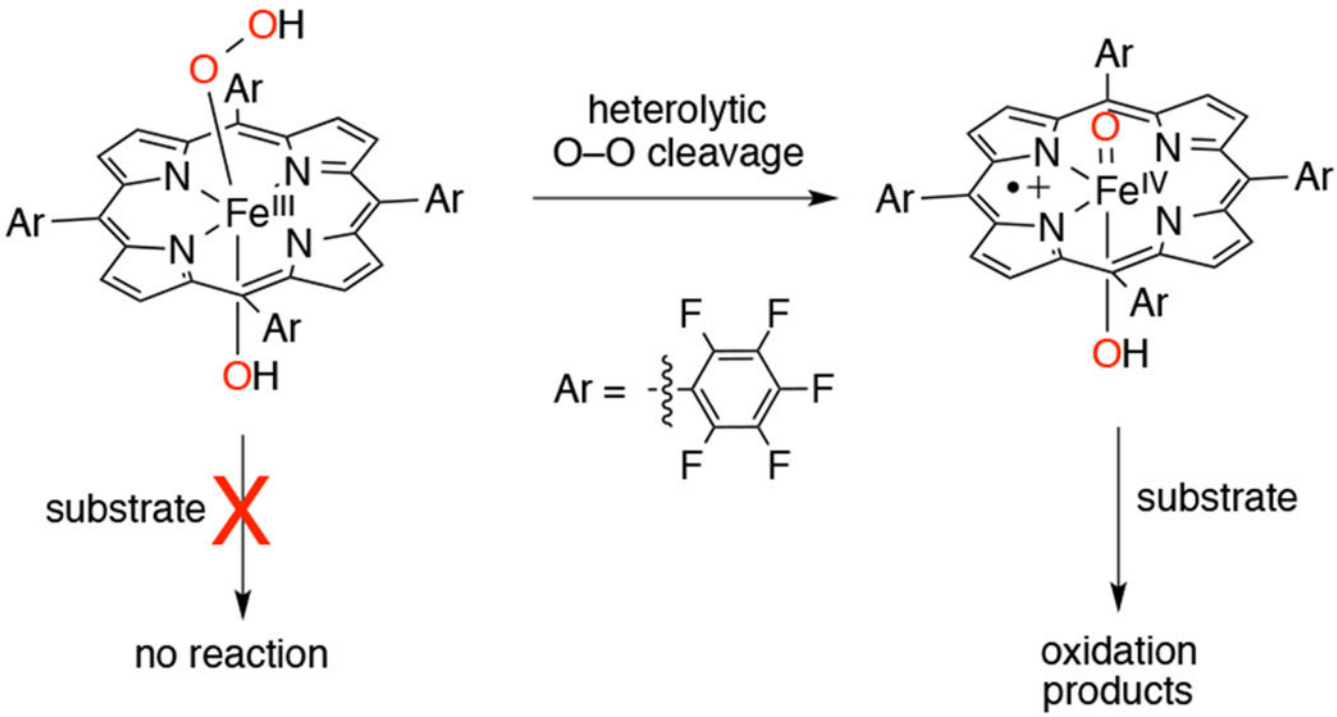

Scheme 42.

Comparative Reactivity of a Ferric-Hydroperoxide Porphyrin and the O–O Bond Cleavage Product, a Cpd-I-like Species

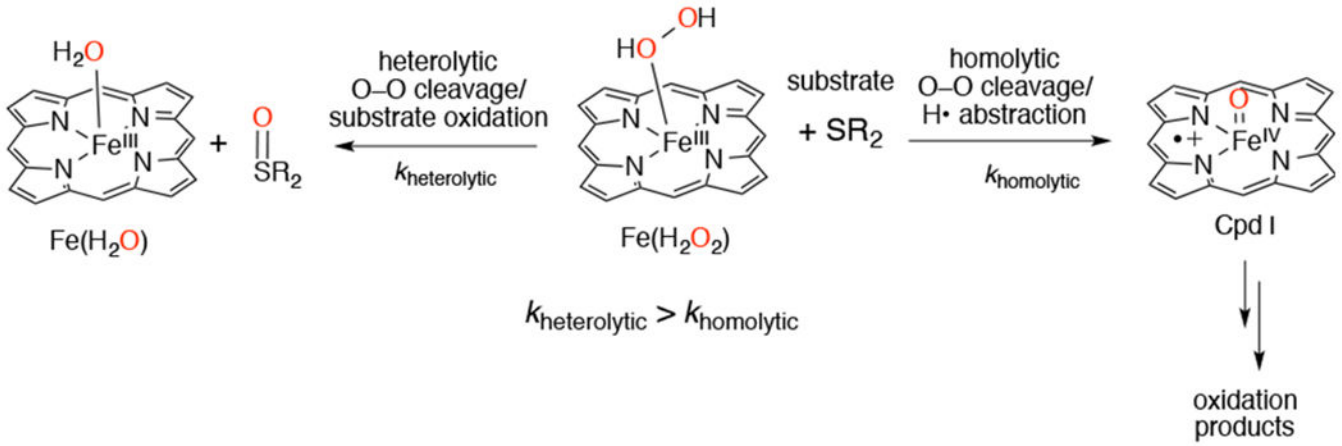

Scheme 43.

DFT Calculations on the Heterolytic vs Homolytic Cleavage Mechanisms in Oxidation of Sulfide Substrates by an $Fe(H_2O_2)$-Porphyrin Complex

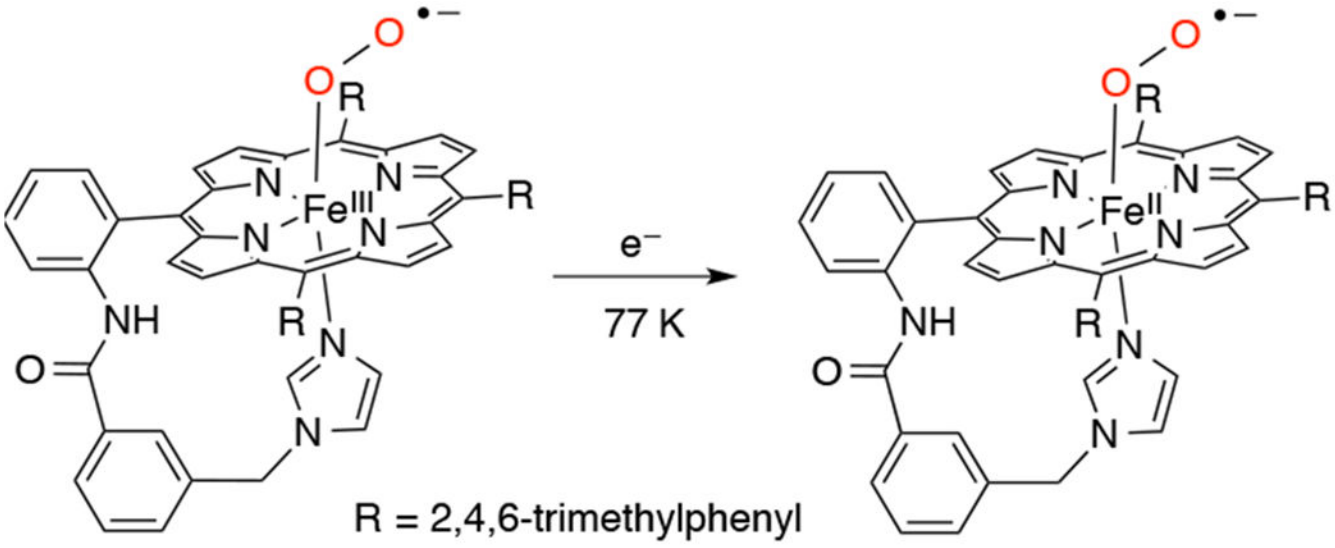

Scheme 44.
Cryo-Reduction of a Ferric-Superoxo to the Ferrous-Superoxo Porphyrin Complex

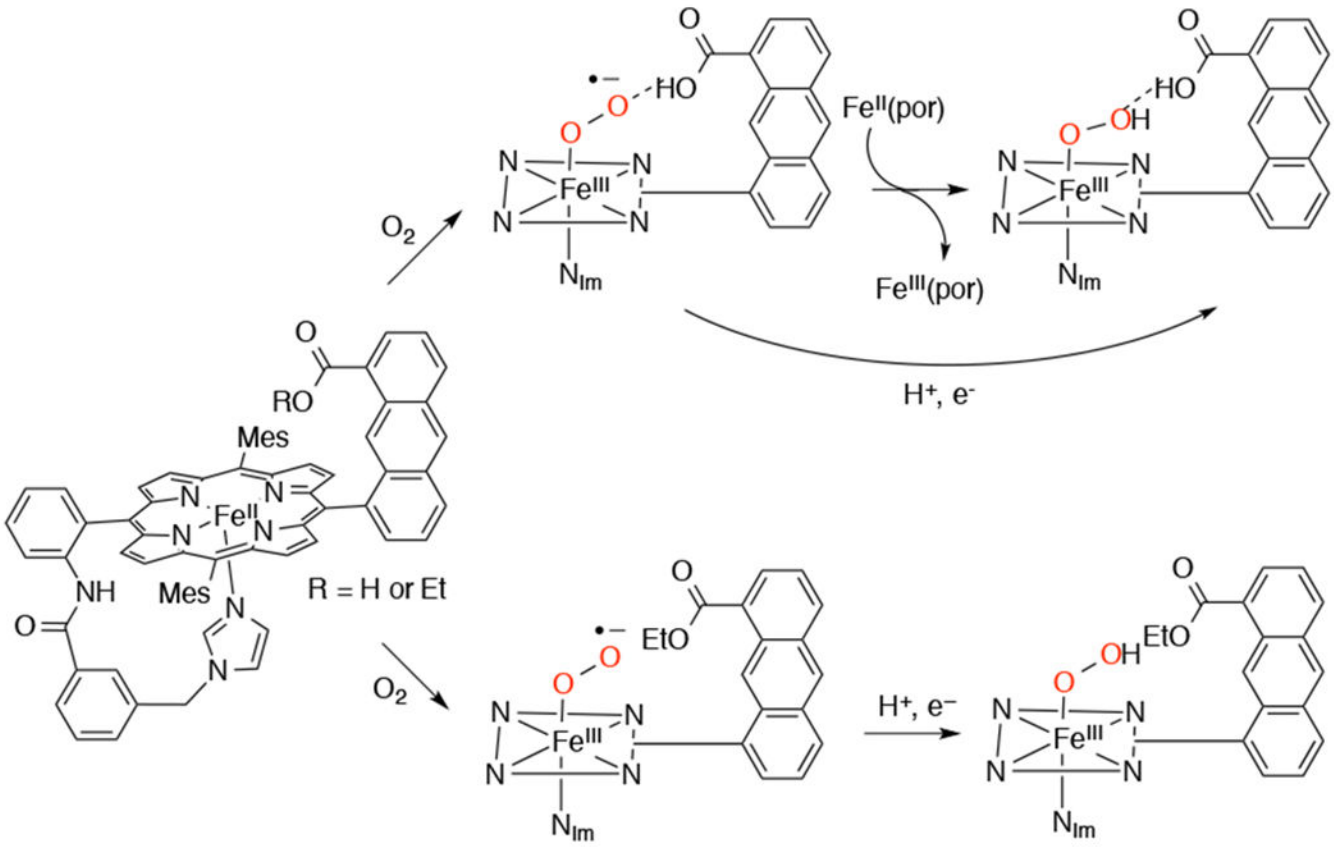

Scheme 45.

Comparison of the Reactivity of a Ferric Superoxo Porphyrin in the Presence and Absence of a Ligand-tethered Proton Donor

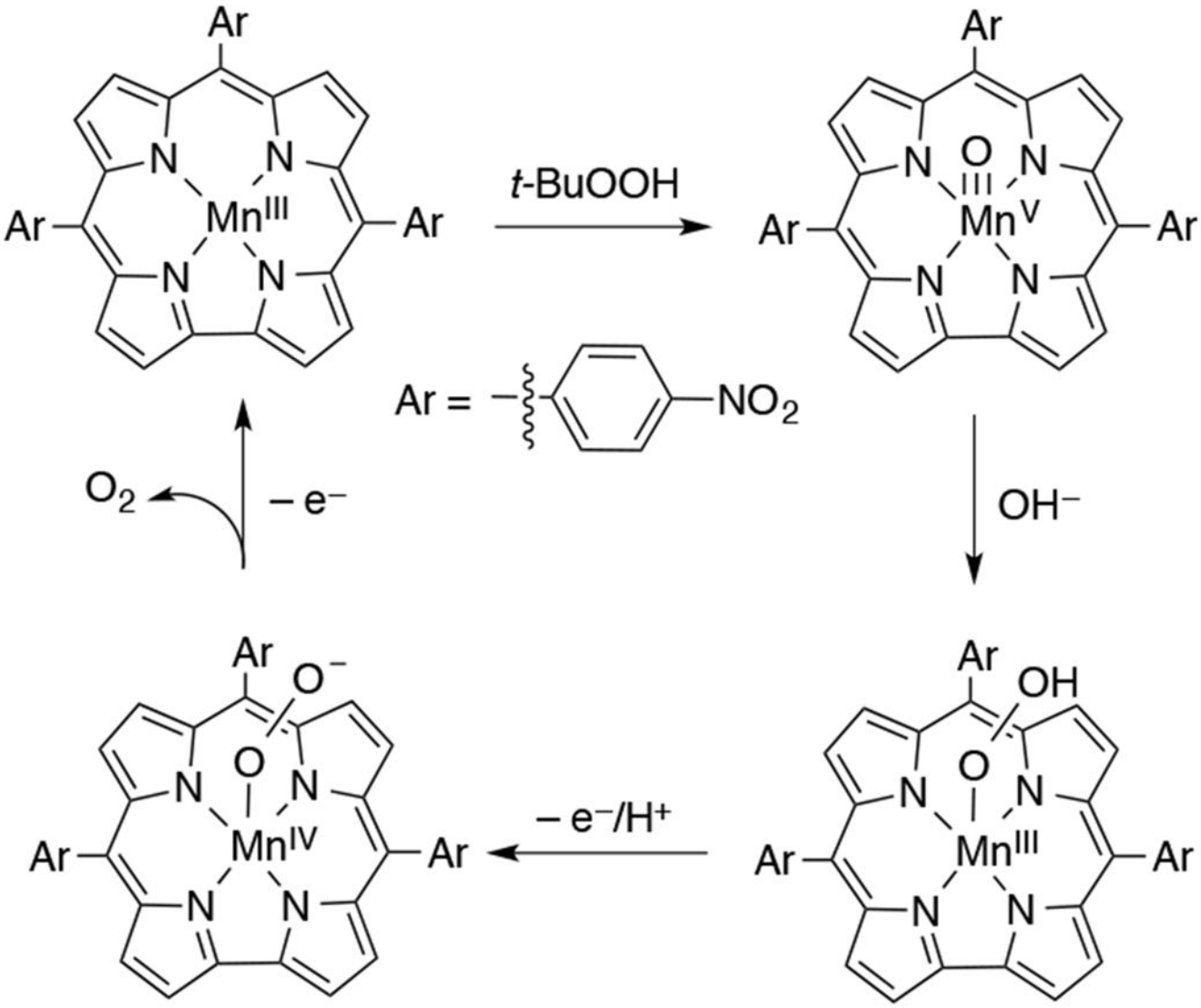

Scheme 46.

O-O bond Formation from Nucleophilic Attack of Hydroxide on a High-Valent Metal-Oxo Corrole

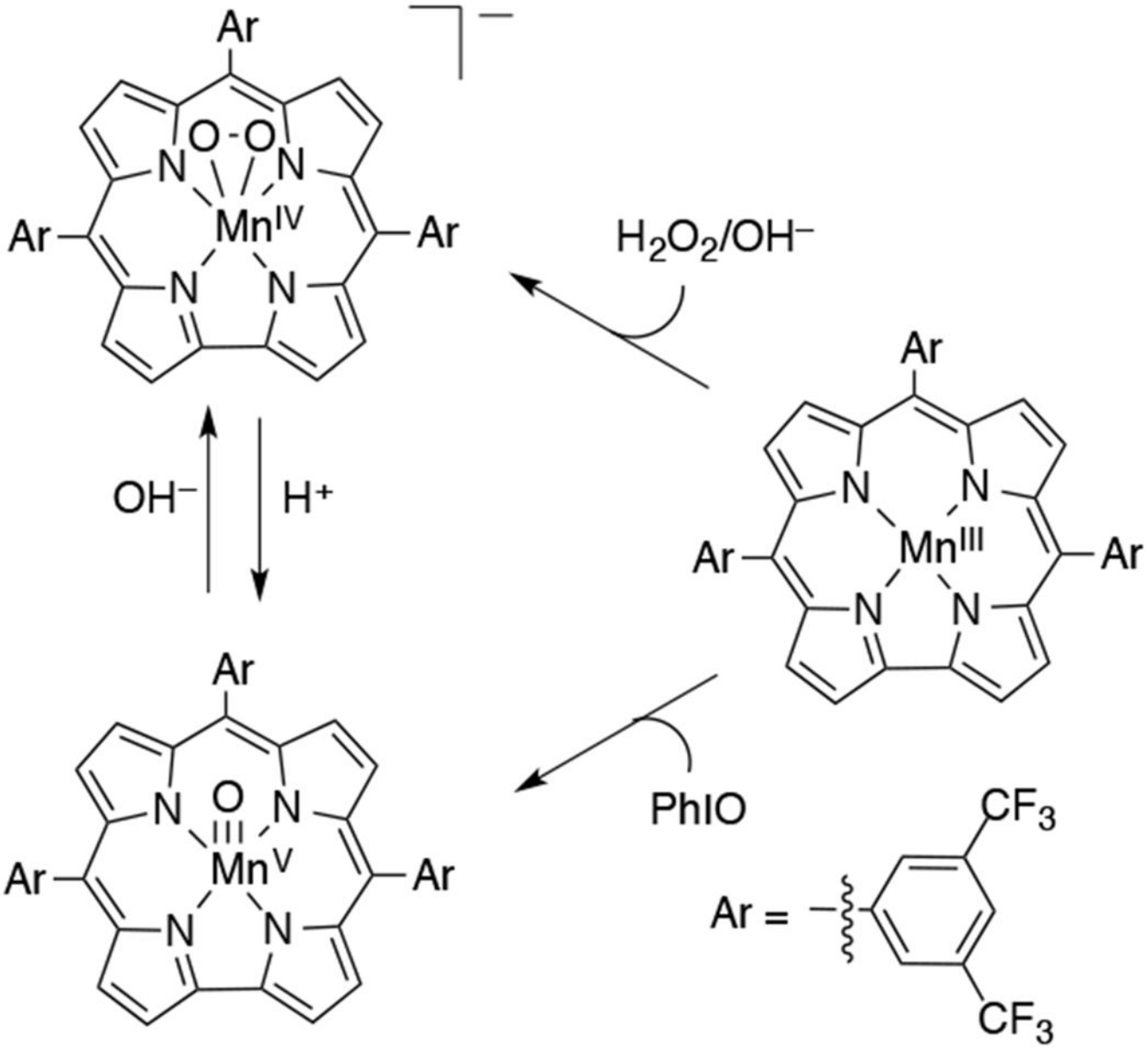

Scheme 47.

Reversible Interconversion of a Manganese-oxo and Manganese-peroxo Corrole Complex in the Presence of Acid or Base

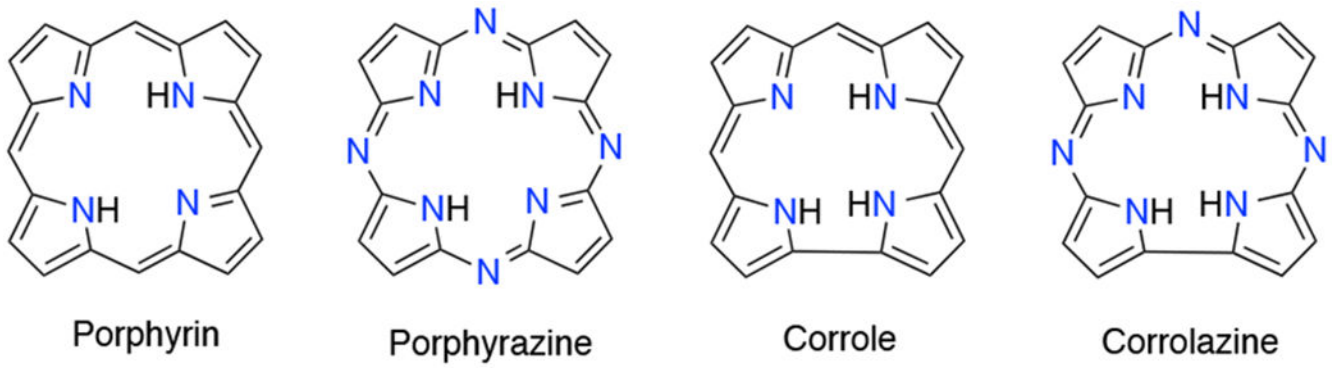

Chart 1.
Core Structures of Common Members of the Porphyrinoid Family Used for Biomimetic Studies

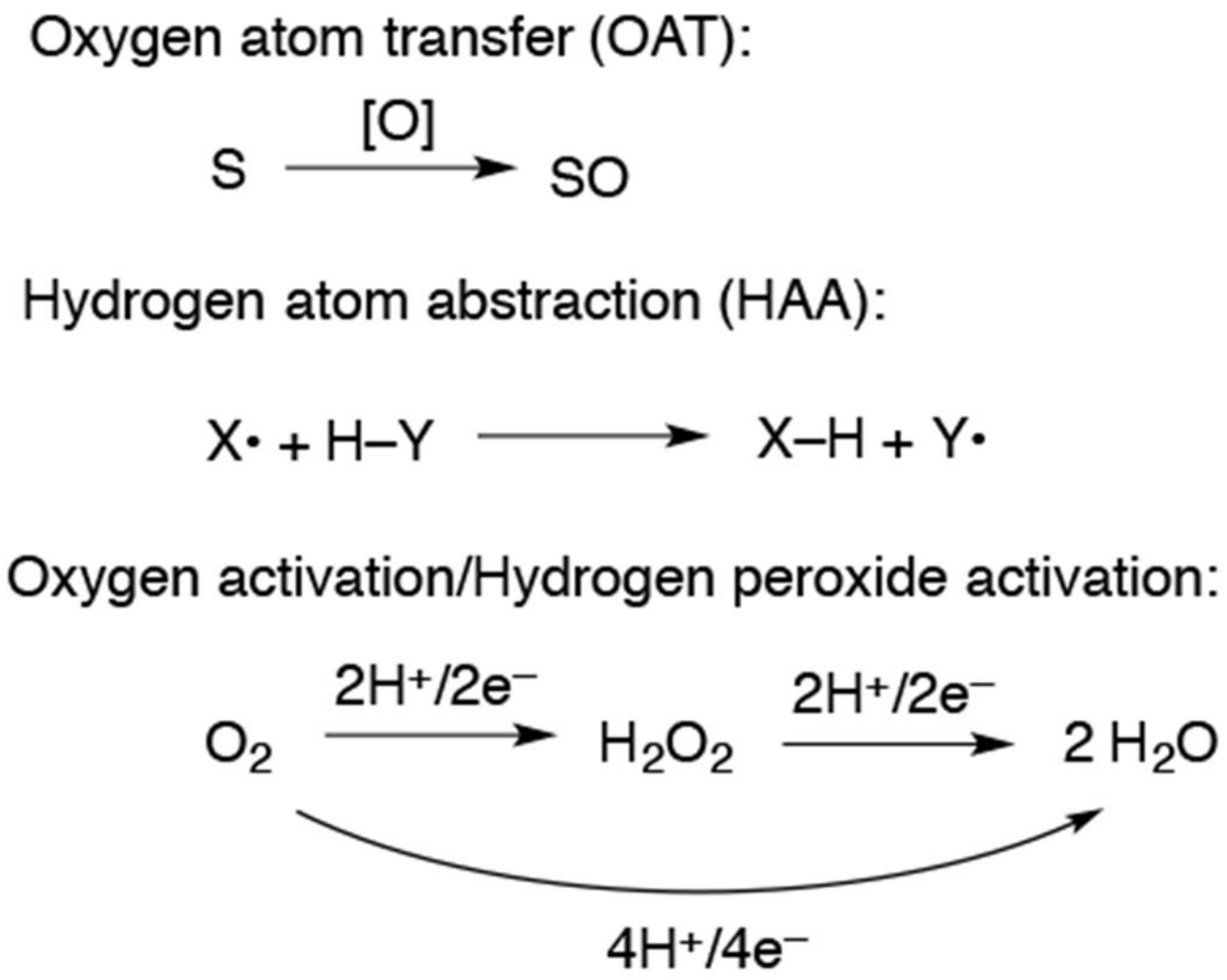

Chart 2.
Biomimetic Reactions Performed by Metalloporphyrinoid Complexes